1-1-2003

Effect of primary silicon crystals on the fluidity of eutectic and hypereutectic Al-Si alloys in lost foam casting

Shailesh Kamble
Ryerson University

EFFECT OF PRIMARY SILICON CRYSTALS ON THE FLUIDITY OF HYPEREUTECTIC ALUMINUM SILICON ALLOYS IN LOST FOAM CASTING

by

Shailesh Kamble
B.E. (Metallurgy), 1997
University of Pune, India

A thesis
presented to Ryerson University
in partial fulfillment of the
requirements for the degree of
Master of Applied Science
in the Program of
Mechanical Engineering
Toronto, Ontario, Canada, 2003

Your file Votre référence
ISBN: 0-612-87158-4
Our file Notre référence
ISBN: 0-612-87158-4

AUTHOR'S DECLARATION

I hereby declare that I am the sole author of this thesis.

I authorize Ryerson University to lend this thesis to other institutions or other individuals for the purpose of scholarly research.

Shailesh Kamble

I further authorize Ryerson University to reproduce this thesis by photocopying or by other means, in total or in part, at the request of other institutions or individuals for the purpose of scholarly research.

Shailesh Kamble

BORROWER'S PAGE

Ryerson University requires the signature of all persons using or photocopying this thesis. Please sign below, and give address and date.

NAME	ADDRESS	DATE

ABSTRACT

EFFECT OF PRIMARY SILICON CRYSTALS ON THE FLUIDITY OF HYPEREUTECTIC ALUMINUM SILICION ALLOYS IN LOST FOAM CASTING

© Shailesh Kamble, 2003
Master of Applied Science
in the program of
Mechanical Engineering
Ryerson University

The hypereutectic Aluminum-Silicon (Al-Si) Alloys are gaining impetus in the automotive components, mainly due to their wear resistance. This property in these alloys is derived from the primary silicon crystals. However, there are unique metal flow and mold filling problems associated with hypereutectic Al-Si alloys in Lost Foam Casting (LFC). This investigation is a pioneering work undertaken to gain a better understanding of the role of primary silicon crystals and other phases in the LFC of hypereutectic Al-Si alloys.

Time-temperature and first derivative curves were used to determine velocity of metal flow and to calculate solid fractions. Process parameters such as superheat, gating design and alloy composition were manipulated to change the morphology of primary silicon crystals. Microscopy and image analysis of castings enabled study of precipitated particles. Solidification, interlocking and melt sluggishness of precipitated particles significantly influenced fluidity, and the routine process parameters played a minor role.

ACKNOWLEDGEMENTS

With great pleasure, I would like to express my gratitude to those who contributed this work.

To work with Dr. C. Ravindran was a lifetime opportunity. His trust in his students, continuous encouragement and being with them during the ups and downs, on the personal and professional front makes a student far better than he is. Certainly, ' It is not the ability of a person that makes people trust in him but it's the trust of people that makes a person able.' Thank you, Sir!

Special thanks are owed to Alan Machin. Alan was a source of information and learning. His inquisitiveness and prompt service to the lab are greatly appreciated.

Colleagues Lukas, Carl and Domenic were part of 'Near Net Shape Research Team'. Healthy competition and constructive criticism in this group motivated my research.

My family had an indirect contribution to this research. Their patience, understanding and emotional support was an inspiration to make things better.

I am also thankful to the Chaudhari family and my friends Gajendra, Sandy, Jayesh, Girish, Sachin and Rakhi for keeping my spirit up.

Finally, I would like to thank God for everything!

To my uneducated Grandparents

... for their extreme faith in education.

TABLE OF CONTENTS

LIST OF TABLES

LIST OF FIGURES

CHAPTER 4

APPENDIX B

APPENDIX C

NOMENCLATURE

Symbol		*Units*
English		
a	Channel radius	cm
A	Mold surface area	cm^2
C	Specific heat of liquid metal	cal/g °C
C_L	Specific heat of an alloy	J/g°C
$\%f_s$	Fraction of solid	Dimensionless
h	Heat transfer coeff. at mold-metal interface	cal/cm^2 s °C
H	Heat of fusion	cal/g
H_e	Heat of fusion of eutectic phase	cal/g
H_p	heat of fusion of proeutectic phase	cal/g
H_E	Decomposition energy of LFC pattern	J/g
k	Critical solid concentration	Dimensionless
k′	Thermal conductivity of mold	cal/s cm°C
L	Latent heat of solidification	J/g
L_f	Fluidity	cm
N	Average grain density	cm^{-3}
P_p	Back pressure	g/cm s^2
R	Average grain radius	cm
S	Circumference of mold channel	cm
t_f	End of solidification/Fluid life	s
t_s	Instantaneous time	s
t_p	Thickness of pattern	mm
T	Temperature of liquid metal	°C
T_{LIQ}	Liquidus temperature	°C
T_{SOL}	Solidus temperature	°C

T_m	Metal melting temperature	^oC
T_r	Room temperature	^oC
ΔT	Superheat	^oC
V	Velocity of metal flow	cm/s
V_1	Velocity of metal flow before enters PSC depleted zone	cm/s
V_2	Velocity of metal flow through PSC depleted zone	cm/s
Δy	Choking range	cm

Greek

α	Thermal diffusivity of mold	cm^2/s
ρ_p	Density of pattern	g/cm^3
ρ_L	Density of molten metal	g/cm^3

Abbreviations

AFS	American Foundry Standards
BGS	Bottom Gating System
cc	Cooling Curve
EPS	Expandable Polystyrene Foam
GFN	Grain Fineness Number
LFC	Lost Foam Casting
pcf	Pounds per Cubic Foot
PMMA	Polymethyl Methacrylate
PSC	Primary Silicon Crystals
PT	Pouring Temperature
RPT	Reduced Pressure Test
SEM	Scanning Electron Microscopy
TGS	Top Gating System
zc	Zero Curve

Definitions

Baume	Unit for measurement of viscosity of water based washes at room temperature.
First derivative curve	First derivative at each point of the cooling curve is equal to the slope of the cooling curve.
Fluidity	Fluidity is the ability of the molten metal to effectively fill the mold.
Fraction of solid	Fraction of solid ($\%f_s$) may be defined as the percentage of solid phase(s) that precipitates between liquidus and solidus temperatures in a solidifying melt.
Freezing range/ Mushy zone	The range between the liquidus and the solidus temperature.
Heat of fusion	The heat that is to be removed during solidification is known as the heat of fusion.
Liquidus	The temperature at which solidification begins.
Local solidification time	It is defined as the time difference between the liquidus and the solidus points.
Total solidification time	It is the time difference between the pouring temperature and the solidification temperature.
Solidus	The temperature at which solidification ends.

CHAPTER 1

INTRODUCTION

Aluminum-Silicon (Al-Si) alloys have been a desirable material for combustion engine blocks and pistons due to their lightweight, high thermal conductivity and adaptability to rapid, precision casting techniques. However, these alloys do not have adequate wear resistance, and this necessitates insertion of liners (usually of iron or steel) in Al block. The liners are expensive, reduce the thermal conductivity and increase the weight almost by three times that of Al alloys.

Reynolds Aluminum Company initiated a comprehensive program in 1958 to develop such an alloy.[1] They developed the 390 Al-Si alloy with good wear resistance. This is a hypereutectic alloy with 17 and 18% Si. The high wear resistance of this alloy was attributed to the precipitation of hard primary silicon crystals during solidification.

Fluidity of hypo and hypereutectic Al-Si alloys was studied by several researchers. [2,3,4,5,6,7] Their results showed an increase in fluidity for the alloys with Si content upto 18% Si. These researchers observed that a decrease in the fluidity for the alloys Si content more than 18%, in spite of the high heat of fusion of Si (350 cal/g, 7 times more than Al). The reasons for this observation include an increase in the freezing range, a decrease in superheat and an increase in the amount of silicon particles.

Although, past researchers suggested that size and distribution of primary silicon crystals might be one of the reasons for decreasing the fluidity above 18% Si content, their results were not supported with corroborating evidence (e.g. micrographs and theoretical calculations). Also there is a need to study the effect of process parameters on the size and distribution of primary silicon crystals (PSC) and the other precipitated particles (such as $CuAl_2$) on the flow stoppage.

Flow stoppage mechanism suggests that in case of hypereutectic Al-Si alloys, the flow stoppage occurs at the end of the casting (not at the start of the casting, as in case of pure metals) due to agglomeration of precipitated particles causing interlocking and melt sluggishness. Thus, it was suggested that precipitated particles also play a role in the flow stoppage, impacting the fluidity of an alloy.

Lost Foam Casting[8,9,10,11] (LFC) is an endothermic process that helps in reducing the freezing range and hence decreases the size of primary silicon, thus avoiding the interlocking of primary silicon crystals. This process also results in smooth distribution of precipitated particles in microstructure due to its lamellar mold filling mechanism.

In this Lost Foam Casting research, the effect of selected process parameters on the morphology of primary silicon particles and fluidity of hypereutectic alloys was studied through thermal analysis, image analysis and fraction of solid determination.

CHAPTER 2

LITERATURE SURVEY

Chapter Summary

A literature survey was conducted to study the fluidity of Al-Si alloys, flow stoppage mechanisms and the role of primary silicon crystals during solidification. Lost Foam Casting was deliberately selected for the processing of hypereutectic Al-Si alloys. Fraction of solid is the amount of solid phase that precipitate during solidification. It is related to thermal and image analysis results. Several methods to calculate fraction of solid were studied.

2.1 INTRODUCTION TO ALUMINUM SILICON ALLOYS:

Section Summary

Cast Al-Si alloys are mainly divided into three groups (hypoeutectic, eutectic and hypereutectic). This division is based on Si content in the alloy.

Up to the eutectic composition (hypoeutectic alloy), the freezing range of alloy decreases by increasing the Si content, whereas the freezing range increases after the eutectic composition (hypereutectic alloy). Alloys in the range of 12-25% Si are of particular interest in this research due to their high wear resistance.

2.1.1 Aluminum Silicon (Al-Si) Alloys

Aluminum silicon alloys (Al-Si) constitute 85-90% of the total Al cast parts produced.[1] Al alloys containing Si as the major alloying element offer excellent castability, good corrosion resistance and good machining /welding characteristics.

The properties of Al-Si alloys are strongly dependent on the casting process used, the chemical additions made, primary silicon crystals (PSC), grain structure and molten metal treatment to reduce hydrogen gas content and remove inclusions. Depending on the amount of Si, the alloys are divided into three major groups:

- Hypoeutectic alloys with Si content between 5-10% Si
- Eutectic alloys with 11-12% Si
- Hypereutectic alloys with 12-25% Si

Addition of Si to Al is similar to the addition of sugar to iced tea. Si dissolves into Al. As addition of Si continues, Al eventually becomes saturated with Si. Above the saturation point, Si precipitates out in the form of hard, primary Si particles similar to the excess sugar in iced tea. Hypereutectic Al-Si alloys are of particular interest in this research.

2.1.2 Hypereutectic Al-Si Alloys (Si Content: 12-25%)

Hypereutectic Al-Si alloys have long been recognized as a potential candidate for automotive applications. The higher Si content causes outstanding wear characteristics. Hypereutectic Al-Si alloys can have a density about one third and a thermal conductivity about three times that of cast iron. High wear resistance, low density and good thermal conductivity eliminate the need for expensive iron or steel cylinder liners in pistons and engine blocks as suggested by Jorstad.[1] Alloy 390 is the most commonly used alloy in the series of hypereutectic alloys. The designation '390' is used with reference to a family of three specific alloys, as given in Table 2.1.

Table 2.1 Composition of 390 Alloys.[13,14]

	Si %	Fe%	Cu%	Mn%	Mg%	Zn%	Al	Process
390	16-18	1.3	4-5	0.10	0.45-0.65	0.10	rem.	Die Casting
A390	16-18	0.50	4-5	0.10	0.45-0.65	0.10	rem	Sand, Plaster mold and Die Casting.
B390	16-18	1.3	4-5	0.50	0.45-0.65	1.5	rem	Die casting, Permanent mold casting.

2.1.3 Al-Si Phase Diagram

With an increase in Si content, the freezing range of the hypoeutectic alloy decreases whereas it increases for hypereutectic alloys (Figure 2.1). This increase in freezing range for hypereutectic alloys by addition of Si causes the following effects:

1. Ineffective degassing: Hydrogen is the only gas that is soluble in Al alloys. Solubility of hydrogen increases with an increase in temperature. Above 780^0C, hydrogen is more soluble in molten metal and hence tablet flux degassing is known to be ineffective at such a high temperature. Degassing will be discussed in more detail in Section 3.2.10.

2. Effective grain refinement: Phosphorous addition and faster cooling are the main methods of grain refinement for hypereutectic Al-Si alloys. With an increase in liquidus temperature, the freezing range also increases. High liquidus temperature increases the cooling rate and results in finer grain size. Grain refinement will be discussed in detail in Section 2.3.5.

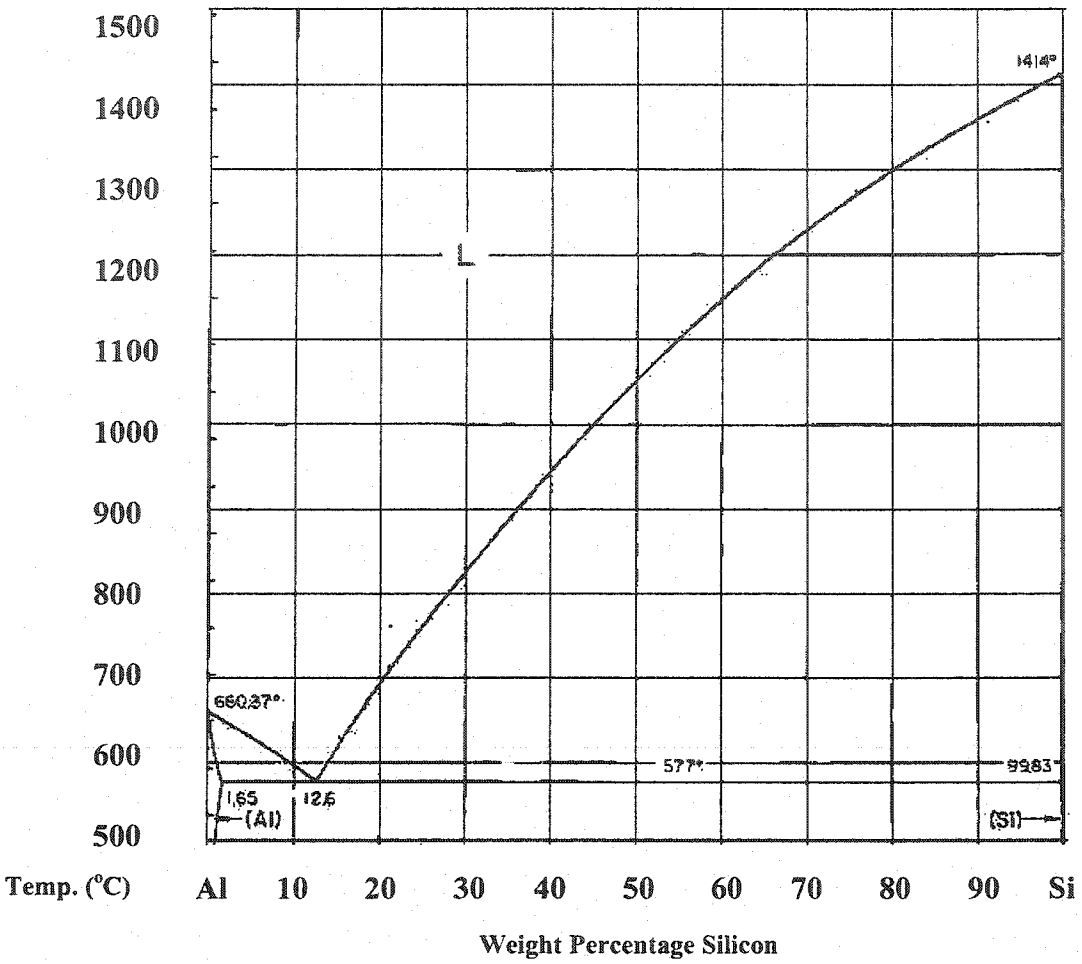

Figure 2.1 Equilibrium Binary Phase Diagram for Al-Si Alloy.[15]

2.2 FLUIDITY OF ALUMINUM-SILICON ALLOYS

Section Summary

Al-Si alloys have a better fluidity due to its high heat of fusion. Effects of several factors on fluidity are summarized in this section. Heat of fusion, superheat, section thickness, mechanism of freezing, alloy additions (Si and Cu) and gating system are of particular interests in this research.

2.2.1 Effect of Heat of Fusion on Fluidity

Fluidity implies an ability to effectively fill the mold. It is how far a molten metal can flow in a mold and how well it is able to fill out fine details, before it becomes too solid to flow further. With higher amount of heat that must be removed to solidify, the alloy will be able to flow further. This heat that is to be removed during solidification is known as the 'heat of fusion'. Al has a high heat of fusion (95 cal/g). It is higher than any other commonly cast metal. Thus in effect, a significant amount of heat must be absorbed by the mold and/or other surroundings during solidification. However, the heat of fusion of Si is 3.7 times greater than that of Al (Table 2.2). So, with more Si in an alloy, the alloy should flow further. Thus the heat of fusion is the most important indicator of fluidity in Al casting alloys.

Element	**Heat of Fusion (Cal/g)**
Si	350
Al	95
Mg	90
Fe	65
Cu	50
Zn	25

Table 2.2 Heat of Fusion of Elements.[2]

While the heat of fusion directly affects fluidity, there are many factors that affect fluidity in some measure.

2.2.2 Other Factors that Affect Fluidity

The factors that improve the fluidity are:

1) Degree of superheat: The Fluidity is known to increase with increasing melt temperatures for a given alloy composition.[2,3] In the case of low superheat, the

nucleation of fine grains is an immediate result. However, for high superheat, nucleation is delayed and results in increased fluidity.

2) Modification: Literature suggested that[4,50] Al-Si alloys with hypoeutectic and eutectic compositions that have been grain refined and strontium modified exhibit an improved fluidity of about 20-30 %, as compared to untreated Al-Si alloys. The addition of strontium to the hypoeutectic and eutectic Al-Si alloys causes the eutectic Si to become fibrous and the solid/liquid interface to become relatively smooth. Both these effects improve fluidity.

3) Mold design: The gating system, pouring head and rate of pouring have a direct effect on fluidity. High rate of pouring, top gating system and high velocity head increase the fluidity. Hence, it is important to be aware of the fluid dynamics of the system.

4) Melt cleanliness: A significant factor affecting fluidity is melt cleanliness. Inclusions within the melt decrease the fluidity. Loper[2] reported a substantial increase in the fluidity of alloy 319 when the melt was cleansed using inert and halogen gases.

The factors that reduce the fluidity are:

1) Cooling rate: Rate of cooling depends on the casting process implemented and the mold medium. High cooling rate decrease the fluidity.

2) Grain refinement: Ti grain refinement reduces the fluidity.[2] Phosphorous (primary silicon refiner) refinement for hypereutectic alloy reduces fluidity by 10-20 % relative to non refined melts.[4] It was suggested that phosphorus causes primary silicon particles to become finer (and numerous), thus increasing melt sluggishness. This reduces fluidity.

3) Surface tension of the molten metal: A high surface tension reduces the fluidity. Many elements are known to reduce the surface tension of molten Al (e.g. Li, Bi, Pb, Mg, Sb, Ca). Si has a limited effect on the surface tension of molten Al. Some elements (e.g. Ge, Zn, Ag, Fe, Mn, and Cu) may slightly increase the surface tension. However, the effect of surface tension is typically masked, or eliminated by the influence of surface oxide films.

4) Formation of surface oxide films: This has a marked effect on fluidity. It has been estimated that the surface tension can be tripled by the formation of aluminum oxides.[2]

5) Formation of non-metallic inclusions in the molten metal: This factor covers inclusions, entrained dross and/or slag and any undissolved additions made during solidification. All these have a negative impact on fluidity. Increase in fraction of solid due to nonmetallic inclusions also reduces fluidity.

2.2.3 Role of Si on the Fluidity of Al-Si Alloys

Fluidity increases with an increase in Si content up to 18-20 % Si and then it decreases (Figure 2.2).

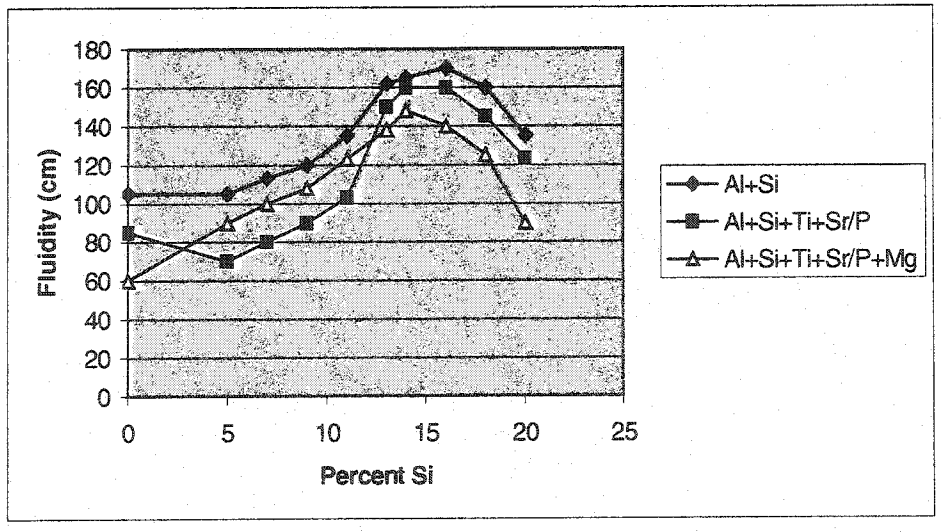

Figure 2.2 Figure Showing Decrease in Fluidity for Higher Si Content.[4]

The reasons for such a behavior was discussed by several researchers, [2,4,16]

- With an increase in Si content, the freezing range of an alloy also increases. This in turn increases the extent of mushy zone and it might impede the flow of melt.
- With an increase in Si content, numbers and size of primary Si particles increases, this might cause resistance to metal flow.
- In case of constant pouring temperature, superheat gradually decreases with an increase in Si content.

2.2.4 Role of Copper (Cu) on the Fluidity of Al-Si Alloys

Cu addition increases strength and fatigue properties. Cu has a low heat of fusion (50 cal/gm). Therefore, to maintain the fluidity of an alloy, Cu is always used in conjunction with Si.[17] Si has little effect on the solubility of Cu in Al. Also, Cu does not change the solubility of Si in Al.[19]

A study by Wang and Apelian[18] revealed that the addition of Cu causes precipitation of $CuAl_2$ phase during solidification. This phase is in the form of coarse blocky particles, ranging in size from 5 to 20 μm. They precipitate with the eutectic Si. Kim and Loper[3] observed a decrease in fluidity with addition of 3.5% Cu for hypereutectic Al-Si alloy. Figures 2.3 and 2.4 compare the change in fluidity by addition of Cu.

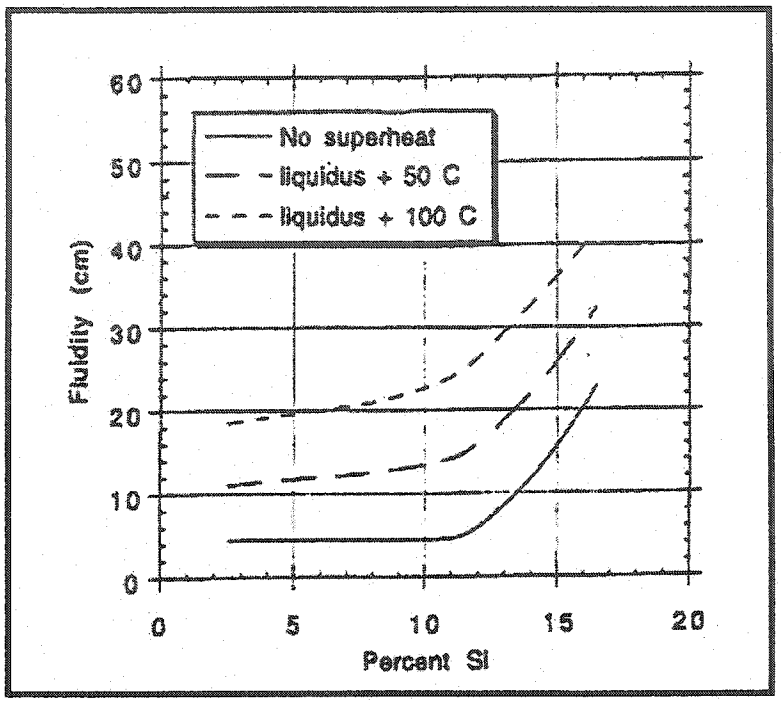

Figure 2.3 Fluidity Curves Without Cu Addition.[3]

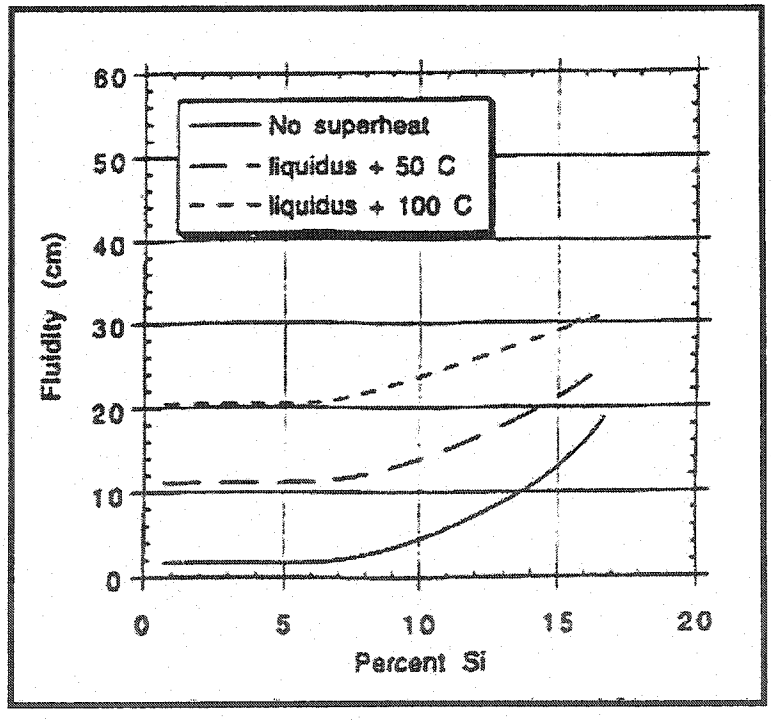

Figure 2.4 Fluidity Curves With 3.5% Cu.[3]

Pan & Hu[5] observed similar results with addition of 2% and 4% Cu.

2.2.5 Effect of Lost Foam Casting (LFC) on the Fluidity

For LFC, the spiral pattern test has been used to determine fluidity. However, differences in gating system, pressure head and fluid flow affect the results and limit the ability to compare such results.

Pan and Liao[6] studied the influence of several processing parameters, including pouring temperature, coating thickness, pattern density, gating system design, and application of vacuum on the fluidity of A356 (hypoeutectic alloy with 7% Si) alloy in LFC. The findings obtained indicate that the fluidity of A356 alloy was positively effected by pouring temperature, pattern thickness and application of vacuum, whereas negatively effected by coating thickness and foam pattern density. Pan and Liao did not study the effects of sprue height and gating ratio or gating system dimensions on the fluidity. They suggested that a casting with a thicker section or with a higher pouring temperature has a higher heat content, and a better fluidity.

2.2.6 Fluidity Model for Hypereutectic Al-Si Alloy

Flemings developed simplified mathematical models for the fluidity of pure metals that are poured into a cylindrical channel mold .[7,20]

$$L_f = \frac{\rho a V (H + C\Delta T)}{2H(T_m - T_r)} \qquad (2.1)$$

Where,

L_f fluidity, cm

V velocity of metal flow, cm/s

a channel radius, cm

ρ density of liquid metal, g/cm^3

H heat of fusion, cal/g

C specific heat of liquid metal, cal/g ^{o}C

ΔT superheat, ^{o}C

T_m metal melting temperature, °C

T_r room temperature, °C

For alloys,

$$L_f = V * t_f$$

Where,

t_f fluid life, s

Hence,

$$L_f = \frac{A\rho V(kH + C\Delta T)}{Sh(T - T_r)}\left(1 + \frac{B}{2}\right) \tag{2.2}$$

Where,

k critical solid concentration (dimensionless fraction)

S circumference of mold channel, cm

h heat transfer coeff. at mold-metal interface, cal/cm^2 s °C

A mold surface area, cm^2

$$B = \frac{h\sqrt{\pi\alpha\,\Delta y}}{k'\sqrt{V}} \tag{2.3}$$

Where,

k′ thermal conductivity of mold, cal/s cm °C

Δy choking range, cm

α thermal diffusivity of mold cm^2/s

This equation was modified for hypereutectic Al-Si alloys by Kim and Loper[2],

$$L_f = \frac{A\rho V_1 (kH_p + C\Delta T)}{Sh\,(T - T_r)}\left(1 + \frac{B}{2}\right) + \frac{\rho A V_2 H_e}{2h(T - T_r)} \qquad (2.4)$$

V_1 velocity of metal flow before enters PSC depleted zone, cm/s

V_2 velocity of metal flow through PSC depleted zone, cm/s

H_e heat of fusion of eutectic phase, cal/g

H_p heat of fusion of proeutectic phase, cal/g

T Temperature of liquid metal, °C

2.3 MICROSTRUCTURAL CHARACTERISTICS

Section Summary

The PSC are the main constituent in the microstructure of hypereutectic Al-Si alloys. They enable improved wear resistance of the alloy. Size and distribution of the PSC need to be controlled to achieve optimum properties. This control mainly depends on the rate of cooling and grain refinement. Faster the rate of cooling, the finer is the size of the PSC. Phosphorous grain refinement is ineffective if the solidification rate is very slow.

2.3.1 Sequence of Phase Precipitation

The main sequence of phase precipitation is as follows.[21]

Hypoeutectic alloy:

1. Formation of a dendritic network of primary α-aluminum.
2. The Al-Si eutectic reaction.
3. Precipitation of secondary eutectic phases like Mg_2Si and Al_2Cu.

Eutectic alloys:

Pre-eutectic reactions may be missing in this case.

Hypereutectic alloys:

1. The primary reaction involves precipitation of Si particles until the eutectic composition is reached.
2. In addition to the main reactions, precipitation of Fe and Mn containing phases may take place. Most common of such phases are listed in Table 4.4. (Please refer Section 4.2.3.)

However, the dominant feature in microstructure of hypereutectic Al-Si alloy is the PSC.

2.3.2 Primary Silicon Crystals

The primary Si phase appears in two different forms as shown in Figure 2.5.

1. Primary Silicon Crystals (PSC): Appear typically as large black 'cuboids'.
2. Eutectic Si: Appear as 'needles'.

PSC are extremely hard, measuring greater than 1100 on the knoop scale.

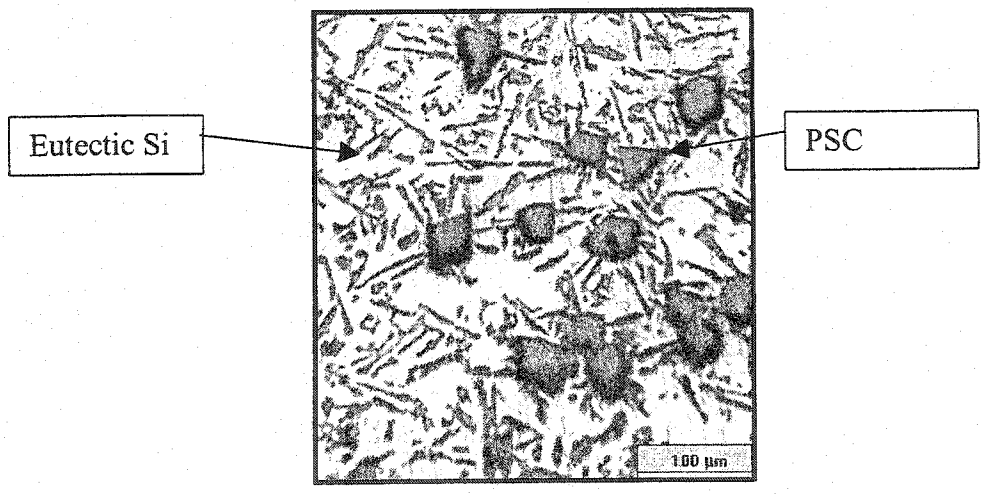

Figure 2.5 Microstructure Showing PSC and Eutectic Si.[19]

PSC originate from transient eutectic colonies, which form at the mold walls during initial stages of solidification and subsequently break up releasing PSC.[22]

Hard PSC increase the wear resistance of the alloy. But if they grow to a larger size (>200μm) during solidification, they cause machining difficulties due to their high hardness. So they must be refined to a reasonably smaller size to economically achieve the wear characteristics for which the alloy is best known. PSC provide wear resistance as well as thermal insulation.[23] In the case of cylinders, the PSC act as an insulator thus retaining heat in the combustion chamber and allowing the rest of the piston to run cooler. Hypereutectic Al-Si has 15% less thermal expansion than conventional piston alloys (usually hypoeutectic Al-Si alloys).

The size of PSC increases with an increase in Si content in hypereutectic alloy. Size for phosphorous-free PSC containing 14% Si and 25% Si typically changes from approximately 40-60 μm to 200-300 μm.[12] Controlled rate of cooling combined with a small addition of phosphorous, provide adequate PSC control. Phosphorous refinement is discussed in detail in Section 2.3.5.

2.3.3 Morphology of PSC

PSC are known to occur as the generic "cuboid" form. However, there can be variations in the morphology. The morphology of PSC is highly dependent on the solidification parameters such as freezing rate, temperature gradient and local liquid composition. These parameters change continuously during the freezing of a casting. So it is not surprising that different Si forms should occur almost side by side. Most common forms are[16]:

- Star Shaped PSC: In this case, PSC form along five axes originating from a single nucleus (several variations of this shape can be found).Refer Figure 2.6(a).

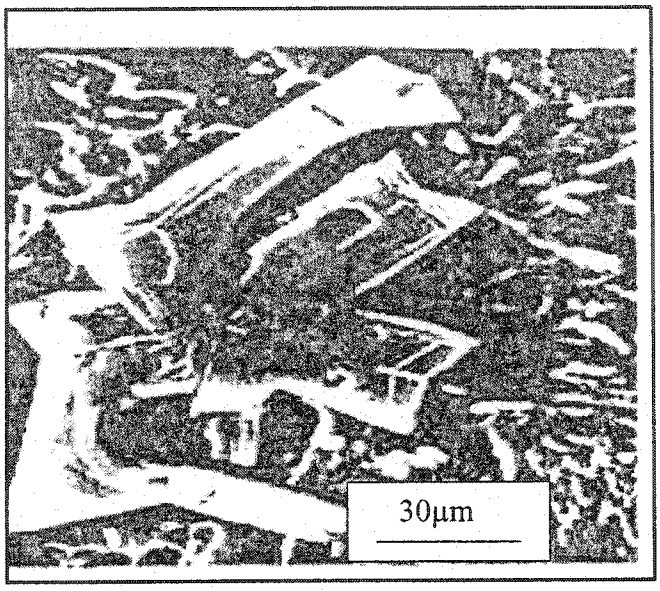

Figure 2.6(a) Star Shaped PSC.

- Polyhedral PSC: In this case, PSC appear hexagonal or octagonal on a polished section. This is the most common shape. Refer to the Figure 2.6(b).

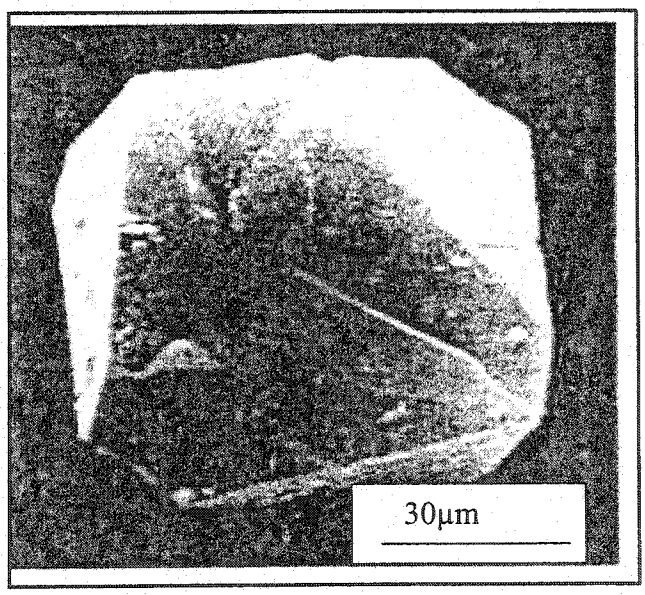

Figure 2.6(b) Polyhedral Shaped PSC

- Dendritic Shaped PSC: In this case, PSC resemble the dendritic form of simple metals, such as the primary Al dendrites in hypoeutectic alloys. Refer to the Figure 2.6(c)

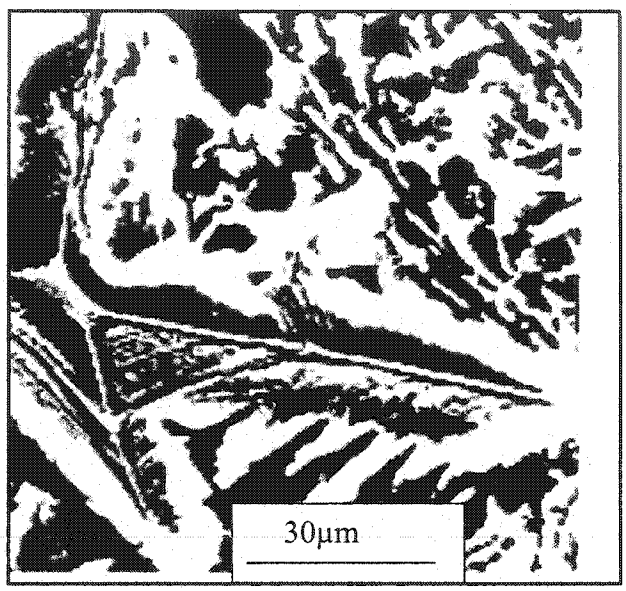

Figure 2.6(c) Dendritic Shaped PSC

The properties of hypereutectic Al-Si alloys (optimum machinablility, improved wear resistance and thermal conductivity) depend on the growth of PSC in microstructure.

2.3.4 Growth of PSC

Optimum wear resistance and mechanical properties of the hypereutectic Si alloys require a reasonably small size and uniform distribution of the primary Si phase. Two factors govern the size and distribution of PSC:

1) Solidification rate
2) Artificial nucleation (refinement)

Normally, the formation of the PSC begins at the liquidus temperature and completes at the solidus temperature. Without a prior refinement treatment, the size is controlled primarily by the rate of cooling through this temperature range, more rapid rates resulting in finer particles. Even in refined melts, with an increased number of nucleation sites, the ultimate size of PSC depends on the solidification rate.[1]

Other reasons for change in PSC size are[12]:

1) Melt holding time increases the possibility of increase in PSC size. It happens due to agglomeration of nuclei.
2) Aggressive degassing causes significant loss of refinement because the nuclei float out of the melt by attachment to the rising gas bubble, whereas mild degassing stirs the melt to produce a more uniform distribution of nuclei.
3) If the melt is cast at higher temperature (~ 900^0C), finer PSC is obtained because of greater solubility of the phosphorous.
4) Remelting at higher temperature results in new nuclei and hence fine grain size can be achieved.

2.3.5 Phosphorous Refinement

Phosphorous refinement is discussed in detail by Gruzleski and Closset.[16] The PSC in hypereutectic alloys are not readily nucleated by the usual impurities present in the alloy. As a result, PSC often do not begin to crystallize until a considerable undercooling is reached below the liquidus temperature. The paucity of nuclei allows only a relatively few Si particles to form, with the result that the microstructure contains extremely large PSC.

Refinement of PSC is usually achieved by the addition of phosphorous to the melt. Phosphorous reacts with the liquid Al to form aluminum phosphide that can act as an effective heterogeneous nucleant. Effect of phosphorous refinement on the size of PSC can be seen in Figure 2.7.

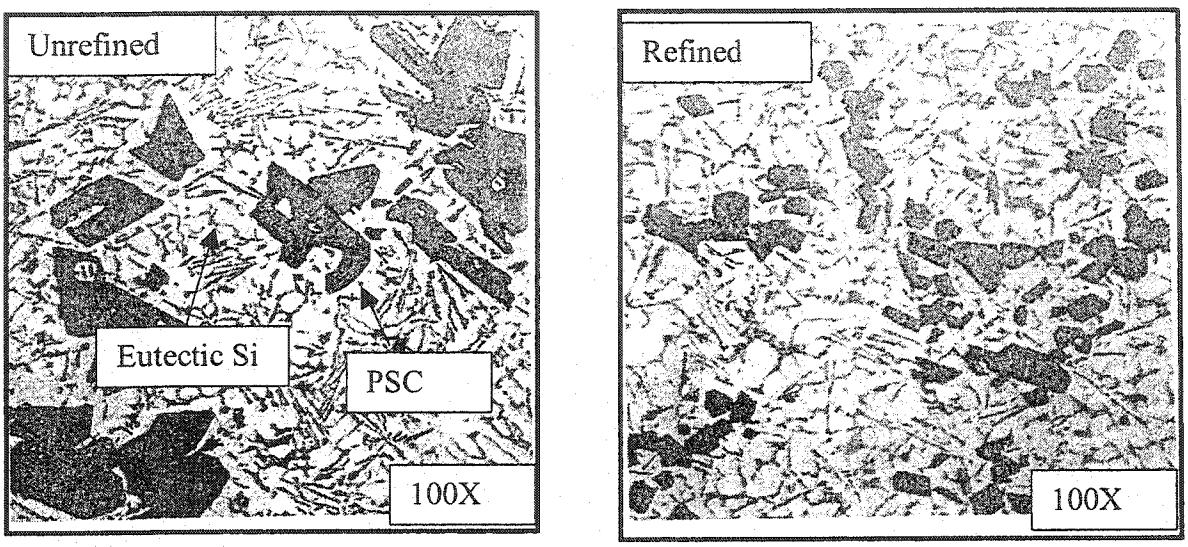

Figure 2.7 Effect of Phosphorus Refinement on Size of PSC[16]

The PSC are also known to play a significant role in flow stoppage during the solidification process.

2.4 FLOW STOPPAGE MECHANISMS

Section Summary

The flow stoppage mechanism is different for pure metal, hypoeutectic and hypereutectic alloys. In the case of pure metal, flow stoppage occurs at the start of the casting whereas in case of hypo and hypereutectic alloys it occurs at the end of the casting. Melt sluggishness and fraction of solid are the main reasons for flow stoppage in hypo and hypereutectic alloys.

2.4.1 Pure Metals

In pure metals, when metal enters the channel of a fluidity test mold, solidification begins at the channel wall and continues by the growth of columnar grains

with a planar interface as metal flows through the channel. Flow ceases when the columnar grains join each other at the channel entrance as shown in Figure 2.8.

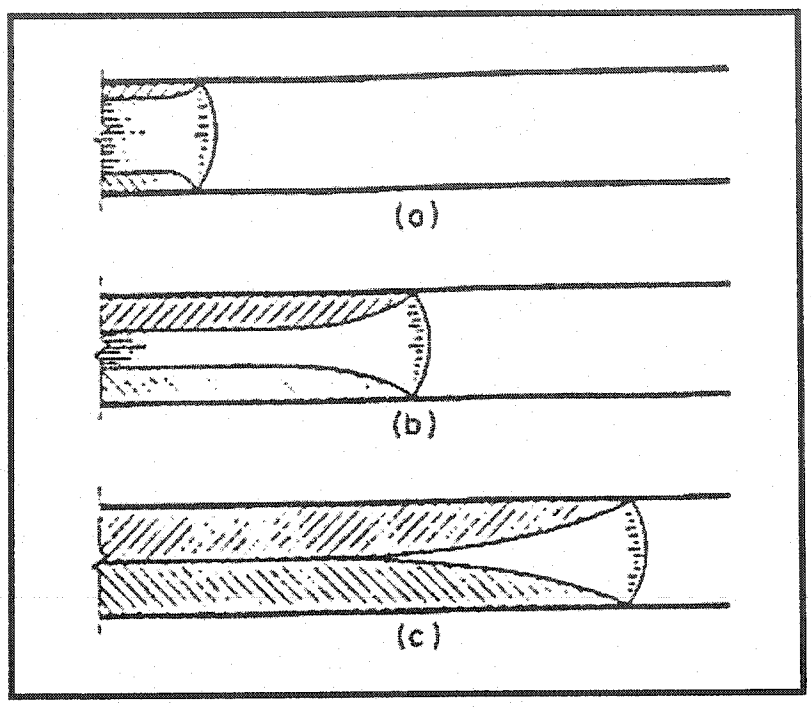

Figure 2.8 Flow Stoppage of a Pure Metal in a Fluidity Channel.[20]
a) Liquid Metal Enters the Channel and Solidification Begins Immediately
b) Solid Continues to Grow as Metal Flow.
c) Flow Stoppage Occurs as a Result of 'Choking' at the Channel Entrance.

2.4.2 Hypoeutectic and Eutectic Alloys

According to literature, [5,22] a well developed Al dendrite skeleton grows from the mold walls to the center of the spiral channel at both the entrance and the mid section of the spiral casting, an indication of progressive solidification. The progressive solidification mode keeps the flow channel open at the center and allows the melt to flow with less resistance Thus, results in enhanced fluidity. Therefore, metal flow stoppage occurs at the tip (end of the casting), when the degree of sluggishness becomes high

enough to cause flow stoppage. The fluidity in hypoeutectic and eutectic composition is mainly governed by degree of melt sluggishness at the flow tip.

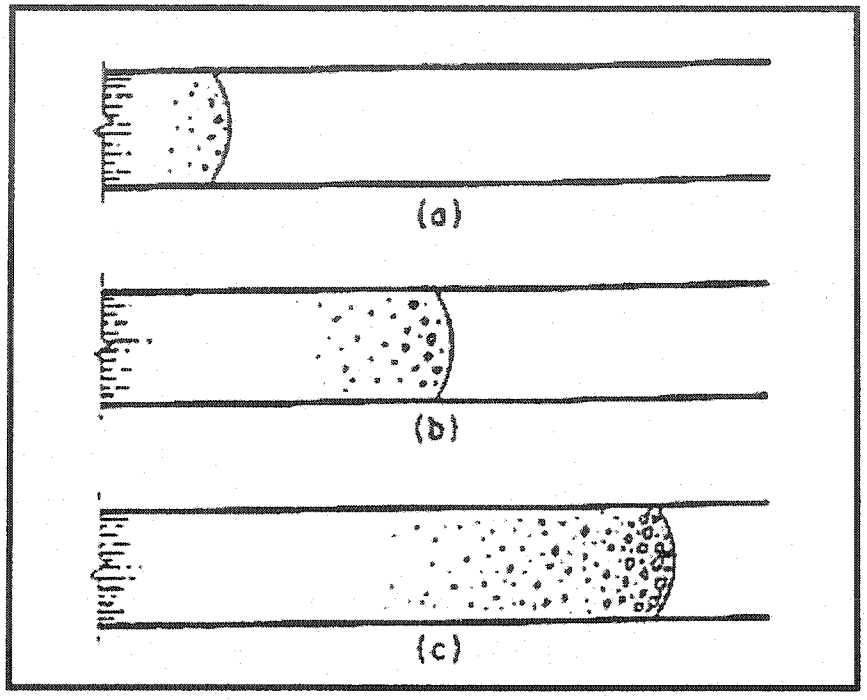

Figure 2.9 Flow Stoppage for Hypoeutectic and Eutectic Alloys.[20]
a) Liquid enters flow channel and fine grains nucleate at tip.
b) Nucleation continues and fine grains grow rapidly as flow progresses.
c) Flow ceases when a critical concentration of solid is reached near the tip.

2.4.3 Hypereutectic Alloys

In Figure 2.10, two distinct zones can be observed at the flow tip: a PSC depleted zone at the very end of the tip (zone 1), and a PSC rich zone (zone 2) immediately behind zone 1. The concentration of the PSC in zone 2 increases as Si content increases. This distinctive morphology is most likely because the PSC that formed do not adhere to the mold walls and can be carried downstream by the flowing metal. These drifting PSC then accumulate at the flow tip and gradually increase the sluggishness of the melt, and finally

the metal flow ceases. However, before the flow completely stops, a small amount of melt would penetrate the opening between the PSC and would form a PSC zone at the very tip of the spiral. Flemings et.al.[7] studied this mechanism in detail. According to them, the value of the critical solid fraction governs the fluidity of the alloy. The higher the critical solid fraction value of an alloy, the better is the fluidity.

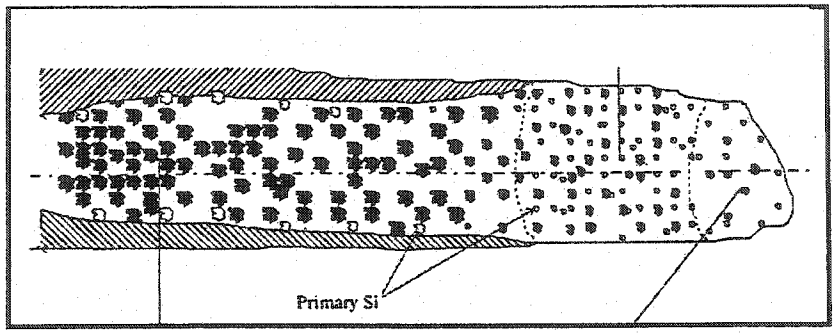

Figure 2.10 Flow Tip for Hypereutectic Al-Si Alloy.[5]

Lost Foam Casting (LFC) provides unique advantages over other conventional casting processes like Sand casting or Die Casting in case of hypereutectic Al-Si alloys.

2.5 LOST FOAM CASTING

Section Summary

Lost Foam Casting is a relatively new casting process for producing near net shape castings. Unique mold filling mechanism of LFC through endothermic degradation of foam has a strong effect on the fluidity and microstructure of an alloy. Lamellar flow of the advancing metal front in LFC unlike turbulent flow in other casting processes has a particular significance in this research.

2.5.1 The Process

The Lost Foam Casting (LFC) or Expendable Pattern Casting (EPC) process was first invented and patented by Shroyer[8] in 1958. While bonded sand was used initially, the process was subsequently improved to use dry unbonded sand. Interest in the LFC process within the foundry industry has increased significantly since the early 1980s. Currently, the LFC process is regarded as a viable alternative to the conventional casting processes for the production of near net shape castings. The process has been applied successfully in making aluminum, brass, bronze, cast iron and steel castings. The LFC process allows the designer flexibility and opportunity that is not possible with conventional casting processes. The primary advantages of this process are the elimination of cores and parting line, improved accuracy and a practical replacement for bonded sand. The process is explained in detail in Sections 3.2.1 to 3.2.4.

2.5.2 Filling Mechanism of LFC

In metal casting, it is necessary to ensure uniform mold filling of the cavity with minimum turbulence at a constant filling rate and this is controlled mainly by the gating system. There are rules to predict the filling time for conventional casting.[9] However, the conventional rules for empty mold casting do not apply to LFC. In empty mold casting, the cross section area of sprue, runner and gate determine the filling time of the mold. In LFC, the fused foam, liquid and gases from the styrene exert a backpressure on the advancing liquid metal. The unique mold filling mechanism in LFC causes lamellar flow unlike turbulent flow in other conventional casting processes. Figure 2.11 represents the schematic shape of a molten metal front.

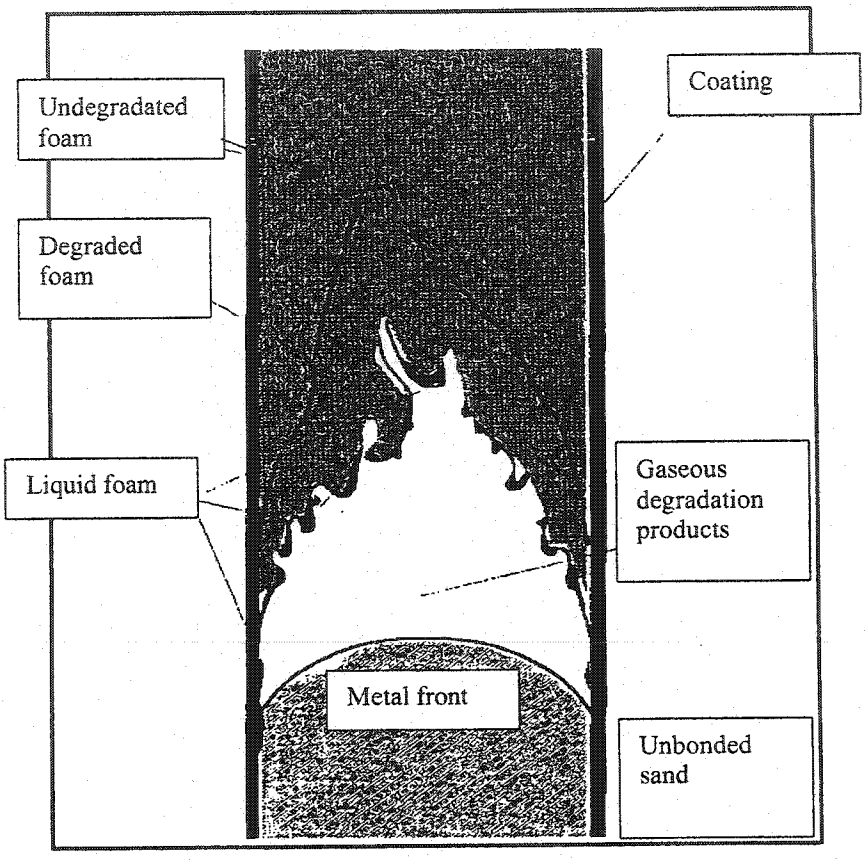

Figure 2.11: Molten Metal Front in LFC.[39]

When molten metal is poured on the foam, the advancing metal front melts and partially vaporizes the polystyrene. The small gap between the molten metal front and foam is filled with a mixture of gases (mostly styrene monomer) and liquid styrene. The gases quickly escape through the permeable coating and the liquid may be absorbed into the coating or may form a thin liquid residue between the casting and the coating. This liquid residue causes the coating to blacken and often leaves a layer of carbon between the casting and the coating. The amount of liquid and gases produced by ablation of foam depends on the molten metal filling temperature and the foam density.[10] For example, with aluminum casting at 750°C the total volume of gases is 40 cm^3 per gram of foam.[23]

It was observed that[10] the gas layer of the molten metal front is essentially negligible when expandable polystyrene (EPS) is used during casting and the molten metal at the moving boundary is almost in direct contact with the polymer at most

locations. Thus, gases formed at the molten metal front are diffused into the sand almost instantly. In the case of polymetheyl methacrylate (PMMA), the gas layer observed in the molten metal front is reported to be as large as 2cm[10] and the amount of gases during the degradation of PMMA is greater than that of EPS.

Thus, fluidity in LFC is controlled primarily by the endothermic polymeric degradation at the metal front and the effective escape of the decomposition products. Also the flow velocity in the lost foam processes is significantly lower than in empty cavity casting processes.[11] Walling and Dantzig[9] have found that the filling rate of the Al in EPC mold was approximately 40-80 mm/sec.

Literature review revealed that for commercial application of hypereutectic Al-Si alloys, Die-casting is the most commonly used process.

2.5.3 Comparison of LFC With Die Casting Process (Commonly Used Process for Hypereutectic Al-Si Alloys)

The main reason behind using Die Casting process for commercial application is its ability to reduce the long freezing range by inherent mold chilling[24] Figure 2.12 is a typical Die Casting machine.

Die Casting Process:

In Die Casting, molten metal is injected into dies and then cooled to form parts. The parts are removed from the dies and machined into their final form.

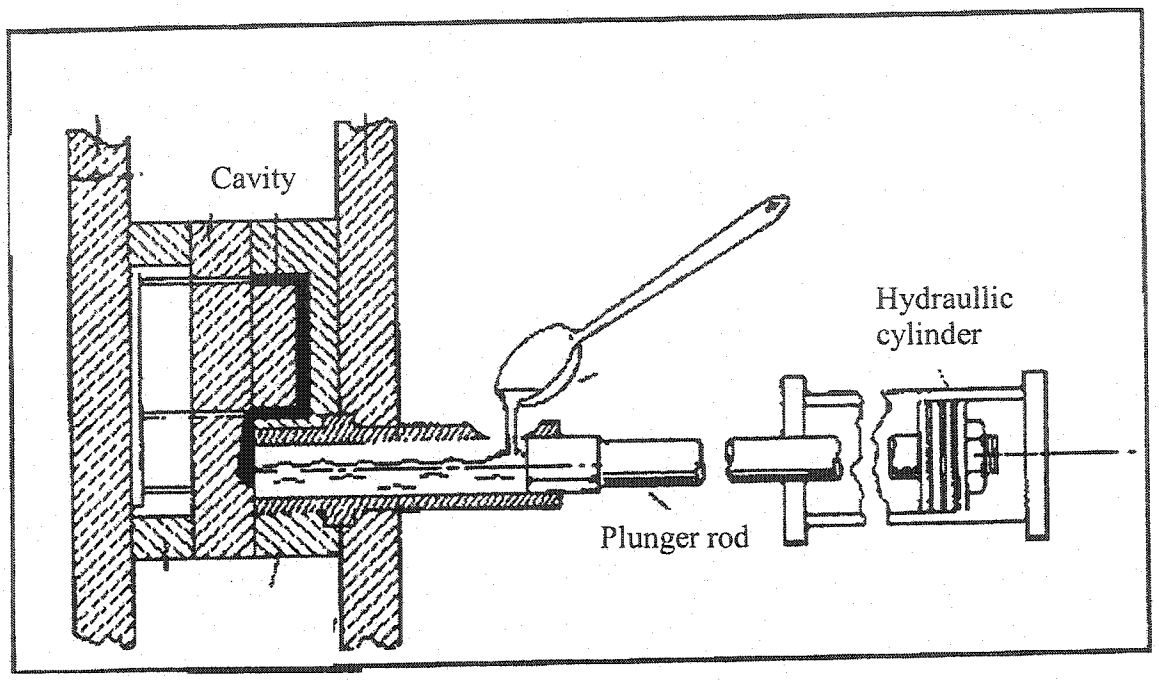

Figure 2.12 Die Casting Process.[24]

Advantages of the Die Casting process

1) Good fluidity: Metal is forced in dies with a very high velocity (typically 30-100 m/s). Thus metal fills all the intricate details of casting.[24]
2) Reduced freezing range: This process has a very high cooling rate due to its inherent mold chilling ability.
3) Good surface finish: Metal mold dies provide good surface finish.
4) High yield: Application of pressure during metal filling avoids gating and risering in mold design.

Although the Die Casting process has several benefits it may not be the first choice for the processing of hypereutectic Al-Si alloys.

Disadvantages of Die Casting process

1) Non-uniform distribution of properties: Die Casting process has a turbulent mold filling mechanism[25] due to high metal velocity (30-100 m/sec) and high pressure (200-800 bar). Turbulent mold filling causes variation in local solidification condition. This results in inhomogeneous grain size in microstructure and hence nonuniform distribution of mechanical properties in casting.
2) Porosity defect: If the metal flow is not controlled precisely it can create defects in the casting. Most flow related casting defects are caused by either trapped gas or premature solidification. Ideally, the liquid metal should displace the cavity gas ahead of the flow front as the cavity fills. As the pressure builds, some of the gas escapes through the vents. But if the advancing metal seals the vents before all the gas escapes, the casting contains gas porosity.
3) Shrinkage defect: High rate of cooling in Die Casting decrease dendritic coherency point.[26] Dendrite coherency point is the point at which dendrites start to impinge on one another and dendrite network becomes coherent. At this point the system behaves less as a liquid and begins to resemble a solid. If the dendritic coherency point occurs before the mold fills completely, the dendrites interlock with each other and resist the flow of metal, thus result in interdendritic shrinkage as shown in Figure 2.13.

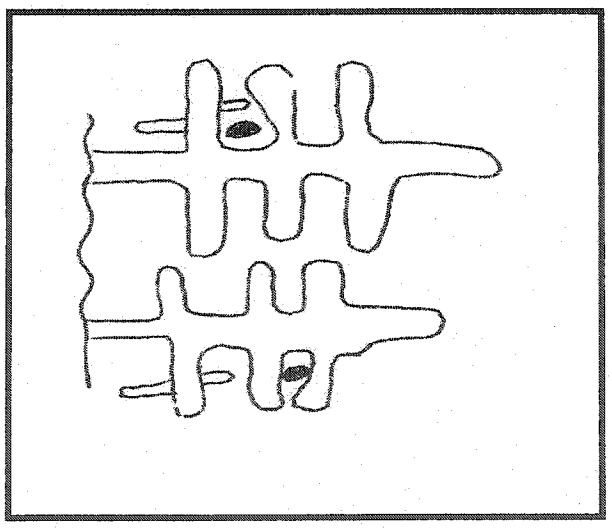

Figure 2.13 Interdendritic Shrinkage Due to Dendritic Coherency in Die Casting.

Similarities between LFC and Die Casting process:

1) Good surface finish: Mainly a result of the application of refractory coating material on foam pattern.
2) High yield: Near net shape casting ability hence no need for gating and risering.
3) Reduced freezing range: LFC is an endothermic process. Decomposition gas products of foam take out heat of molten metal during solidification.

Advantages of LFC over Die casting process:

1) Lamellar flow of metal: Due to its unique mold filling mechanism (refer to Section 2.5.2). LFC has a lamellar flow mechanism unlike turbulent flow in die-casting, thus resulting smooth distribution of properties in microstructure.
2) Porosity: Literature[27,28] mentioned that LFC has 20-30% less porosity as compared to Die Casting. Gases can easily escape through unbonded sand, surrounding foam pattern, thus resulting less porosity.
3) Less shrinkage defects: Rate of cooling is not as high as Die Casting, hence less probability of interdendritic shrinkage.

2.6 FRACTION OF SOLID AND FIRST DERIVATIVE CURVES

Section Summary

Fractions of solid ($\%f_s$) and first derivative curves are described in this section. During solidification of hypereutectic Al-Si alloys, PSC nucleate and release latent heat. Determination of $\%f_s$ is an important step in the correlation of interlocking and melt sluggishness of precipitated particles (e.g. PSC, $CuAl_2$ etc.) with the fluidity of an alloy.

2.6.1 First Derivative Curve

First derivative at each point of the cooling curve is numerically equal to the slope of the cooling curve. Increase in derivative indicates decrease in cooling rate during

solidification. Usually, the decrease in cooling rate is caused by the appearance of a new phase and relates to the release of latent heat. First derivative curves can be used to predict the amount of phase precipitation during solidification as well as to determine the time of complete solidification. In this thesis, the first derivative curves were used for fraction of solid calculations and to observe the variations in phase precipitation for various alloy compositions.

Figure 2.15 is an ideal first derivative curve of cooling curve shown in Figure 2.14. As shown in Figure 2.14, Δt is the difference in time between the liquidus and the end of solidification. At the beginning of the first derivative curve, the melt is liquid. At point 1 of the curve, there is a sharp deviation from the zero curve (refer Section 2.6.2). Zero curve is shown by dotted line in Figure 2.15. This rapid heat release is caused by the sudden nucleation of Al grains in the sample. With time, the rate of nucleation subsides and frontal growth of Al dendrites occurs into the center from slightly cooler mold walls (region 2). After some time, the dendrites fill the casting, and further growth of dendrites can only occur laterally. (region 3). The curve is still above the zero curve. This indicates that latent heat is being released by the continuing growth of Al crystals. At point 4 there is another rapid increase in the derivative, which corresponds to the nucleation of PSC. The growth of Si continues in region 5 of the curve. Finally, at point 6, the Mg_2Si phase appears. The appearance of this is not noticeable in the cooling curve, but it is quite marked in the first derivative curve.

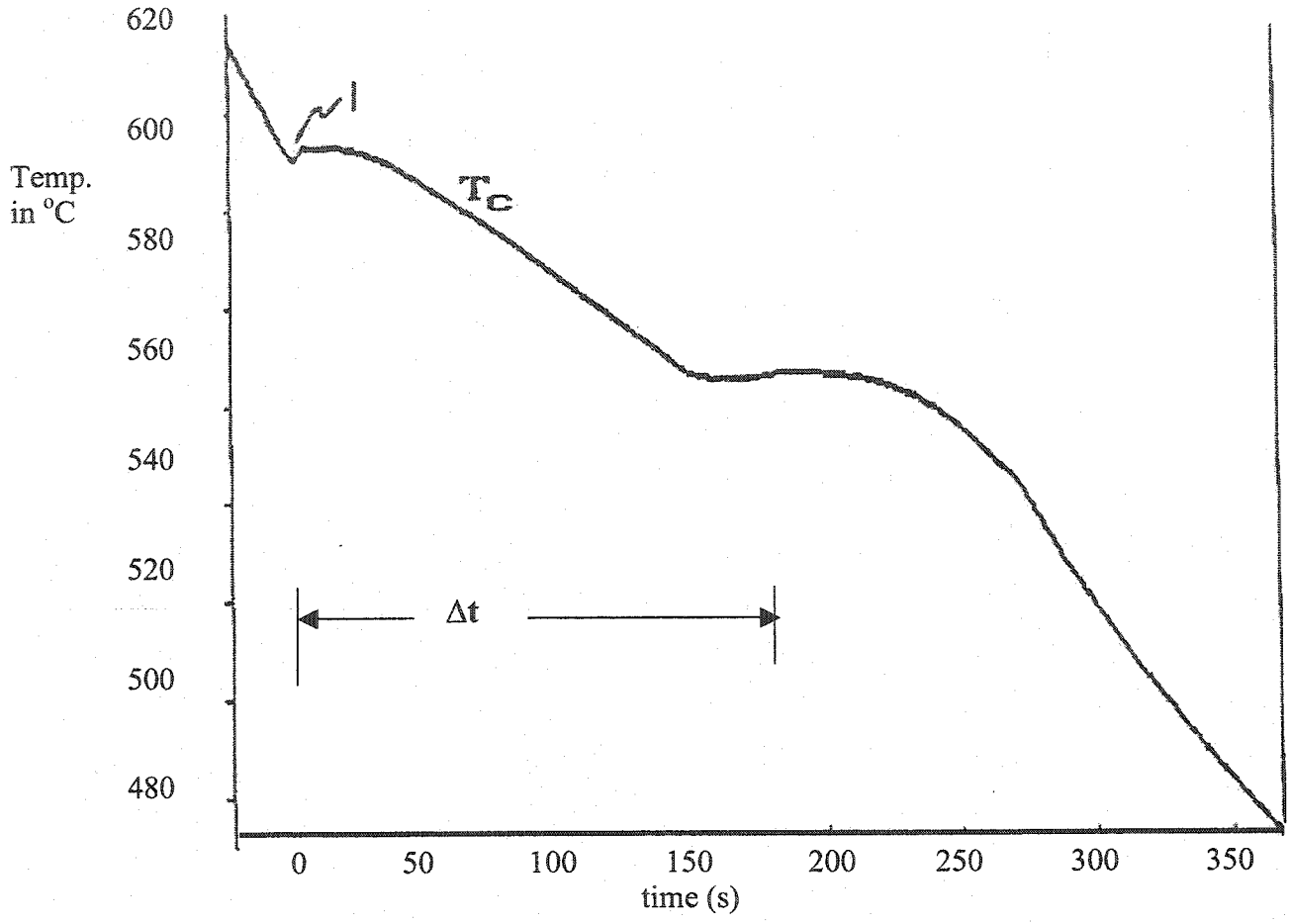

Figure 2.14 Cooling Curve for A356 Alloy.[29]

2.6.2 Zero Curve (Null / Baseline curve)

This curve mathematically represents the cooling curve without phase(s) precipitation and transformation. Generally this curve is a straight line that joins start of the solidification and end of the solidification (complete solidification) as shown by the dotted line in Figure 2.15.

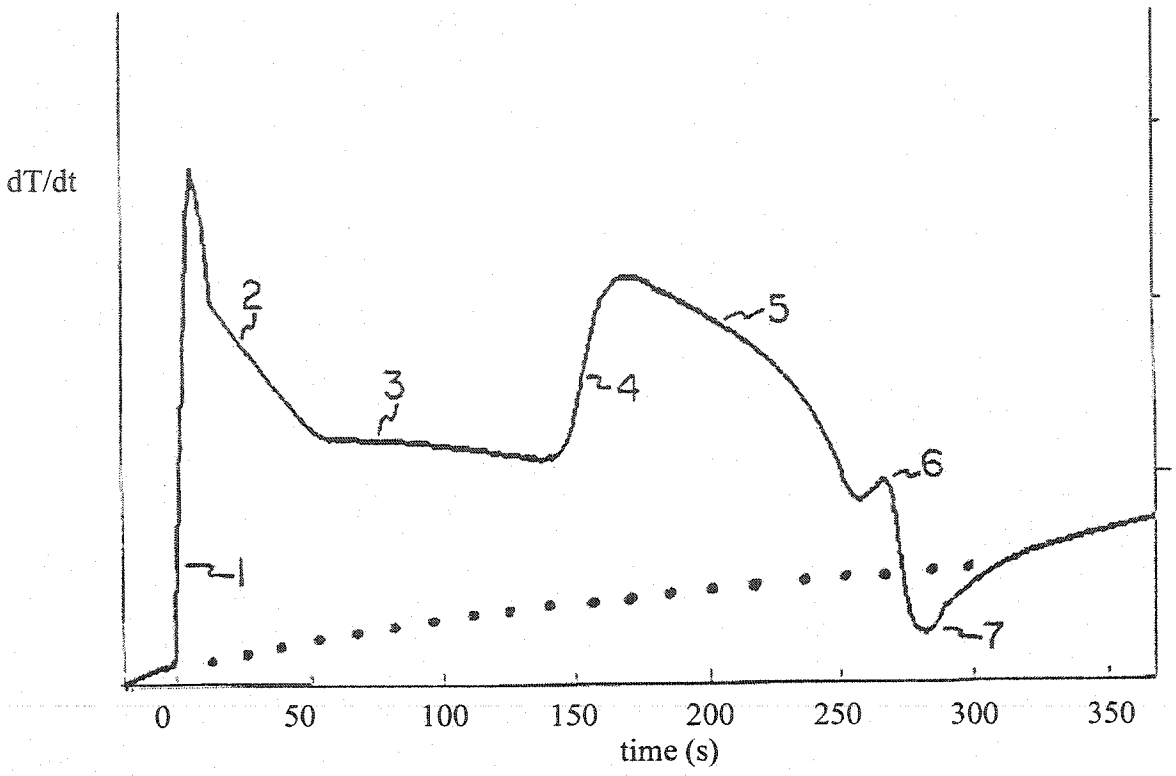

Figure 2.15 First Derivative Curve for A356 Alloy.[29]

2.6.3 Fraction of Solid

Fraction of solid ($\%f_s$) may be defined as the percentage of solid phase(s) that precipitates between liquidus and solidus temperature in a solidifying melt. Calculation of fraction of solid can be used to predict fluidity and microstructure of the casting. It can also be useful in understanding flow stoppage and interlocking mechanism. Literature suggests several methods to calculate the fraction of solid.

2.6.4 Pan and Hu' s Approach for Fraction of Solid

Pan and Hu[5] calculated the fraction of solid at the instant of flow stoppage. According to them, the time when the temperature reaches the peak corresponds to the instant of flow stoppage.

The solidification cooling curve is obtained at the thermocouple where the temperature peak is higher than that of any other thermocouple. (Thus in case of a spiral pattern, the thermocouple at the entrance should provide a reference curve for deriving the fraction of solid vs. time curve). In the present study, the temperature peak was observed at the bottom end of the 24 mm thickness casting bar.

The procedure for the determination of the fraction of solid at the instant of flow stoppage at any specific thermocouple location is as follows.

First, determine the duration (Δt) between the time of flow stoppage and the time of complete solidification from the cooling curve. The time of flow stoppage has already been discussed in the first paragraph of this section. The time of complete solidification can be obtained from the first derivative curve as explained in Section 2.6.2.

Second, determine the instant of flow stoppage (t_s) in the diagram of the $\%f_s$ vs. time (Figure 2.16) by backing a time period of Δt from the end of solidification t_f. Third, draw a vertical line from t_s (the time of flow stoppage) that will intersect the $\%f_s$ vs. time curve at point P. Finally, from point P, draw a horizontal line to obtain the fraction of solid ($\%f_{s\,(p)}$) value for that specific instant (t_s).

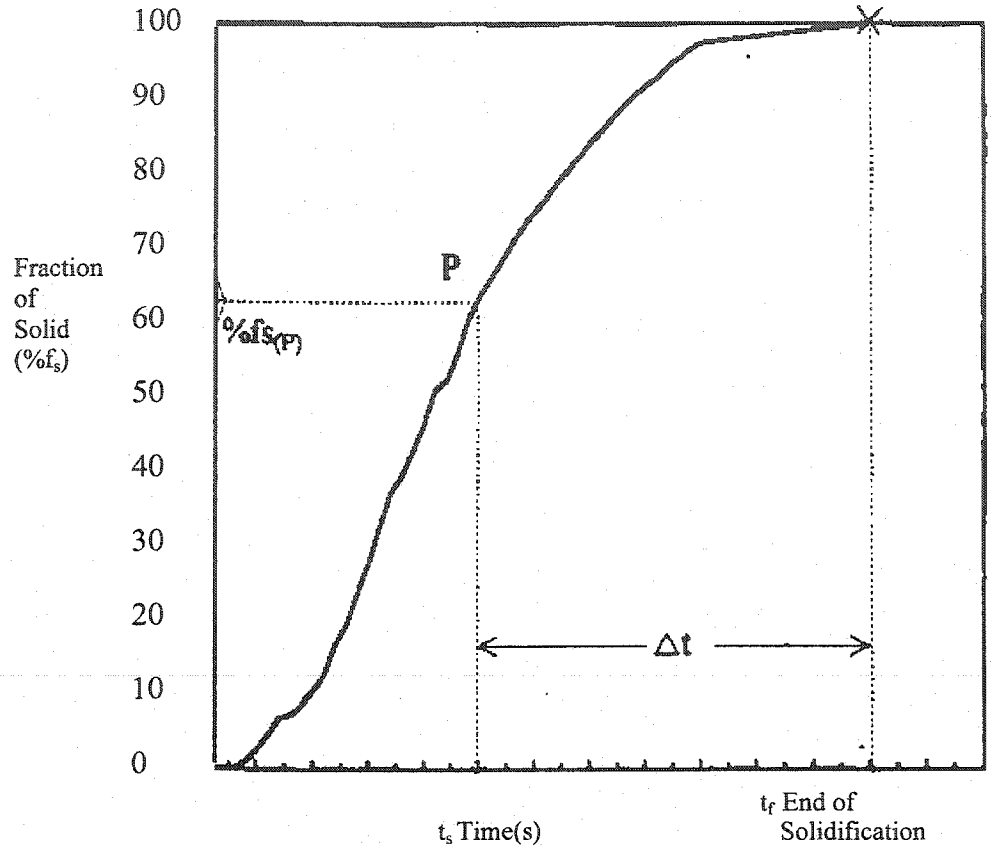

Figure 2.16 Procedure for Determining Fraction of Solid at the Instant of Flow Stoppage.[5]

2.6.5 Some Other Methods to Calculate the Fraction of Solid

The literature[30,47,48] presents several other methods for determining the fraction of solid. These include the following,

1) Quantitative Metallography[47]:

An image analysis can be used to measure the fraction of solid. This technique requires the use of small samples that have rapid cooling rates, in order to preserve the structure present at a given temperature.

2) Linear[47]:

$$\%f_S \equiv \frac{T_{LIQ} - T}{T_{LIQ} - T_{SOL}} \tag{2.5}$$

Where,

T_{LIQ} Liquidus temperature, °C

T_{SOL} Solidus temperature, °C

T Instantaneous temperature, °C

In this model, Latent heat is assumed to vary linearly between liquidus and solidus temperature.

3) Lever Rule[47]:

$$\%f_S = \frac{1}{1-k}\frac{T_{LIQ} - T}{T_m - T} \text{ where, } k = \frac{T_m - T_{LIQ}}{T_m - T_{SOL}} \tag{2.6}$$

Where,

k Distribution coefficient of binary alloys.

T_m Melting temperature of pure Al, °C

Very slow solidification rate is assumed in this model.

4) Scheil's Equation[47]:

$$\%f_S = 1 - [\frac{T_m - T}{T_m - T_{LIQ}}]^{\frac{1}{k-1}} \tag{2.7}$$

This model assumes that no solute diffusion occurs in the solid phase and liquid is perfectly homogeneous.

5) Grain Nucleation[47]:

$$\%f_S = 1 - \exp(\frac{4}{3}\pi R^3 N) \tag{2.8}$$

Where,

R Average grain radius, cm

N Average grain density, cm^{-3}

This model assumes that the shape of the grains is spherical.

6) Heat Balance[30]:

$$\%f_S = \frac{\int_0^t [(\frac{dT}{dt})_{cc} - (\frac{dT}{dt})_{zc}]dt}{\int_0^{ts} [(\frac{dT}{dt})_{cc} - (\frac{dT}{dt})_{zc}]dt} = \frac{c_L}{L}\int_0^t [(\frac{dT}{dt})_{cc} - (\frac{dT}{dt})_{zc}]dt \tag{2.9}$$

Where,

C_L Specific heat of an alloy, J/g °C

L Latent heat of solidification, J/g

dT/ dt First derivative

t End of solidification, s

t_s Instantaneous temperature, s

cc cooling curve

zc zero curve

CHAPTER 3

EXPERIMENTAL PROCEDURE

Chapter Summary

The experimental procedure consists of four parts. The first section describes pattern making and casting for an assembly of patterns of four different thicknesses by changing process parameters (composition, gating system, superheat). The second section describes procedure for thermal analysis (cooling rate and velocity calculations). The third section explains procedure for image analysis (size and distribution measurement of PSC) and the final section focuses on plotting of first derivative curve and fraction of solid calculations. Block diagram of experimental trials is included in Section 3.1.

3.1 BLOCK DIAGRAM/OUTLINE OF THE THESIS:

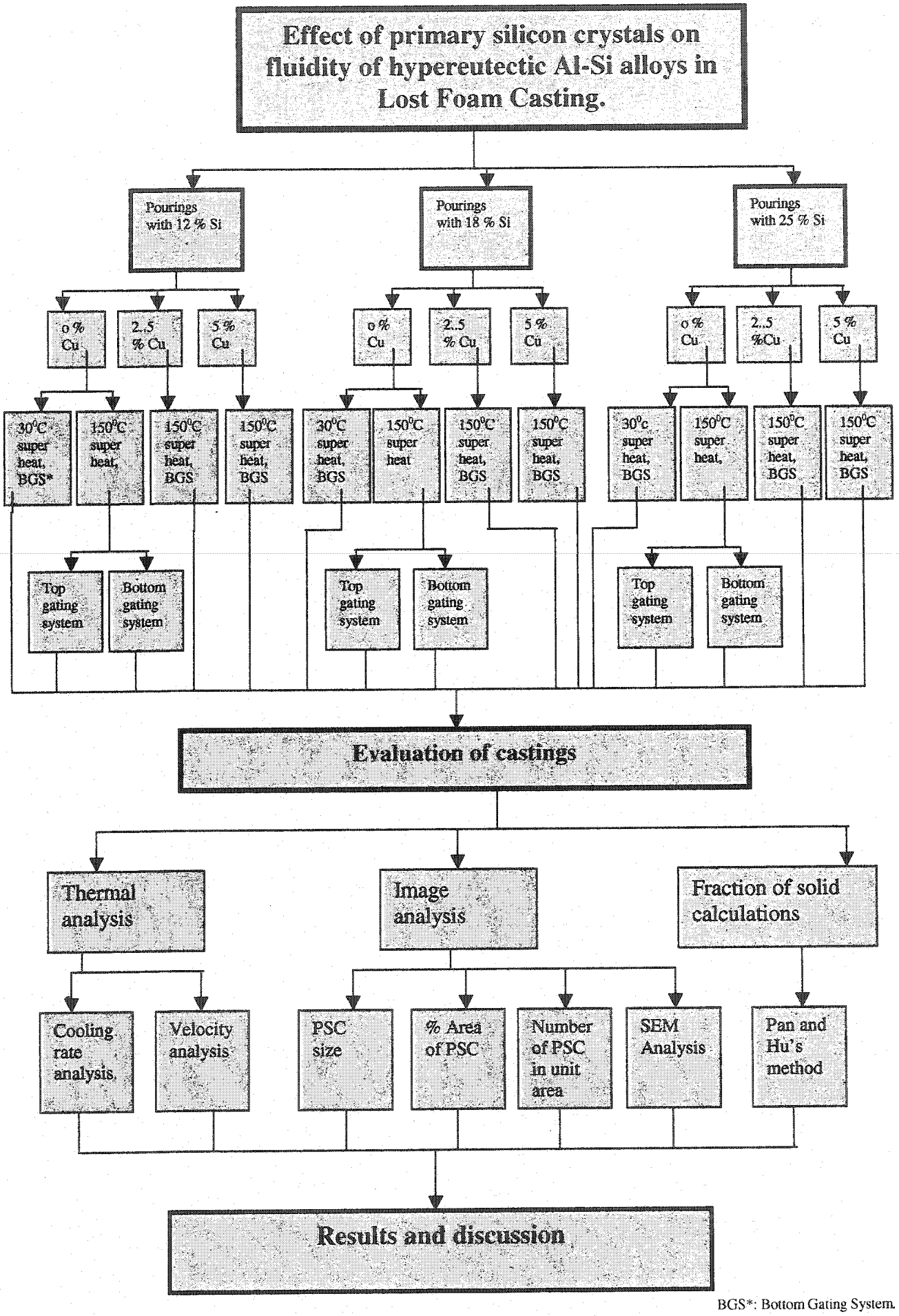

BGS*: Bottom Gating System.

3.2 PATTERN MAKING, MELTING AND POURING

Section Summary

This section covers preparation of foam patterns (designing, cutting, gluing, coating and drying), temperature and composition control, melting procedure for two different furnaces (gas fired and electric resistance) and reduced pressure test (RPT) to control the porosity.

3.2.1 Pattern Making

Expandable Polystyrene (EPC) foam slabs, 1.6 pcf (0.026 g/cm^3) in density were supplied by Foseco-Morval Inc. Rectangular plate patterns of foam, 130 mm long and 35 mm wide were cut to various thicknesses of 6,12,18 and 24 mm. A hot wire was used to cut the foam material (accuracy ± 2mm) and to prepare the pattern assembly.

The gating system consisted of a sprue [185 mm (height) x 35 mm (width) x 35 mm (thickness)], a runner [10 mm (length) x 35 mm (width) x 30 mm (thickness)] and a pouring cup [85 mm (length) x 35 mm (width) x 35 mm (thickness)]. The dimensions of the pattern are shown in figure 3.1. Attempts were made to maintain the standard gating ratio as suggested by Dwyer[31]. Care was taken during foam cutting to minimize adhesive joints because glue increases products of decomposition and can retard metal flow. Four bars of different thickness (6,12,18 and 24 mm) were attached to the gating system with a hot melt adhesive (supplied by Grow Glue Inc.) to form the final cluster with bottom or top gating system (Figures 3.2 and 3.3). The pattern assemblies were then coated with a ceramic slurry (refractory coating) and dried.

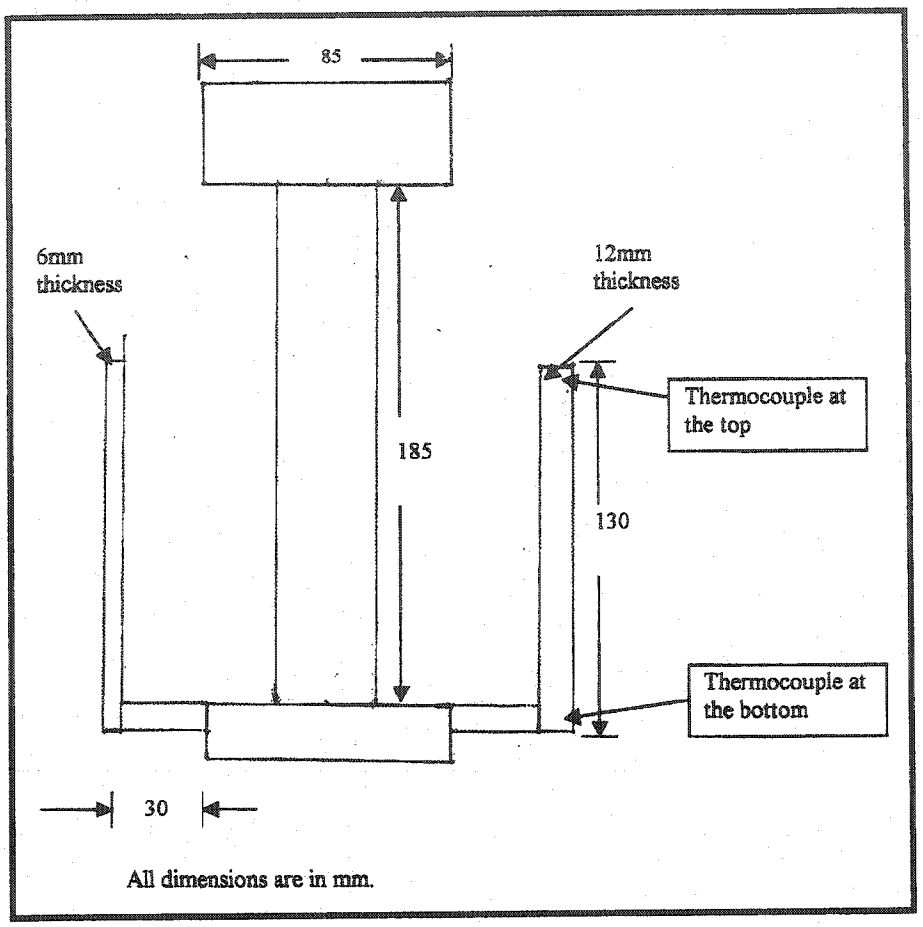

Figure 3.1 Pattern Geometry.

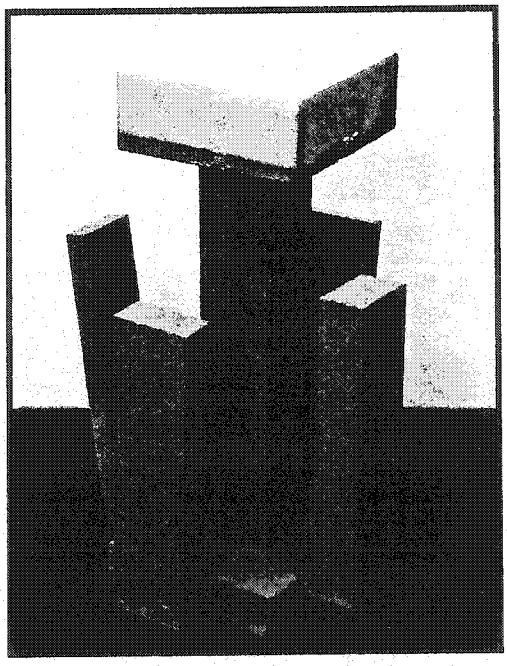

Figure 3.2 Bottom Gating System.

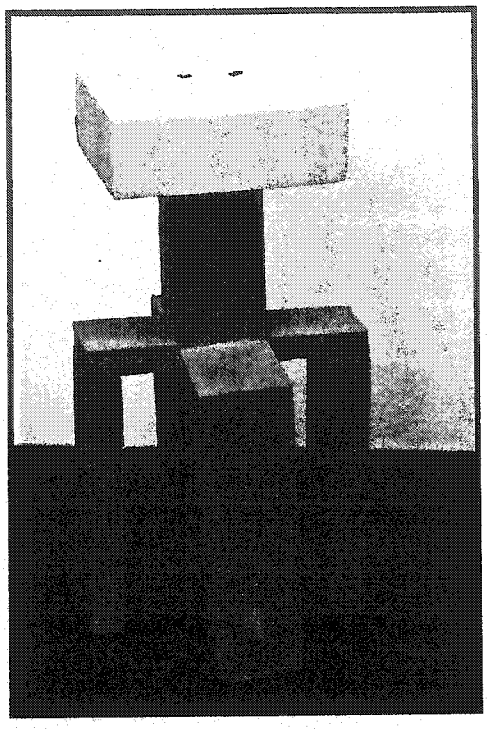

Figure 3.3 Top Gating System.

3.2.2 Pattern Coating and Drying

The refractory coating used for these experiments is Thiem Pink Styrokote 145.3. It is an alumina–water based refractory. This refractory coating mainly serves following purposes:

1) The insulating characteristic of the coating reduces heat transfer from the liquid metal to the sand mold, thereby increases the flow length of the casting.
2) It effectively allows pyrolysis products of degradation (gaseous and liquid) to escape into the surrounding sand and thus decreases the porosity.
3) It avoids direct contact of foam pattern with mold (sand) resulting in improved surface finish.

The refractory coating was adjusted to 40-45 baume by adding water into the slurry and mixing for about 15 minutes in the laboratory mixer (Figure 3.4). Coating can either be applied on pattern by brushing or by dipping. In these experiments, dipping was

preferred for its simplicity and uniformity of coating. The foam cluster was dipped in the refractory slurry and was shaken to drip dry. The coated cluster was then placed in a temperature controlled drying oven. Two variable speed fans enabled circulation of air in the oven. The temperature in the oven was set at 60°C. The cluster was left to dry for almost 8 hours. The thermocouples were inserted in dried and coated pattern for time-temperature data collection.

3.2.3 Temperature Measurement

Thermocouple wires (k-Type, 26 gauge) were inserted into the ceramic insulator tube. The positive and negative ends of two wires were welded to form the couple and the thermocouple tip was inspected for proper weld. They were tested at 100°C in boiling water to determine their temperature measurement accuracy. Finally, the thermocouples were inserted at the bottom and top end of the pattern as shown in Figure 3.1. Thus, the temperatures were measured at the start and at the end of the casting bar. The thermocouples were then connected to a data acquisition system. This system made it possible to record temperature to an accuracy of ± 2°C at eight locations (4 x 2) of the pattern assembly at 0.1 second intervals. This data acquisition system can be used to record temperature at 16 locations at the same time. The pattern assembly was placed in a steel bucket partially filled with silica sand as the mold material.

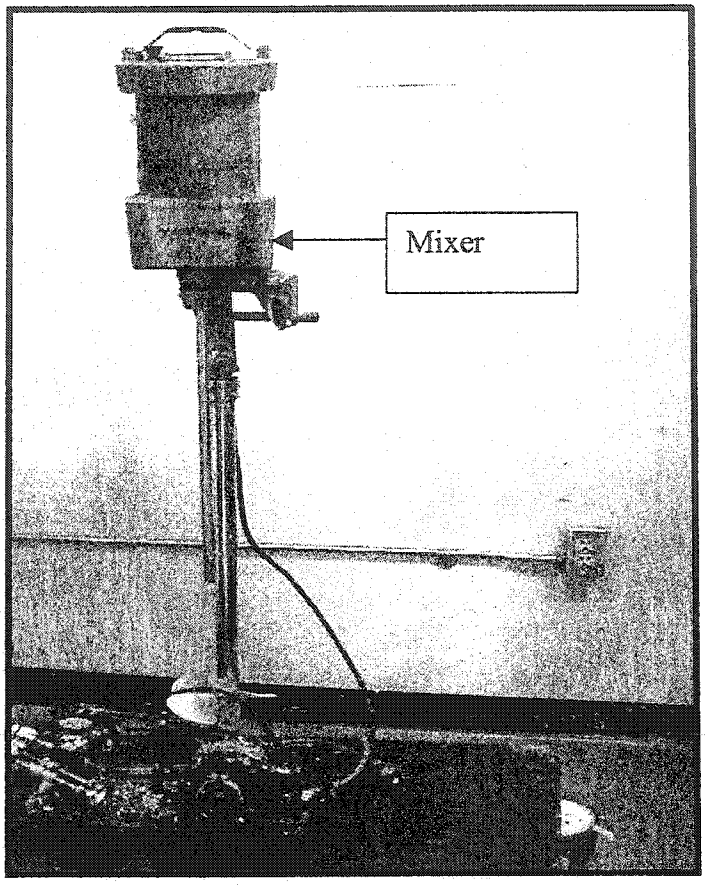

Figure 3.4 Laboratory Mixer for Refractory Coating.

3.2.4 Vibration

The unbonded silica sand (AFS-GFN 35-40) was rained into the steel bucket to surround the pattern assembly. A vibrating table (Figure 3.5) was used to compact the sand in the bucket at 1.2g for 40-50 seconds following the procedure developed by Ravindran et.al.[32] Because the orientation of the pattern assembly was vertical, the vibration was horizontal rather than vertical to prevent mold collapse. After vibration the steel bucket was lifted by using an overheat hoist and placed near melting and pouring station.

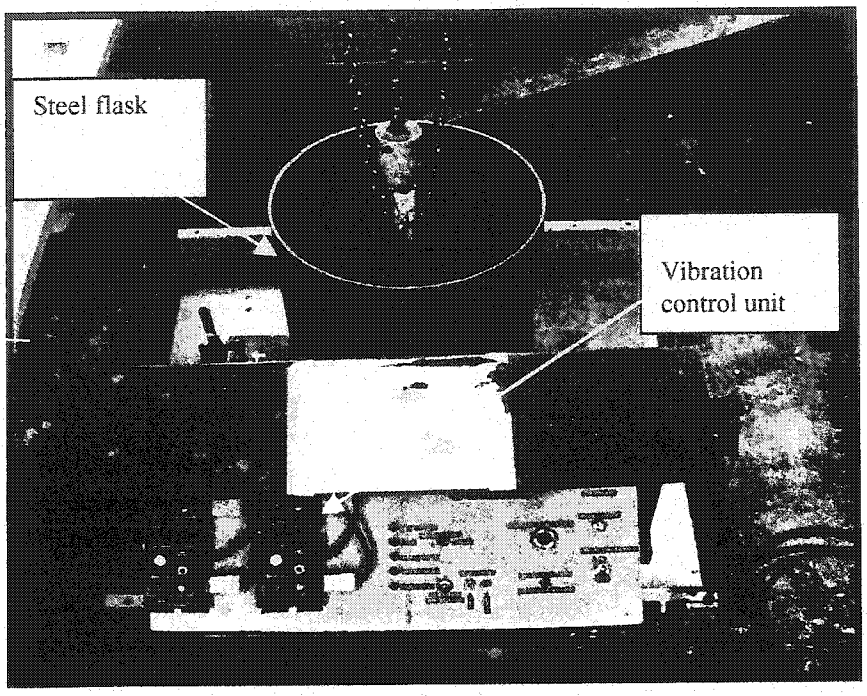

Figure 3.5: Vibration Table

3.2.5 Melting Procedure

The melting procedure was carried out at two different superheats.

1. 30°C superheat: Speedy melt model B-300 gas fired furnace with a graphite crucible (Figure 3.6) was used for melting.
2. 150°C superheat: Electric resistance furnace with protective atmosphere (Figure 3.7) was used.

The reason for using two furnaces is explained in the next paragraph.

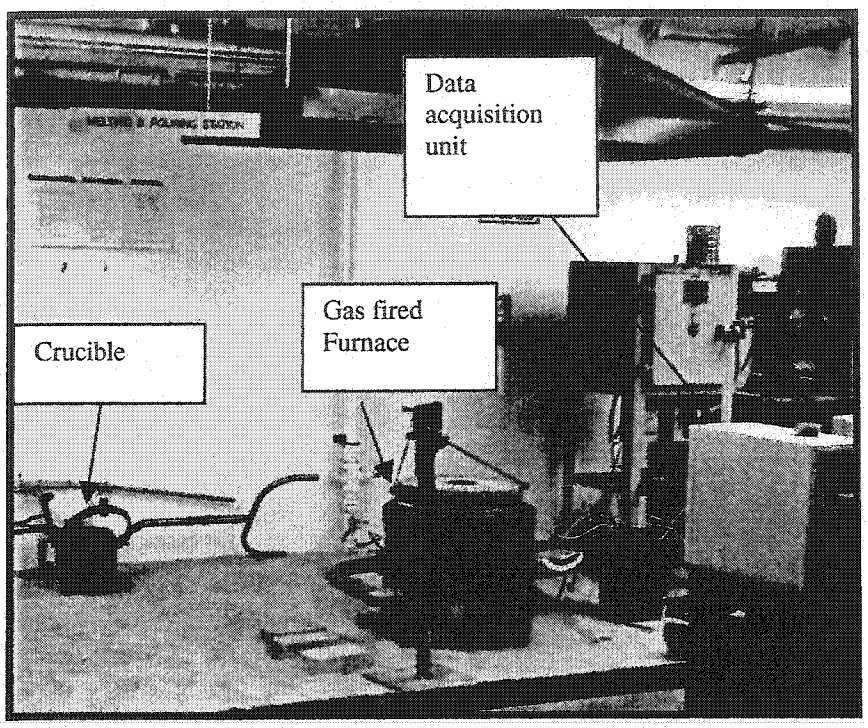

Figure 3.6 Gas Fired Furnace

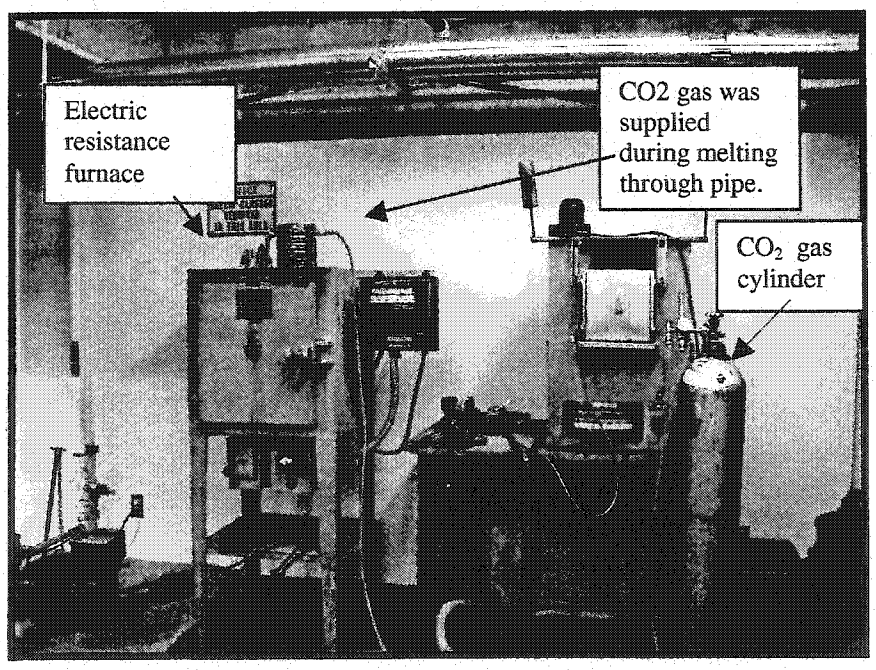

Figure 3.7 Electric Resistance Furnace

The solubility of hydrogen in the Al alloy increases significantly above 780°C. The liquidus temperature for 25% Si is in the range 770-790°C (Table 3.1). The 150°C superheat effectively increases the pouring temperature to the 920-940°C range. At such a high pouring temperature the tablet degassing is ineffective (degassing is discussed in detail in section 3.2.10) and may result in large amount of porosity. Hence an innovative technique was developed to avoid hydrogen contamination at high temperature using an electric resistance furnace. CO_2 gas was supplied during melting inside the furnace chamber through pipe. CO_2 gas is heavier than hydrogen gas and hence it remained at the top of molten metal throughout melting and avoided hydrogen contamination. Reduced Pressure Test (RPT) was used to control the porosity at an acceptable level in the castings (RPT is discussed in detail in Section 3.2.11).

The liquidus temperatures for known levels of Si and Cu were determined using the Al-Si-Cu ternary phase diagram (Figure 3.8). The liquidus temperatures for all the alloy compositions are tabulated in Table 3.1

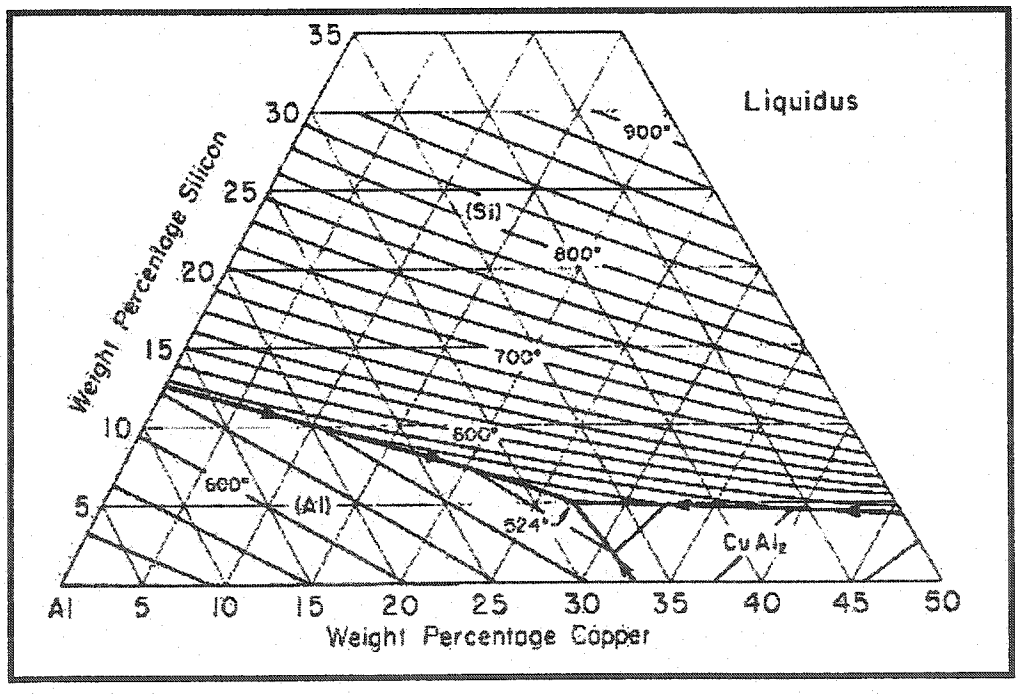

Figure 3.8 Al-Cu-Si Ternary Diagram for Determining the Liquidus Temperature.[19]

Table 3.1 Liquidus Temperature for Various Alloy Compositions.

Alloy composition		Liquidus temperature in °C
%Si content	% Cu content	
12	0	560
18	0	660
25	0	770
12	2.5	524
18	2.5	700
25	2.5	780
12	5	580
18	5	710
25	5	790

3.2.6 Composition Control

A356 alloy (Table 3.2) was used as the base metal. Predetermined quantities of Al-25% Si master alloy and Al-20% Cu master alloy were added to prepare experimental alloys of known composition (Table 3.1).

Table 3.2 Composition of A356 Alloy.[34]

Si	Cu	Fe	Mg	Mn	Ti	Zn	Ca	Sr	P	Al
7	0.01	0.10	0.38	0.01	0.09	0.09	0.0020	0.019	0.0004	Rem.

3.2.7 Casting Procedure

The procedure used for casting in the present study is listed in Table 3.3.

Table 3.3 Casting Procedure.

#	Action	Temp. °C
1	Preheat the furnace	-
2	Add the charge	-
3	Add the first part of flux	~ 600
4	Stop the furnace	PT * + 60
5	Add the second part of flux	PT + 60
6	Degassing	PT + 90
7	Remove crucible from furnace	PT + 40
8	Skimming	PT + 30
9	RPT test	PT + 20
10	Pouring	PT

PT*: Pouring Temperature.

A portable pyrometer with an adequate measurement range (0-1999°C) was used to monitor the melt temperature. Fluxing and degassing is discussed in Section 3.2.9 and 3.2.10. Grain refinement and eutectic Si modification were avoided during melting.

3.2.8 Grain Refinement and Modification

Modification alters morphology of the eutectic Si particles from a coarse flake like form to a fine fibrous one. Strontium (0.02-0.04%) and sodium (0.005-0.01%) are most commonly used modifier in case of Al-Si alloys. It was suggested[33] that modifying additions suppress the growth of PSC within the eutectic. Phosphorous grain refinement controls the size of PSC as discussed in Section 2.3.5. Both these treatments were

avoided during melting in order to isolate and study the effect of selected process parameters on the morphology of the PSC.

3.2.9 Fluxing

In Al alloy melting, oxide formation and nonmetallic impurities are common.[35] Impurities appear in the form of liquid and solid inclusions. Inclusions can originate from dirty tools, sand and other molding debris, sludge, metalworking lubricant residues, and the oxidation of alloying elements and/or the base metal. Fluxing is the technique to clean the melt containing such impurities and inclusions. Fluxing facilitates the agglomeration and separation of such undesirable constituents from the melt.

Pyrotek Canada, supplied the flux (Pyroflux N-20). Fluxing (0.1% of the total melt) was carried out in two parts. The first part of flux was added as soon as the metal melted and the second part was added after reaching the pouring temperature.

3.2.10 Degassing

Hydrogen is the only gas that is appreciably soluble in Al alloys and is the major contributor of porosity. Its solubility varies directly with temperature and the square root of pressure.[35] Several methods can be used to remove the dissolved hydrogen from the melt.

1. Gas purging or gas flushing
2. Tablet flux degassing
3. Mechanical mixer degassing

In the present study, degassing was carried out by submerging the degassing tablet (0.1% of the total melt) into the melt. Degasser was provided by Foseco Morval Inc. Tablet degassing using hexachloroethane (C_2Cl_6) is the most common method in foundry applications. The tablet decomposes in the Al melt to form gaseous $AlCl_3$. The rising $AlCl_3$ gas bubbles then collect hydrogen gas and deliver the gas to the melt surface for release.

Tablets were added when the melt temperature is still 60-70°C above required pouring temperature because tablet degassing was known to reduce the melt temperature by 40-50°C. The tablet was slowly plunged to the bottom of the melt with a dry, preheated bell plunger. Plunging was continued until there was no evolution of gas. The crucible was then taken out of furnace and the liquid metal was skimmed to remove any excess dross and slag. The data acquisition system for the pattern assembly was activated at this point. The metal was poured into the mold at a steady rate by manually controlling the constant metallostatic head. Before pouring the metal into the mold, the Reduced Pressure Test (RPT) was carried out.

3.2.11 Reduced Pressure Test (RPT)

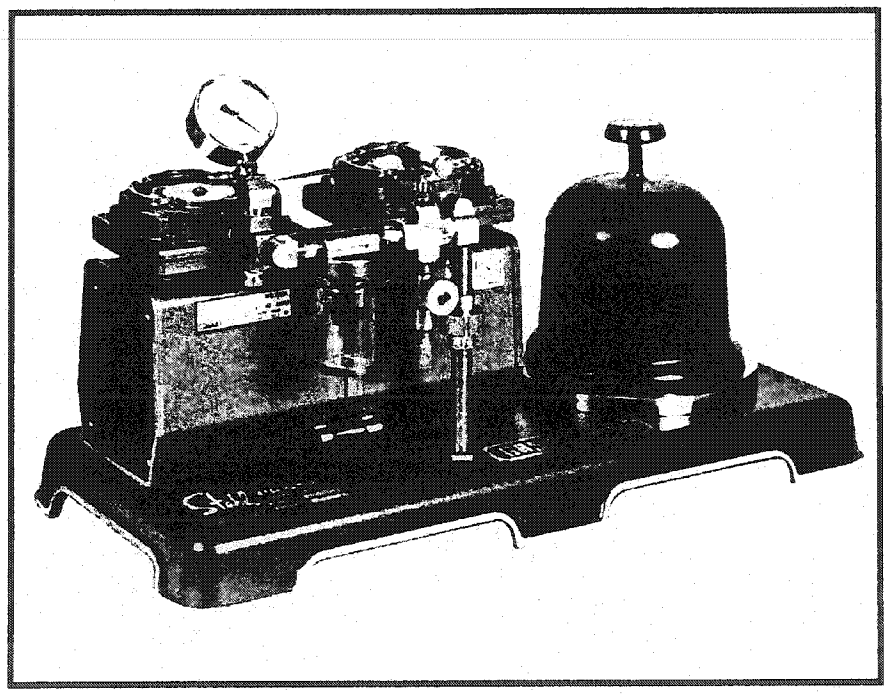

Figure 3.9 Gas-Tech Equipment for Reduced Pressure Test.[36]

Gas-Tech equipment was used for RPT (Figure 3.9). Gas-Tech equipment was located adjacent to metal being sampled. The molten metal was skimmed 2-3 times by small crucible, held in tongs to remove oxides and to preheat crucible prior to taking

sample. Then sample was taken by dipping crucible into molten metal. The crucible with sample was placed on refractory disc in vacuum chamber base plate and covered. Vacuum pump was started and held under reduced pressure for approximately 7 minutes. Vacuum was set at 26 inches of mercury. After 7 minutes, the vacuum pump was turned off; the pressure was released by depressing vacuum release button. The crucible was taken out and sample was removed. The sample was cooled under water. Then the sample was cut in half and polished on 120 grit abrasive papers. RPT exaggerates porosity in the casting thus avoiding the use of microscopy. This exaggerated porosity can be compared with the charts (Figure 3.10) provided by Gas-Tech to verify the acceptability of the porosity (thus determining the acceptability of the melt for pouring). The acceptability limit suggested by Gas-Tech was between picture number 0-6 as shown in Figure 3.10

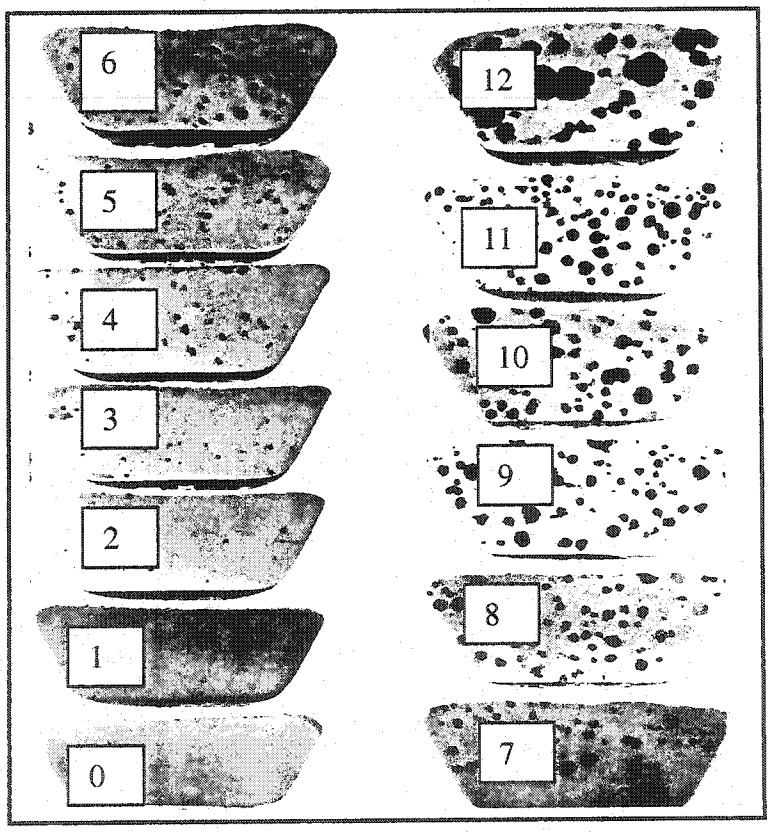

Figure 3.10 Porosity Chart.[36]

RPT test were carried out for gas fired furnace pourings as well as electric resistance furnace pourings. A significant amount of decrease in the porosity was observed by the use of 'atmosphere controlled' electric resistance furnace as can be seen in Figure 3.11 and 3.12.

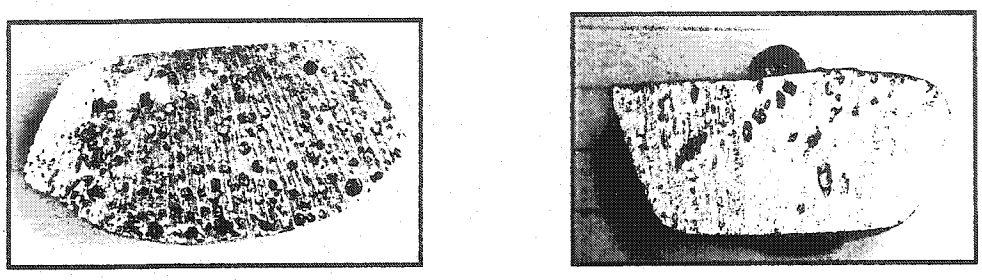

(A) (B)

Figure 3.11 Comparison of Porosity

(a): RPT Sample of the pouring at 920°C in gas fired furnace.

(b): RPT Sample of the pouring at 920°C in electric resistance furnace.

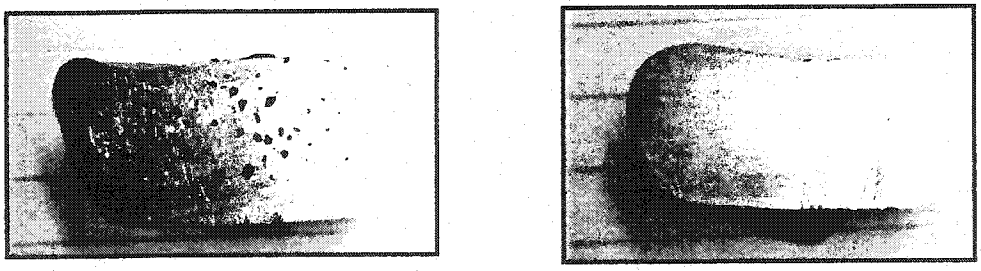

(A) (B)

Figure 3.12 Decrease in Porosity by Decreasing Pouring Temperature

(a): RPT Sample of the pouring at 810°C in electric resistance furnace.

(b): RPT Sample of the pouring at 710°C in electric resistance furnace.

3.2.12 Chemical Analysis

Samples for chemical analysis were taken for each melt. The chemical analysis of the samples was carried out at Gamma Foundries, Toronto. The actual element additions

for various alloys as obtained from chemical analysis at Gamma Foundries are listed in Appendix A

3.3 THERMAL ANALYSIS

Section Summary

The procedure for thermal analysis is explained in this section. Cooling curves were used to plot the cooling rate and velocity curves against the thickness.

3.3.1 Cooling Curves

Using the temperature data recorded by eight thermocouples for each pourings, the cooling curves were plotted. For each pouring, the temperature data were recorded for first 1200 seconds. Cooling curve is the temperature time relation obtained during the solidification of an alloy. It is a valuable tool to study the changes occurring during the solidification process.

3.3.2 Cooling Rate

The cooling rate shows the rate of change of temperature over time during solidification. The cooling rate was calculated by dividing local solidification temperature with local solidification time. Local solidification was defined as the difference between the liquidus and the solidus points. Local solidification time was chosen as the primary parameter to study for two reasons:

1. There is extensive literature suggesting the use of local solidification time as the primary parameter.
2. In this research, pouring temperature is not constant. Total solidification time (the time difference between the pouring temperature and the solidification temperature) cannot be comparable under such conditions.

3.3.3 Velocity

In general, spiral fluidity test patterns were used to measure fluidity of an alloy. But straight patterns could also be used to predict fluidity by calculating velocity. Use of velocity as a measure of fluidity was more simple, accurate and feasible method with available resources. The distance between thermocouples at the start of the casting bar and at the end of the casting bar was kept constant for all the patterns (11.5 mm).

Thus,

Velocity = Distance between two thermocouples / Time taken by molten metal to travel from thermocouple 1 and thermocouple 2.

3.3.4 Repeat Experiments

The results of experiments were confirmed by repeating following pourings:

1. With the alloy of 12% Si content at 30°C superheat and bottom gating system.
2. With the alloy of 18% Si content at 150°C superheat and bottom gating system
3. With the alloy of 25% Si content at 30°C superheat and bottom gating system.

Results of these experiments were similar to the original experimental trials. Also, the change in process parameters resulted in similar results for cooling rate and velocity analyses thus, supported the authenticity of experiments. Further, the authenticity was supported by adding cooling rate and velocity curves for the pourings with 15 and 18% Si content that showed similar results.

3.4 IMAGE ANALYSIS

Section Summary

This section covers microstructure preparation, image analysis and scanning electron microscopy.

3.4.1 Sample Preparation for Microstructural Analysis

Two samples were cut from each casting bar near the thermocouple location. Each casting that poured consisted of 4 bars of different thicknesses (6,12,18,24 mm) hence total of 120 samples were cut from all the pourings. The samples were prepared for image analysis by following steps:

- Coarse grinding with a belt sander using 80 grit papers.
- Fine grinding with 240,320 ,400 and 600 grit papers.
- Fine polishing on rotating velvet cloth with alumina powder and diamond paste.
- Etching by using Keller's reagent (HF, HCL, HNO_2 and H_2O in equal parts) for 15 seconds.

After etching the samples were ready for image analysis. Mounting of samples was not carried out due to large number of samples.

3.4.2 Image Analysis

The samples were observed using optical microscopy at a magnification of 50X-500X. Size of PSC, number of PSC per unit area (650 X 850 μm) and % area of PSC were measured using the Buehler's image analyzing system. A routine was developed to determine aforesaid parameters. Ten different regions for each sample were selected to determine the average reading.

3.4.3 Scanning Electron Microscopy (SEM)

The size of $CuAl_2$ phase observed was in the range, 5-30μm. This phase precipitates with eutectic Si. Thus it is difficult to differentiate this phase from other primary phases. The SEM work was carried out at the University of Toronto.

3.5 FRACTION OF SOLID

Section Summary

First derivative curves were plotted using Microsoft Excel software and fraction of solid was calculated using the method described by Pan and Hu.

3.5.1 First Derivative Curve

Change in temperature with respect to change in time (dT/dt) was plotted using Microsoft Excel software. Temperature data were recorded by thermocouples at every 0.1 second time interval for 1200 seconds, hence first derivative points were scattered after plotting. Smoothening of these curves was achieved by 'moving average' in Microsoft Excel.[48] Moving average uses a specific number of points (set by user), averages them and uses the average value as a point on the line.

3.5.2 Fraction of Solid Calculations

It was clear through thermal and image analysis that morphology of PSC play a significant role in flow stoppage mechanism. Thus it was useful to calculate the amount of solid formed (precipitation of phases) at the instant of flow stoppage and compare the results with thermal and image analysis.

After reviewing different models for fraction of solid calculations, the Pan and Hu's[5] model was selected for further calculations for all the pourings. This model was explained in Section 2.6.4. This model was selected because it was based on calculation of fraction of solid at the instant of flow stoppage.

CHAPTER 4

RESULTS AND DISCUSSION

Chapter Summary

The chapter is divided into three main parts. Results of experimental trials are discussed through a) thermal analysis, b) image analysis and c) first derivative curves and fraction of solid calculations. Results are confirmed by comparing these three methods of analysis with each other.

4.1 THERMAL ANALYSIS

Initial experiments were conducted with pourings at 12, 15, 18, 21 and 25% Si content. Soon after it was observed that results of pourings with 15 and 18% Si content were in the similar range. Also, the results were similar for 21 and 25% Si content (refer Appendix B). Hence pourings with Si content 12,18 and 25% were pursued for further pourings.

Section Summary

Thermal analysis of all the pourings was carried out through plotting cooling rate and velocity against thickness of casting bar. Micrographs and SEM results are added in this section for a better understanding of thermal analysis.

4.1.1 Cooling Rate Analysis

Cooling rates were plotted against thickness for all the pourings. Cooling rate analysis was of particularly interest because of differences in latent heat release by different phases precipitating during solidification.

4.1.1.1 Pourings at 30°C Superheat

The change in cooling rate with pattern thickness for various compositions is shown in Figures 4.1,4.2 and 4.3. The bottom curve is for the thermocouple data recorded at the bottom end of the casting bar (start of the casting bar) and the top curve is for top end of casting bar (end of the casting bar) for all the pourings made with bottom gating system.

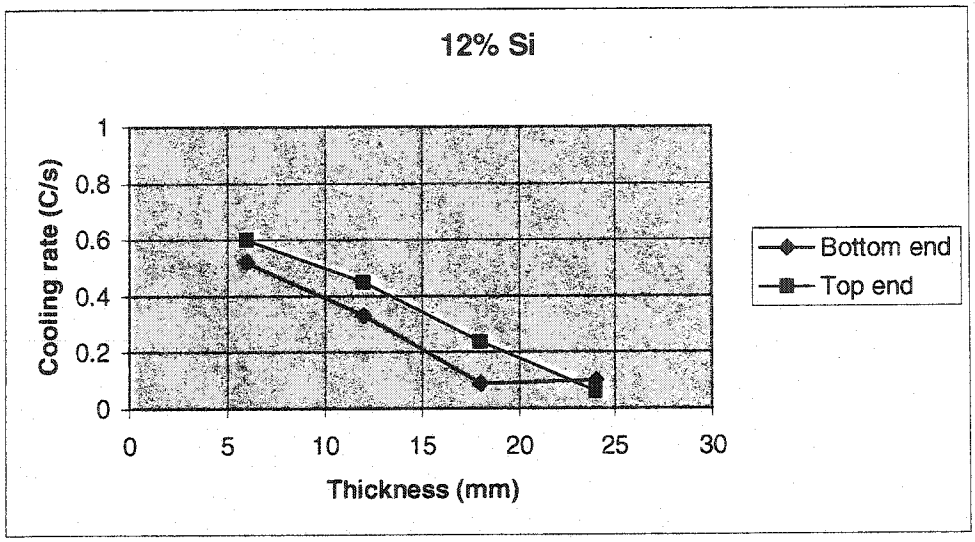

Figure 4.1 Cooling Rate Curve for 12% Si Content at 30°C Superheat.

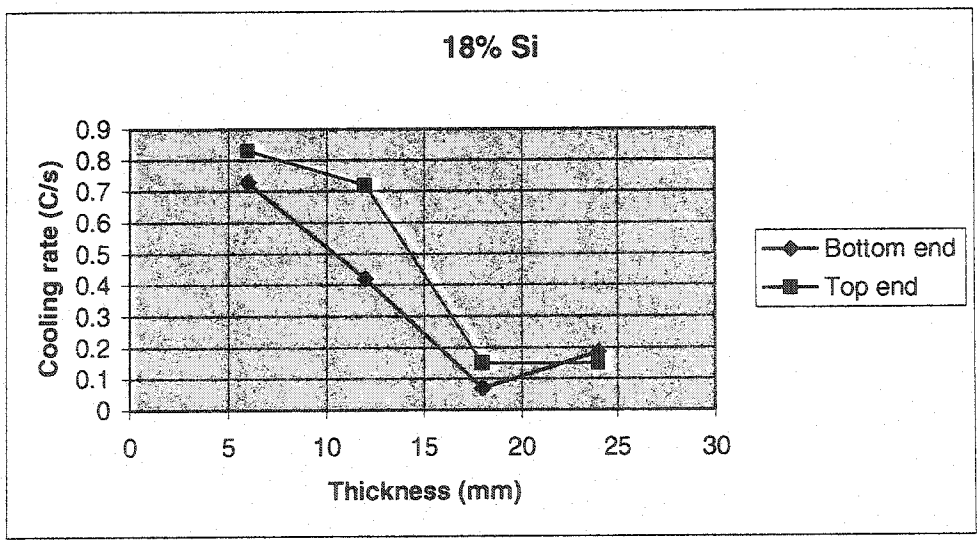

Figure 4.2 Cooling Rate Curve for 18% Si Content at 30°C Superheat.

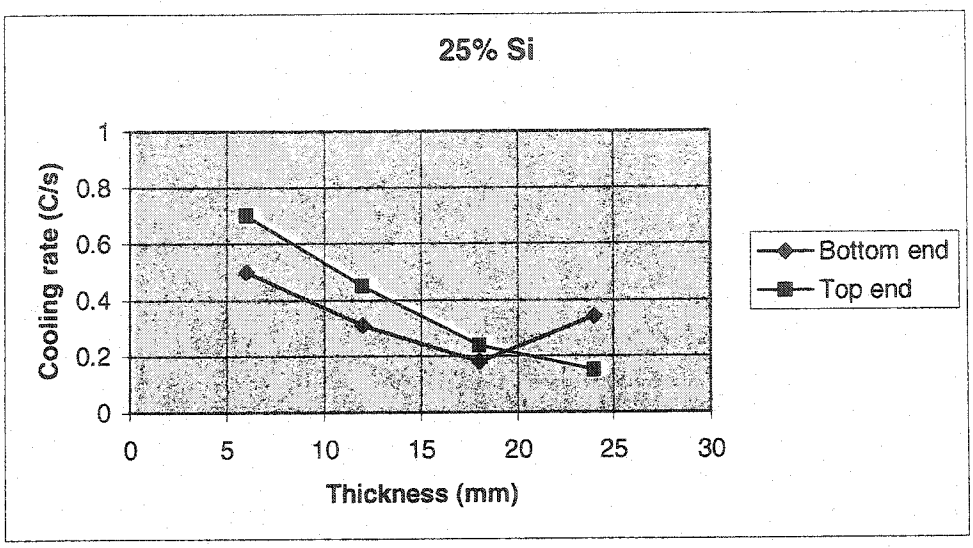

Figure 4.3 Cooling Rate Curve for 25% Si Content at 30°C Superheat.

Observations and discussion:

- The cooling rate observed at the top end of casting bar was higher than that at the bottom end. This was expected as most of the gaseous products of foam decomposition escaped through top end and enabled removal of the heat of molten metal.

- For all three compositions, the cooling rate decreased with an increase in section thickness up to 18mm. Beyond this thickness of 18mm, the cooling rate increased. This behavior of curves was observed prominently for the bottom end of castings. Energy balance equation for LFC was developed by Pan and Liao.[37] This equation confirmed that cooling rate decreases with an increase in the section thickness.

$$\frac{\Delta T}{L_f} = \frac{\rho_p H_E}{C_L 2.2 t_p \rho_L} \qquad (4.1)$$

-Energy balance equation for LFC

Where,

ΔT Superheat, °C

L_f Flow length , cm

ρ_p Density of pattern, g/cm^3

H_E Decomposition energy of LFC pattern, J/g

C_L Specific heat of molten metal, J/g °C

t_p Thickness of pattern, mm

ρ_L Density of molten metal, g/cm^3

The cooling rates in the present study are in contradiction of the energy balance equation for larger section thickness. This contradiction could be explained through Flemings' solidification model.[7,20] This model is based on flow stoppage mechanism. Flow stoppage mechanism for hypereutectic alloys was discussed in Section 2.4.3.

Flemings studied solidification of pure metals and of alloys in the channel of fluidity test mold to understand the flow stoppage mechanism. He explained that during solidification of alloys, columnar dendrites form at mold walls. These dendrite fracture forming equiaxed grains (for solute rich alloys). The equiaxed grains flow downstream with the liquid metal, until the critical solid concentration (k) exceeds (please refer to Section 2.2.6) resulting in a cessation of flow. In the case of hypoeutectic Al-Si alloys, dendrite arms flow downstream with liquid metal whereas in case of hypereutectic alloys, the PSC flow. Pan and Hu[4] suggested that the PSC do not adhere to mold walls and hence they can be easily carried away with the flow of molten metal. According to this model, it could be said that the PSC were more at the end part of the casting as compared to the beginning of the casting.

This flow stoppage mechanism and differences in the heat of fusion of Al and Si affect the cooling rate curves. Heat of fusion was discussed in detail in Section 2.2.1.

The standard heat of fusion of Si is 350 cal/g and that for Al is 95 cal/g. In the region of higher PSC content, Si is expected to release more heat during solidification and thus decreases the cooling rate. As explained in earlier paragraph, the PSC were carried away with metal flow to the end of casting. The casting had a bottom gating system hence metal flowed from bottom to top. Thus, a deficiency of the PSC at bottom end of bar possibly caused an increase in the cooling rate for higher section thickness (i.e., 18mm and more). The relative ease of the PSC flow at larger section thickness was supported by the results of Liu et.al.[38] They also suggested an increase in fluidity with an increase in section thickness.

Lamellar mold filling mechanism of LFC also plays a role in controlling the cooling rates. This mechanism was discussed in Section 2.5.2. It results in smooth distribution of PSC in microstructure during solidification. Other conventional casting processes like Sand casting or Die-Casting may not result in smooth distribution of PSC due to their turbulent mold filling mechanism. LFC was compared with Die Casting process in Section 2.5.3.

- At the top end of casting bar, the higher concentration of the PSC should decrease the cooling rate in proportion to the increase in cooling rate at bottom end. This did not happen because the cooling rate at top end was always high due to escape of foam decomposition products. Thus filling mechanism of LFC appeared to counteract the effect of high heat of fusion of Si.

- High Si content caused formation of more number of the PSC and hence a larger deflection in the cooling rate was observed for alloys with 25% Si (Figure 4.3).

4.1.1.2 Pourings at 150°C Superheat

The change in cooling rate with pattern thickness for various compositions is shown Figures 4.4,4.5 and 4.6

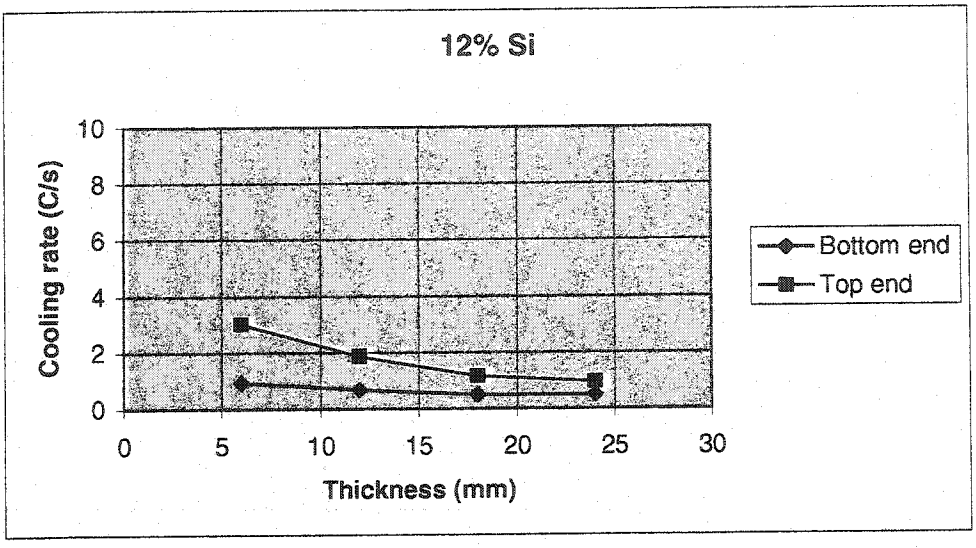

Figure 4.4 Cooling Rate Curve for 12% Si Content at 150°C Superheat.

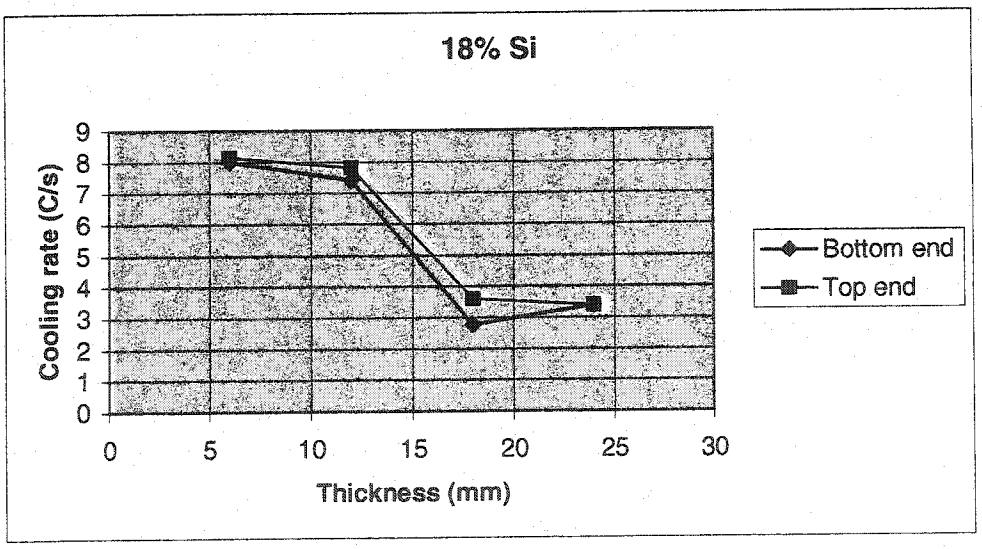

Figure 4.5 Cooling Rate Curve for 18% Si Content at 150°C Superheat.

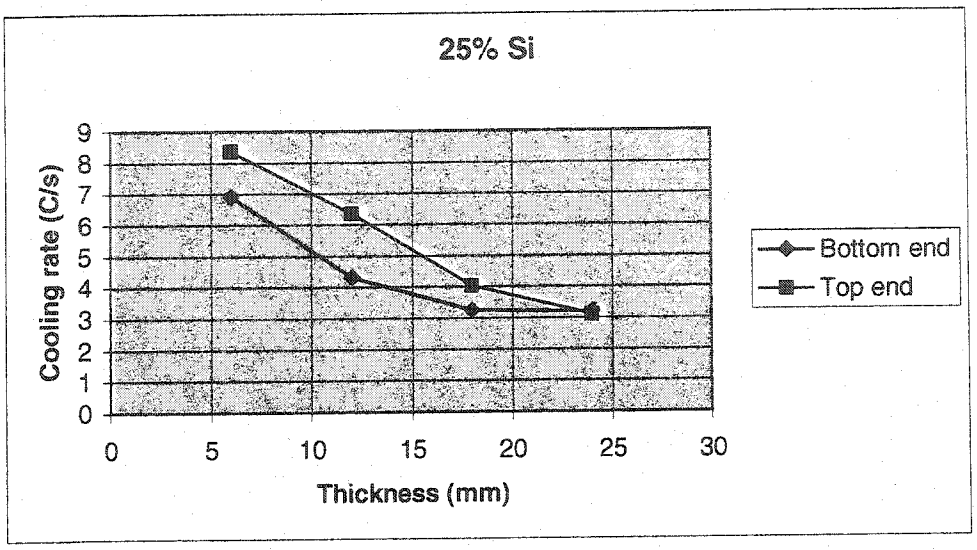

Figure 4.6 Cooling Rate Curve for 25% Si Content at 150°C Superheat.

Observations and discussion:

- The cooling rate curves in this case showed a behavior similar to the one for 30°C superheat pourings except the cooling rates were higher in this case. The higher cooling rates were obvious due to high pouring temperatures.

- It was also observed that the increase in the cooling rate due to flow of PSC was started at lower section thickness bar (12-18mm), whereas it was observed at 18mm bar for 30°C superheat curves (refer to Section 4.1.1.1) This could be justified through the remelting of PSC nuclei. In the case of high temperature pourings, the PSC nuclei possibly remelt and go back to the liquid due to high temperature of melt. Sometimes the nuclei can break and each part of broken nuclei act as a separate nuclei. Thus, at higher temperature more number of PSC of smaller size form. These smaller PSC can be easily carried away with melt to the end of casting even in a lower section thickness bar. This causes deflection of curve at lower section thickness. The relation between size of the PSC and pouring temperature is discussed in more detail in Section 4.2.1.

4.1.1.3 Pourings with 2.5% Cu Addition at 150°C Superheat

The change in cooling rate with pattern thickness for various compositions is shown Figures 4.7,4.8 and 4.9.

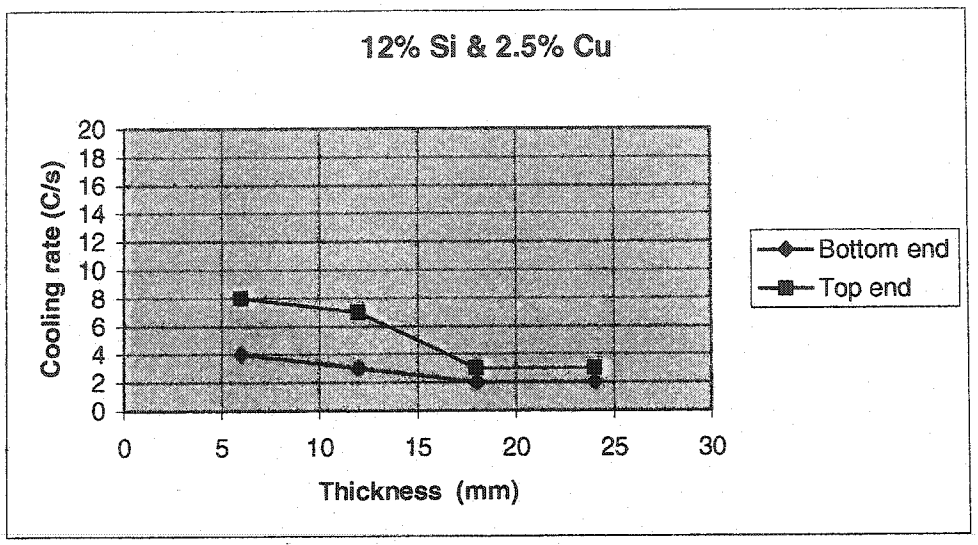

Figure 4.7 Cooling Rate Curve for 12% Si, 2.5% Cu Content at 150°C Superheat

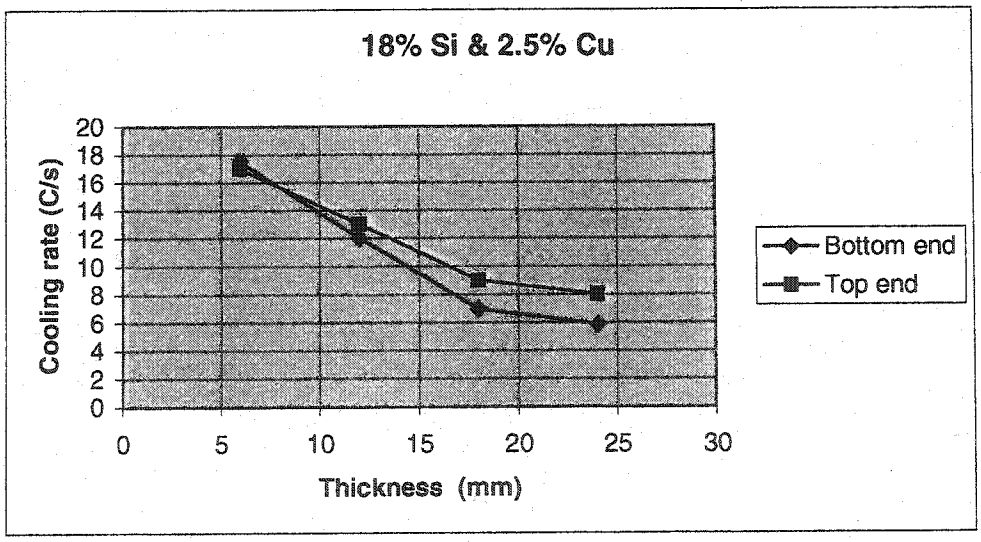

Figure 4.8 Cooling Rate Curve for 18% Si, 2.5% Cu Content at 150°C Superheat

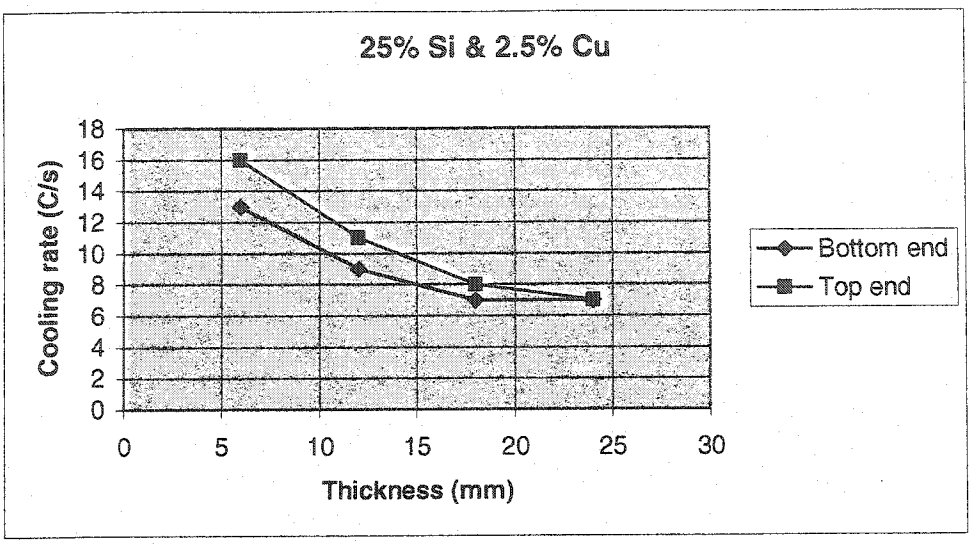

Figure 4.9 Cooling Rate Curve for 25% Si, 2.5% Cu Content at 150°C Superheat.

The cooling behavior observed by addition of 2.5% Cu follows the similar trend like the earlier curves without Cu addition. Cooling rate was comparatively high in this case. The reason could be low heat of fusion of Cu (50 cal/gm, approximately $1/7^{th}$ of the value for Si). Hence Cu could act as a chill in Al-Si alloys. Therefore addition of Cu allowed the melt to cool faster and hence increased the cooling rate. The cooling rates for all these pourings are tabulated in Table 4.3.

To confirm the effect of Cu addition on cooling rate and velocity, one more set of pourings with 5% Cu were made. Similar trend of results were obtained with these pourings. The cooling rate and velocity curves with addition of 5% Cu are plotted in Appendix C.

4.1.1.4 Pourings With Top Gating System at 150°C Superheat

Top gating system results in turbulent mold filling (unlike lamellar mold filling in the case of bottom gating system). Bottom gating system results in comparatively less defects in casting than top gating system.[39] Effect of the gating system on the distribution of PSC during solidification and its effect on cooling rate can be a separate thesis topic. In this research, one set of pourings were made with top gating system to confirm and emphasize that the distribution of PSC during solidification is the prime factor in controlling the cooling rate of an alloy.

The change in cooling rate with pattern thickness for various compositions is shown Figures 4.10,4.11 and 4.12. In this set of pourings, top curve is the start of the casting bar whereas the bottom curve is the end of the casting bar.

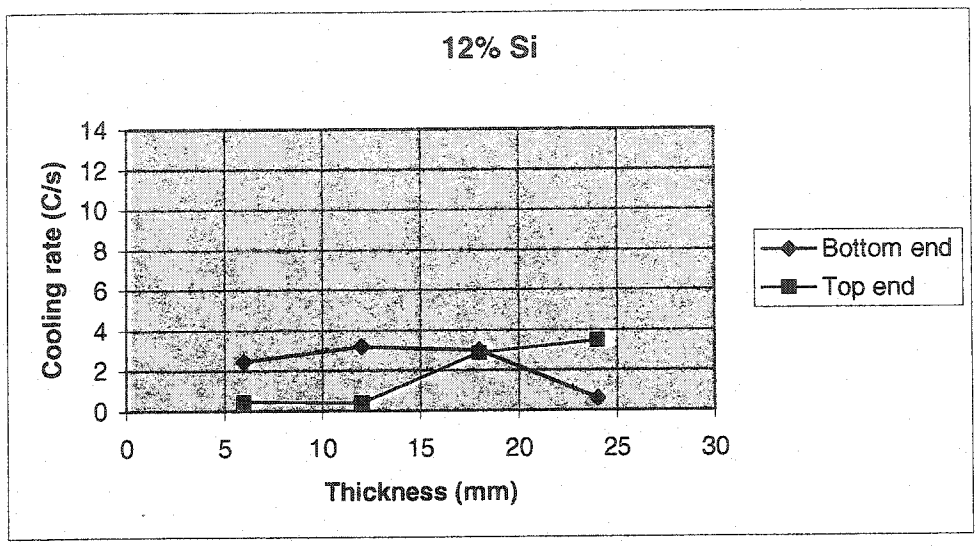

Figure 4.10 Cooling Rate Curve for 12% Si at 150^{0}C Superheat, Top Gating System.

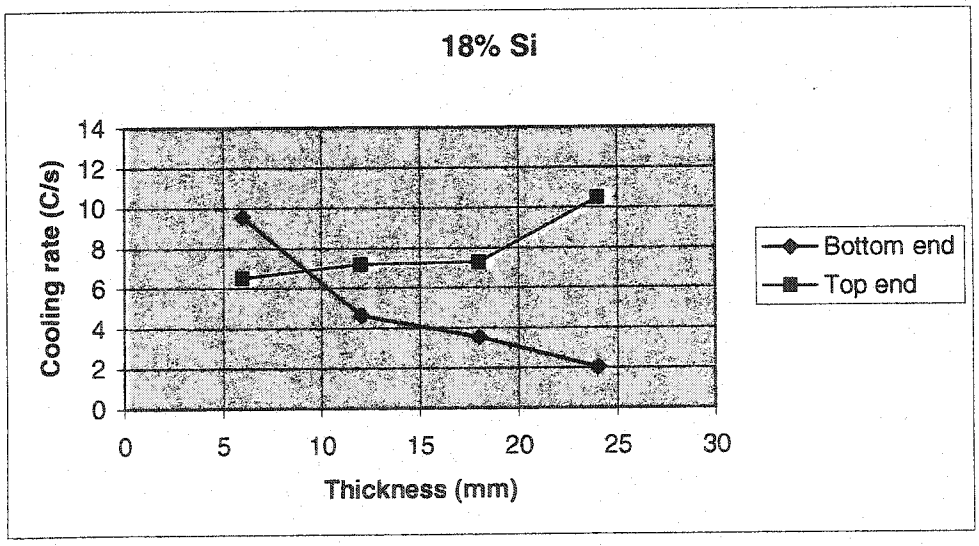

Figure 4.11 Cooling Rate Curve for 18% Si at 150^{0}C Superheat, Top Gating System.

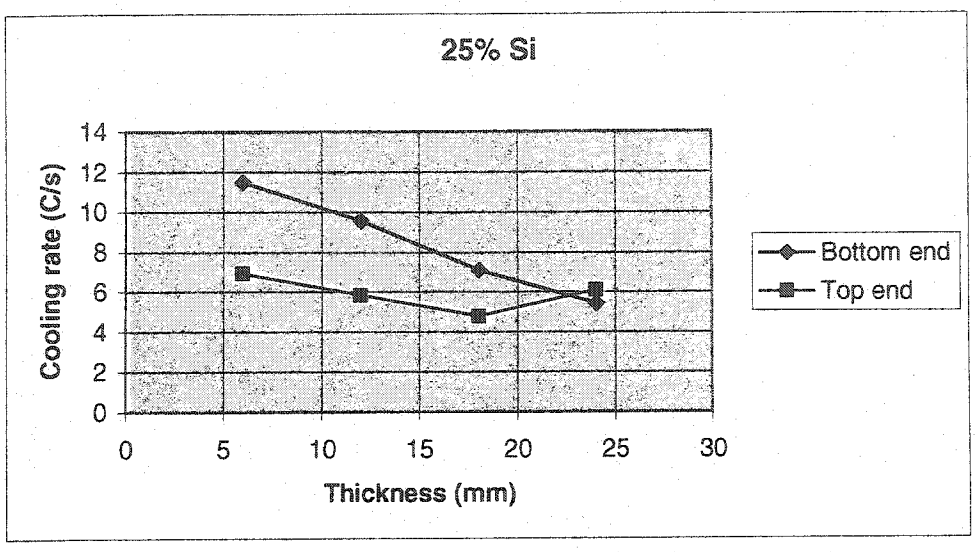

Figure 4.12 Cooling Rate Curve for 25% Si at 150°C Superheat, Top Gating System.

Observations and discussion

- For lower section thickness (6-12mm) cooling rate was high for bottom end of the bar whereas it was low at the top end of bar. This could be explained through LFC filing mechanism as explained in Section 2.5.2. It was suggested that gaseous products of foam decomposition escaped through the bottom end enabling removal of heat of molten metal and hence increased the cooling rate at bottom end.

- Crossing of curves at higher section thickness confirmed that precipitated particles (PSC) were carried with molten metal towards the end (bottom) of casting and due to this high heat of fusion, the cooling rate decreased at the bottom end of bar whereas it increased at the top end of the bar.

Distribution of PSC in the casting bar during solidification was explained through cooling rate analysis. Flow stoppage mechanism was used to explain the distribution of PSC in the microstructure. Next section will discuss about the effect of this distribution of PSC on fluidity (velocity) of an alloy.

4.1.2 Velocity Analysis

Velocity is a measure of the fluidity of the alloy in the solidification system. Several factors that affect the fluidity (velocity) were summarized in Section 2.2.2. Care was taken in all the experiments to keep all these factors constant except composition, superheat, gating system and the pattern dimensions. They were maintained constant to highlight the effect of selected process parameters on morphology of PSC and ultimately on the fluidity of an alloy.

4.1.2.1 Pourings at 30°C Superheat

The variation in metal flow velocity for various compositions is shown in Figure 4.13. This data were recorded for 30°C superheat.

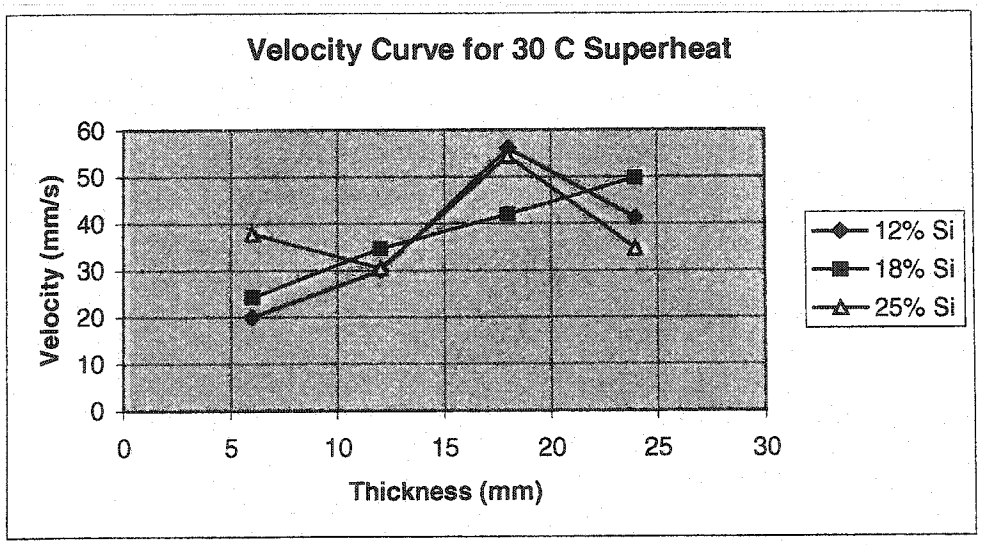

Figure 4.13 Velocity Curves at 30°C Superheat.

Observations and discussion:

1) There is a non-linearity of the curves for 12% and 25% Si content, however the curve is linear for 18% Si alloy. Considering the high heat of fusion of Si (Table 2.2), fluidity was expected to increase with an increase in Si content. Pan and Hu[4] studied the fluidity of hypereutectic Al-Si alloys (Section 2.2.3) Their results

showed that fluidity increased with an increase in Si content upto 18% Si content, but it decreased for Si content higher than 18%. These authors suggested that interlocking of PSC might be one of the reasons to cause resistance to flow.

Even after a significant difference between Pan and Hu's work and the present study, results of both the studies were similar. In this study, superheat was kept constant whereas Pan and Hu had constant pouring temperature. Fluidity was recorded at its high for 18% Si content in both the studies. This emphasized that the role of the PSC morphology and their interlocking was more dominant in controlling the fluidity than pouring temperature. Loper[2] also observed that an increase in Si interferes with fluidity by reducing it.

Although past work suggested that interlocking could be one of the reasons for the decrease in fluidity above 18% Si, corroborating evidence (e.g. micrographs and theoretical calculations) was not presented. Hence in this research, the effect of interlocking and melt sluggishness on fluidity was further studied in detail through image analysis, first derivative curve and fraction of solid calculations.

2) Non-linearity at 12% Si content was due to low pouring temperature (577°C + 30°C). At such a low temperature with bottom gating system metal reached the casting bar well after the liquidus point (the end part of mushy zone). Tseng et.al.[40]also suggested decrease in metallostatic head pressure at bottom gating system and hence delay in mold filling.

3) Nonlinearity at 25% Si content for low section thickness could also be related to the low pouring temperature as explained in previous paragraph. This nonlinearity of curves was not observed for pourings with 150°C (refer Figure 4.14).

4.1.2.2 Pourings at 150°C Superheat

The variation in metal flow velocity for various compositions is shown in Figure 4.14. This data was recorded for 150°C superheat.

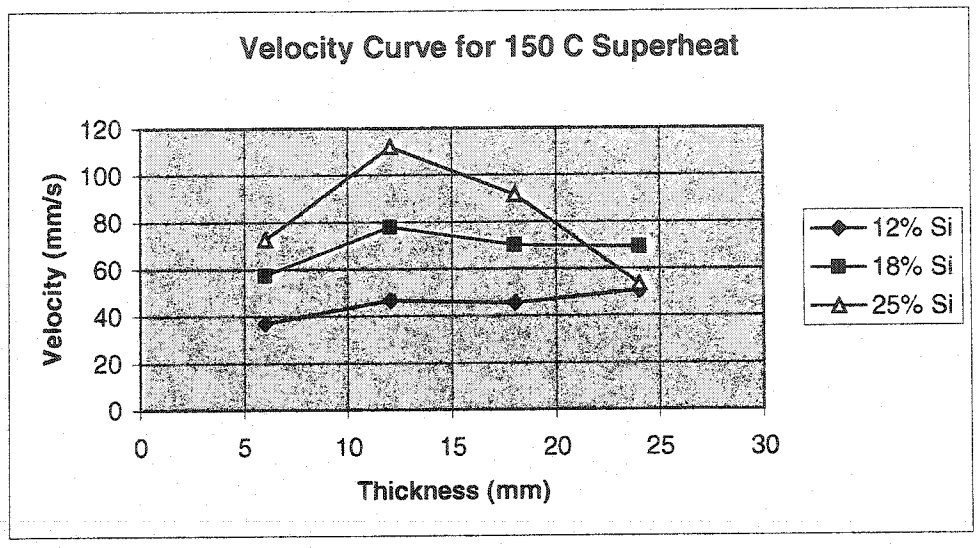

Figure 4.14: Velocity Curves at 150°C Superheat

The Velocity Curves were similar to those observed for 30°C superheat (Figure 4.13). This behavior emphasizes that interlocking of PSC plays a major role in controlling fluidity whereas superheat and heat of fusion play minor roles.

The velocity was observed higher than that for 30°C superheat. This was expected because an increase in pouring temperature increases the fluidity.[2,3,41] Linearity in the curve was observed for 12% Si content in this case unlike the one at 30°C superheat. This was attributed to an increase in the pouring temperature (577°C + 150°C), and the metal reached the casting bar at the early stage of mushy zone.

The micrographs in Figures 4.15,4.16 and 4.17 demonstrate interlocking of PSC and the resistance to flow of metal at 25% Si content that was not observed at 12% and 18% Si content.

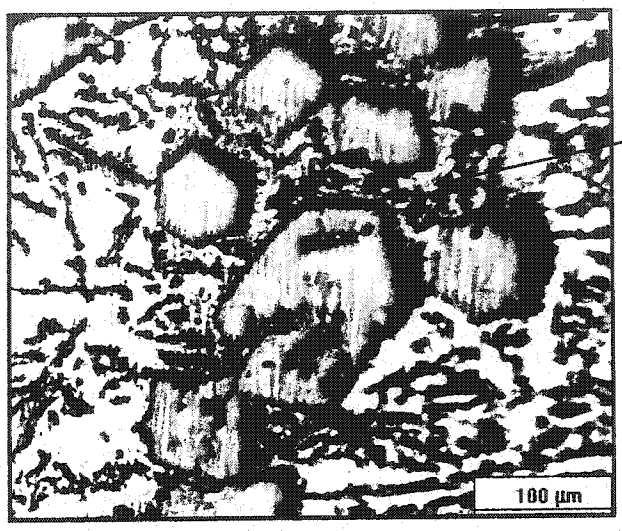

Interlocking of PSC at 25% Si content.

Figure 4.15 Micrograph for 25% Si Content, 30^{0}C Superheat.

PSC are not interlocked at 18% Si content.

Figure 4.16 Micrograph for 18% Si Content, 30^{0}C Superheat.

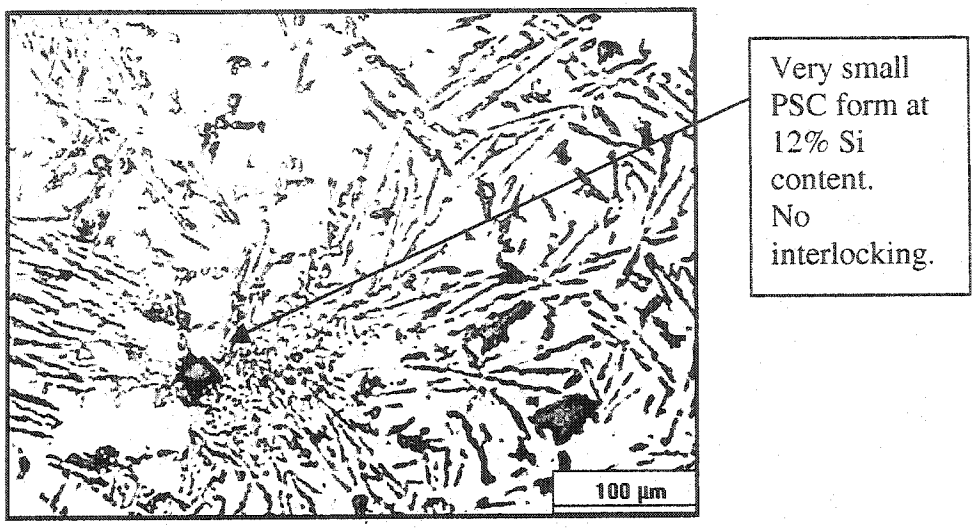

Figure 4.17 Micrograph for 12% Si Content, 30°C Superheat.

4.1.2.3 Pourings With Addition of 2.5 % Cu at 150°C Superheat

The variation in metal flow velocity for various compositions at 150°C superheat is shown in Figure 4.18. However, these alloys contain an addition of 2.5% Cu.

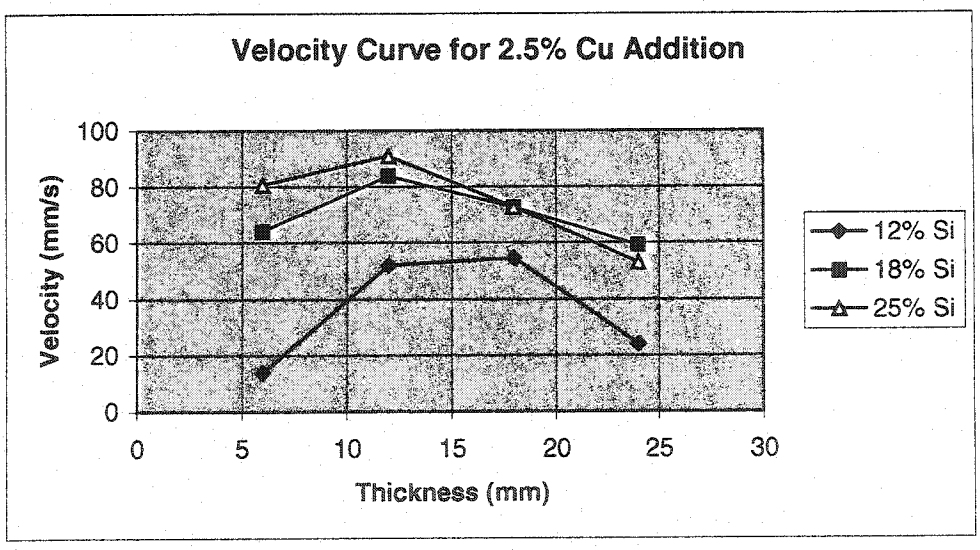

Figure 4.18 Velocity Curves at 150°C Superheat, with 2.5% Cu Addition.

Nonlinearity was observed at all three compositions as can be seen in figure 4.18. Velocity decreased even at 18% Si content unlike previous sets of pourings. Literature[3,5,6]

suggested that addition of Cu caused precipitation of $CuAl_2$ phase together with the eutectic Si. Precipitation of $CuAl_2$ phase might have increased the melt sluggishness and hence caused nonlinearity in all the curves. Micrograph 4.19 shows the $CuAl_2$ phase and micrograph 4.20 shows melt sluggishness caused by $CuAl_2$ phase. SEM analysis showed that $CuAl_2$ phase has different odd shapes (Figures 4.21 and 4.23), which effectively increased the possibility of interlocking with the other phases. SEM analysis also showed that the $CuAl_2$ phase included agglomeration of other phases (Table 4.4) of Si and Fe resulting in increased melt sluggishness (Figures, 4.22 and 4.24).

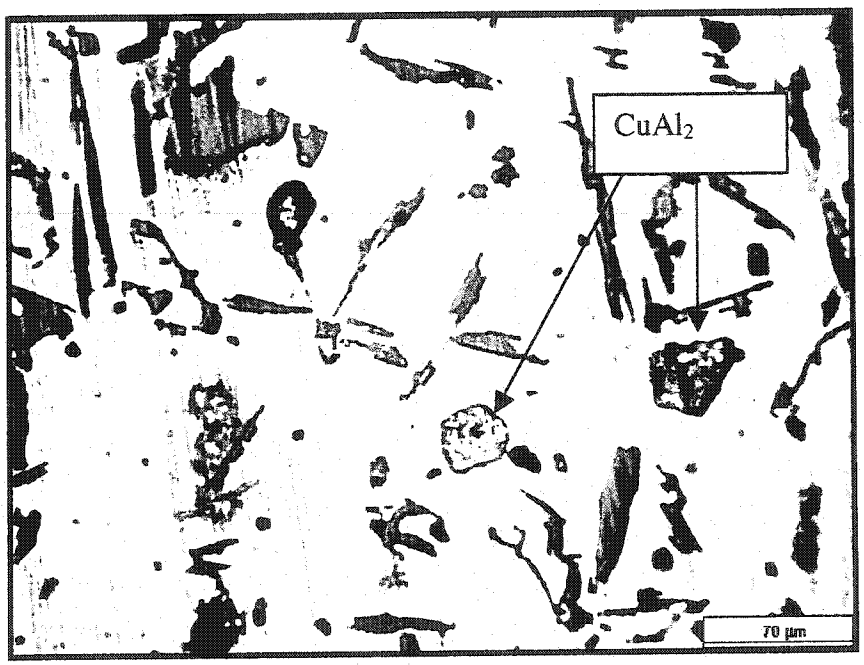

Figure 4.19 Micrograph Showing $CuAl_2$ Phase.

Figure 4.20 Melt Sluggishness Caused by Very Small $CuAl_2$ Phases.

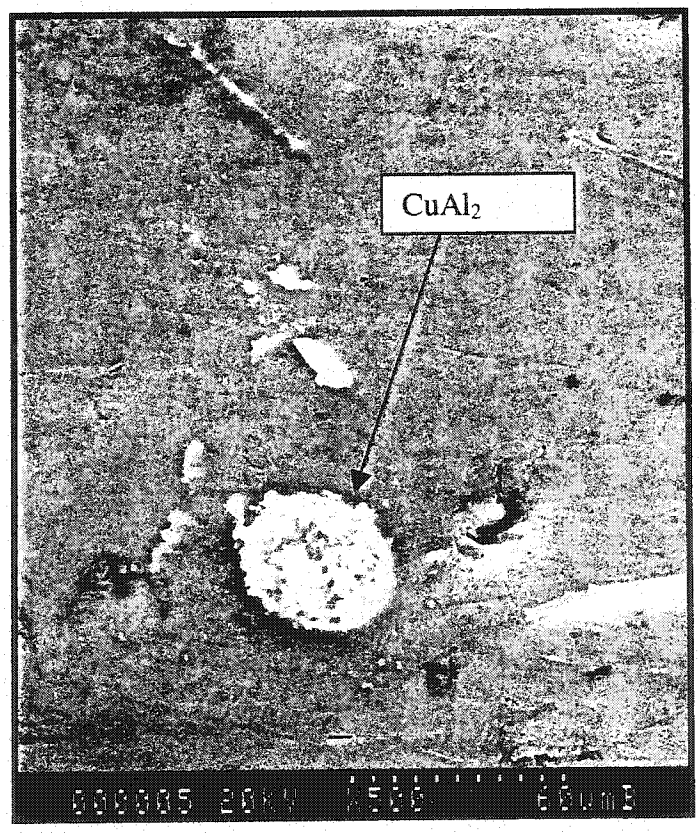

Figure 4.21 $CuAl_2$ Phase in a Globular Shape.

Table 4.1 SEM Analysis of Globular Shaped $CuAl_2$ Phase Shown in Figure 4.21.

Element	Wt%
Al	42.76
Cu	57.24
Total	100.00

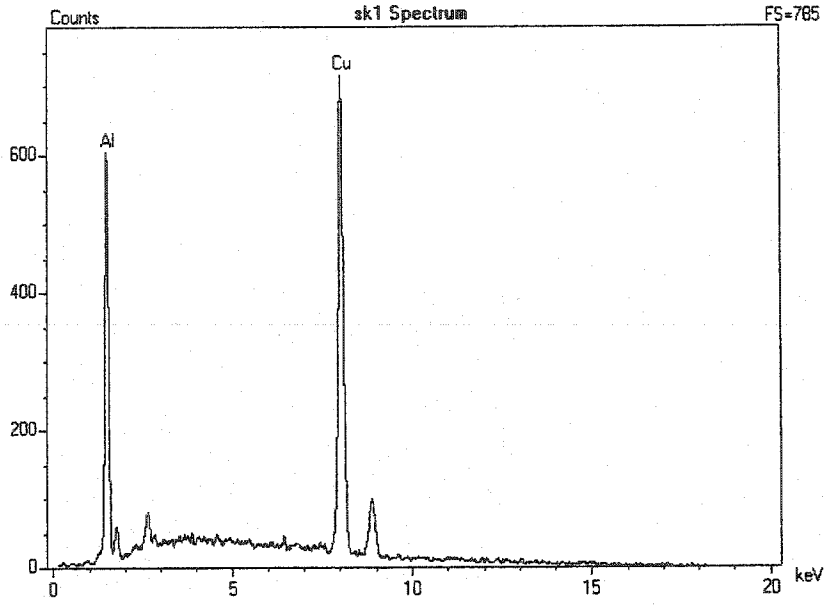

Figure 4.22 EDX Analysis of $CuAl_2$ Phase shown in Figure 4.21.

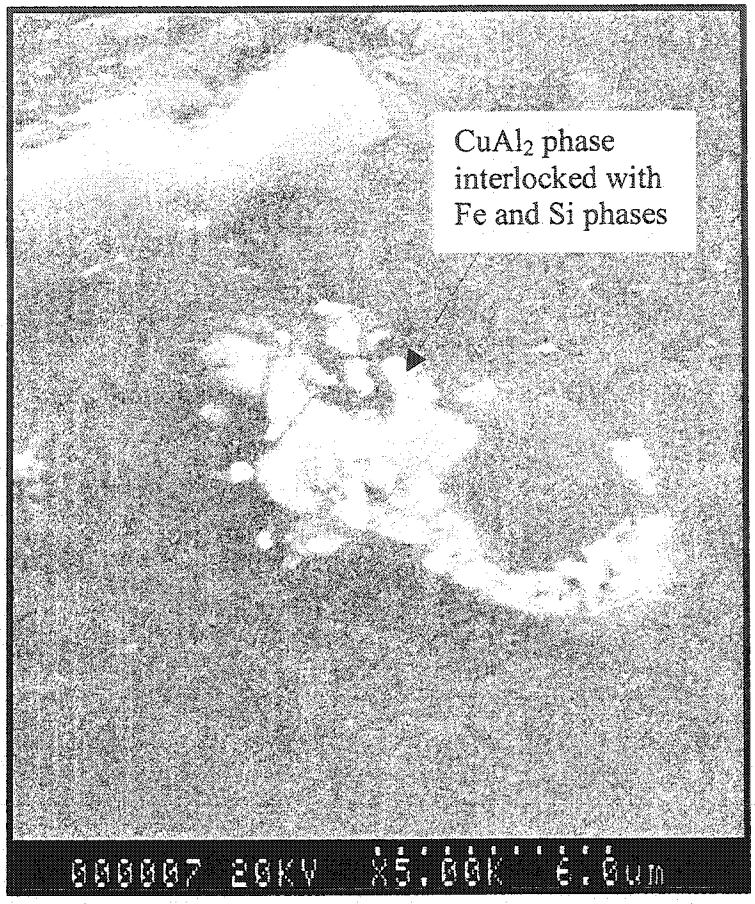

Figure 4.23 $CuAl_2$ phase in Odd Shape.

Table 4.2 SEM Analysis of Odd Shaped $CuAl_2$ Phase Shown in Figure 4.23.

Element	Wt%
Al	49.29
Si	5.29
Fe	22.47
Cu	22.95
Total	100.00

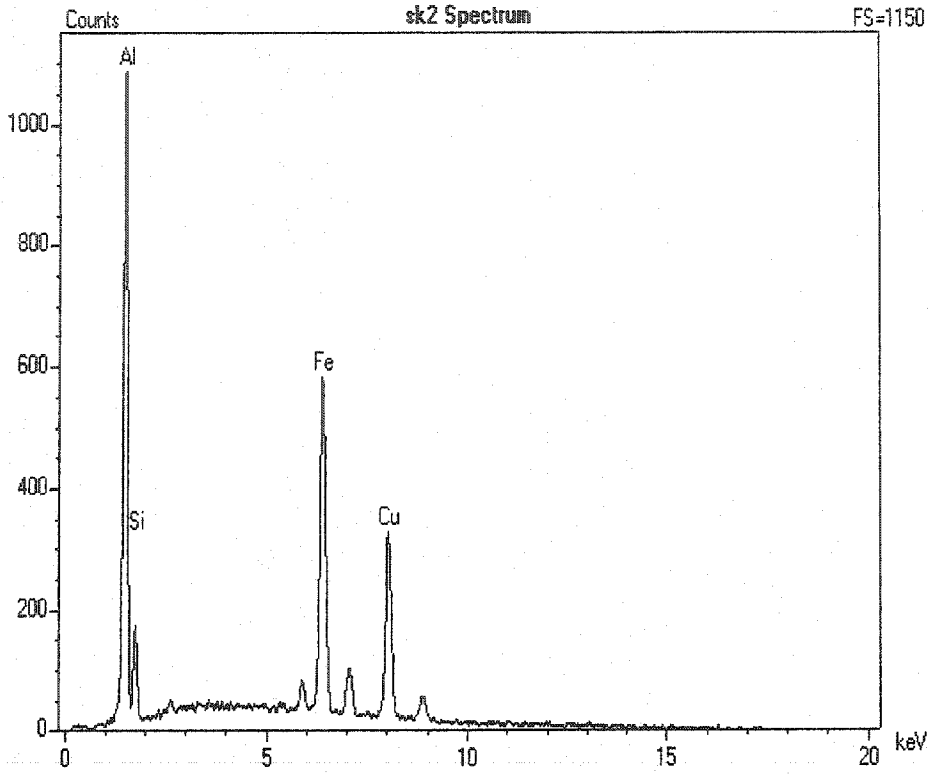

Figure 4.24 EDX Analysis of $CuAl_2$ Phase Shown in Figure 4.23.

4.1.2.4 Pourings With Top Gating System at 150°C Superheat

The variation in the metal flow velocity for various compositions is shown in Figure 4.25. This data were recorded for 150°C superheat.

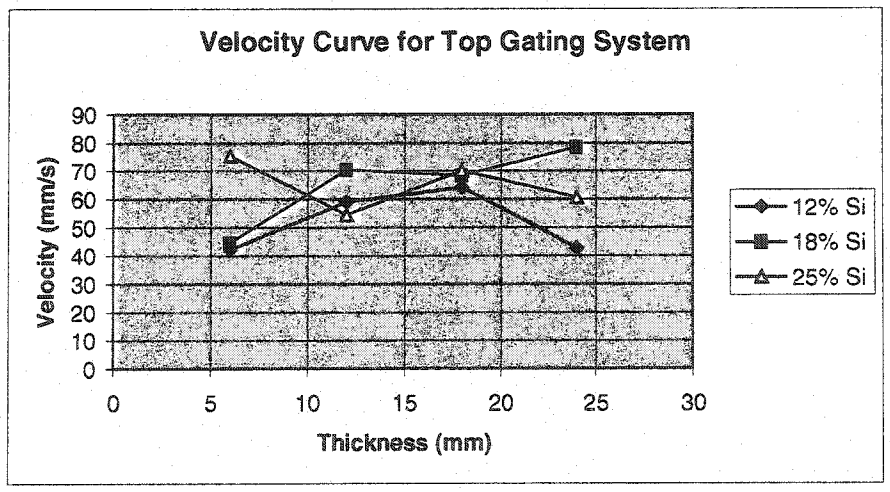

Figure 4.25 Velocity Curves for Top Gating System at 150°C Superheat.

Observation and discussions:

The velocity curves were similar to those for bottom gating system (Section 4.1.2.1 and 4.1.2.2). Nonlinearity in curves for the alloys with 12 and 25% Si was observed whereas linearity in curve for 18% Si was observed. Again, interlocking of PSC appears to play a major role in controlling the fluidity of an alloy even for a different gating system.

The decrease in fluidity at 12% Si at larger section thickness may be explained through backpressure due to of gaseous and liquid products of foam decomposition during pouring. The less heat content of the melt due to less Si content in the melt and the low pouring temperature causes liquid products of foam decomposition(in addition to gaseous products). The top gating system produces backpressure of 0.4 kpa-1.4 kpa[42], thus reducing the metal flow velocity. Yao and Shivkumar [43] suggested that volume of gases produced interferes with fluidity.

According to the equation 2.4 in Section 2.2.6, the fluidity of an alloy depends on several factors including critical solid concentration (k). The thermal analysis of present experiments suggested that the critical solid concentration at the mold tip was a major factor to control the fluidity of an alloy.

4.2 IMAGE ANALYSIS RESULTS

Section Summary

Thermal analysis suggested that melt sluggishness and interlocking of PSC have a significant impact on fluidity of an alloy. In order to understand the effect of size and distribution of PSC on melt sluggishness and ultimately on fluidity of an alloy, image analysis was carried out. Results of thermal analysis, image analysis and fraction of solid are tabulated and discussed in this section.

4.2.1 Pourings with 30^{0}C Superheat

Figures 4.26, 4.27 and 4.28 show the variation of the size of PSC against the thickness of casting bar for pourings at 30°C superheat with 12, 18 and 25% Si content.

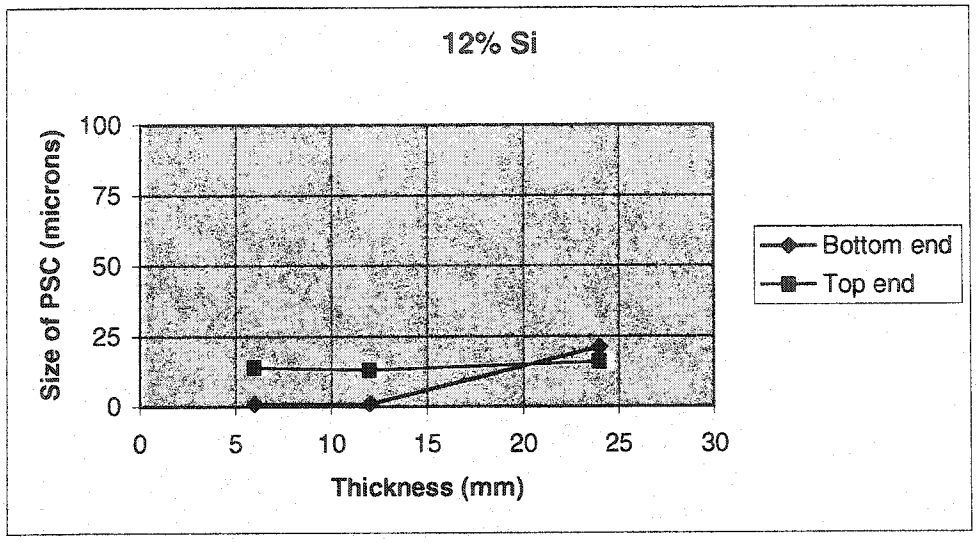

Figure 4.26: Size of PSC Curve for 12% Si , 30°C Superheat.

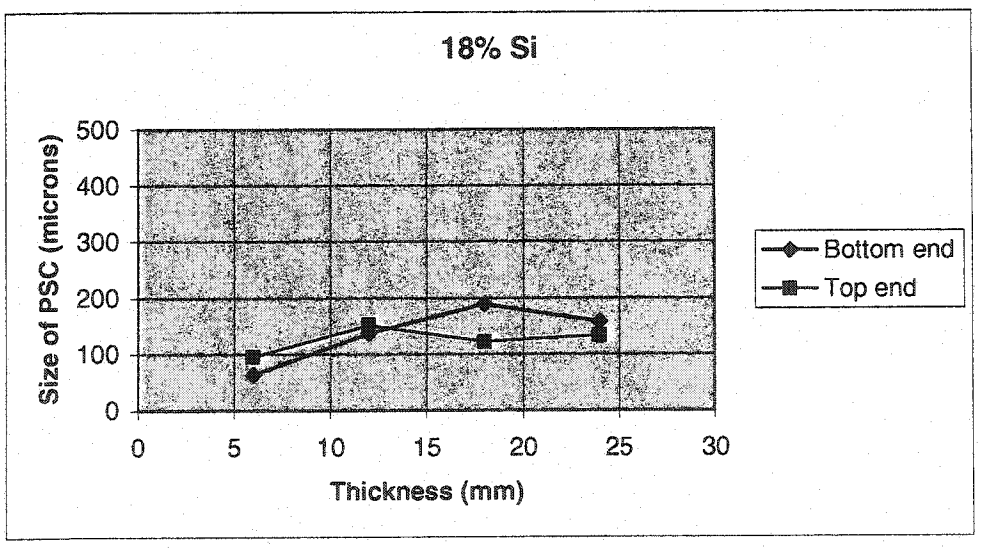

Figure 4.27 Size of PSC Curve for 18% Si , 30°C Superheat.

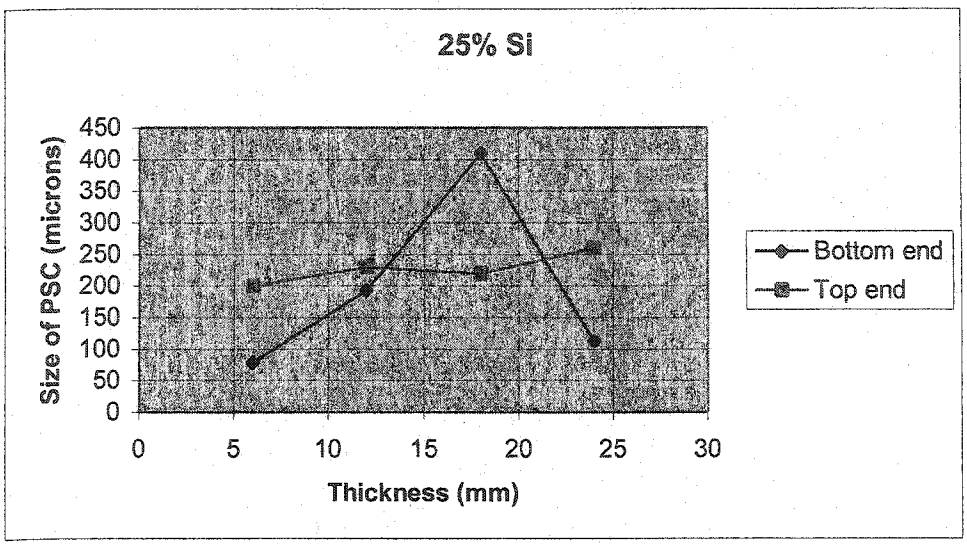

Figure 4.28 Size of PSC Curve for 25% Si , 30°C Superheat.

Observations and discussions:

- The size of PSC increased with an increase in Si content of the alloy.

- The size of PSC increased with an increase in section thickness.

- For higher section thickness, the PSC size for bottom end decreased (Figures 4.27 and 4.28) however for top end the size increased, thus the curves crossed each other for higher section thickness. This behavior was similar to that observed for the cooling rate curves (Section 4.1).

  Crossing of the curves at higher section thickness bars in these curves can be related to the explanation based on energy balance equation (Section 4.1.1.1.) At higher cooling rate, more PSC form and in smaller size. At low cooling rate, less PSC form and in larger size. Size of PSC for all the pouring sets is tabulated in Table 4.3.

- Size of PSC was higher for low pouring temperature (30°C superheat) than that for high pouring temperature (150°C superheat). Refer to Table 4.3.

The relation between size of PSC and pouring temperature is explained here through the nucleation and growth of PSC. PSC originate from eutectic colonies formed in chill zone near the mold medium (silica sand). PSC do not nucleate by usual impurities present in melt, as a result PSC do not crystallize until a considerable undercooling is reached below the liquidus temperature.[16, 49] If temperature of the melt is high enough, then the growth of PSC nuclei stop and they remelt. Thus smaller size PSC, more in numbers form at high pouring temperature. If the pouring temperature is low then PSC do not remelt and growth of nuclei occur and hence larger size PSC, small in numbers form.

- Size of PSC was observed in an acceptable range (<100μm for good machinability) at 150°C superheat. This was achieved without phosphorous grain refinement and eutectic Si modification. This can be explained through LFC filling mechanism (Section 2.5.2). LFC reduces freezing range due to its endothermic nature. Reduced freezing range resulted in smaller size PSC (Section 2.3.4).

First derivative curves and calculation of fraction of solid at the instant of flow stoppage were useful to explain the effect of precipitation of phase on fluidity.

4.2.2 Comparison of Thermal, Image and Fraction of Solid Analyses

Average value of the results of four section thicknesses for each pourings was used for comparison. The comparison between thermal analysis, image analysis and fraction of solid determination with velocity at 24mm section thickness (largest section thickness used for present study) was made in the Table 4.3.

Table 4.3 Comparison of Cooling Rate, Size, Distribution of PSC and Fraction of Solid with Velocity.

Details of Pouring	**% Si**	**Avg. Cool. Rate (C/s)**	**Avg. Size of PSC (± 5 µm)**	**Avg. # of PSC in Unit Area (650x850 µm) (± 10µm)**	**Avg. % Area of PSC**	**Avg % f_s (± 10)**	**Velocity at 24mm Casting Bar (mm/s)**	**Fluidity Ranking (1: best, 14: worst)**
30°C superheat, BGS, 0% Cu.	12	0.3	15	30	0.1	70	40	11
	18	0.4	90	28	0.55	42	50	7
	25	0.45	240	40	2.5	25	33	12
150°C superheat, BGS, 0% Cu.	12	1.1	12	70	0.15	55	50	7
	18	5.1	17	75	0.24	50	68	2
	25	5.2	30	40	0.25	35	55	5
150°C superheat, TGS, 0% Cu.	12	2.8	13	65	0.17	62	44	9
	18	6	15	72	0.23	45	78	1
	25	6.2	29	55	0.29	33	60	4
150°C superheat, BGS, 2.5% Cu.	12	4.1	11	60	0.16	57	24	13
	18	9.1	16	70	0.22	53	63	3
	25	9.2	28	60	0.28	38	53	6
150°C superheat, BGS, 5% Cu.	12	4.2	12	62	0.16	72	21	14
	18	9.8	14	78	0.24	58	43	10
	25	10.1	27	69	0.28	45	45	8

Observations and discussions from Table 4.3:

- Maximum velocity was observed with top gating system for the alloy with 18% Si content, without Cu addition at 150°C superheat. But the minimum velocity was

observed with bottom gating system at 150°C superheat for the alloy with 12% Si and 5 % Cu content.

- Similarity in the size of PSC was observed for the alloys with 18% Si content with and without Cu addition. But the maximum velocity was recorded in case of the alloy with 18% Si and without Cu addition. This emphasized the role of $CuAl_2$ phase, causing melt sluggishness and hence resistance to the flow of melt.

- The fraction of solid was observed for the alloy with 12% Si content was higher than that for alloys with 18% and 25% Si content. This is expected due to less heat content in the melt for the alloy with 12% Si content resulting in a higher fraction of solid at the instant of flow stoppage.

- A lower fraction of solid was observed for the alloy with 25% Si content as compared to the alloy with 18% Si content. This was again related to the heat content of the melt as explained in the previous paragraph. The lower fraction of solid at the instant of flow stoppage should increase the velocity, which did not happen. This could be explained through first derivative curves (Figures 4.30 and 4.31). The First derivative curves suggest that for the alloy with 25% Si content, heat released was more than that for alloy with 18% Si content. But, the number of different phases precipitated also increased with an increase in Si content, resulting in melt sluggishness and hence a decrease in metal flow velocity.

- It was suggested (Section 4.1.2.3) that the addition of Cu resulted in increase in the cooling rate and melt sluggishness. This can be observed through first derivative curves (Figures 4.32, 4.33 and 4.34). Release of latent heat decreased in this case as compared to the curves without Cu addition (Figures 4.29, 4.30 and 4.31). This can be seen by comparing peaks in the first derivative curves. Also number of phase precipitation increased with addition of Cu, resulting in melt sluggishness and hence a decrease in the fluidity.

4.2.3 Precipitation of Phases in Al-Si Alloys

First derivative curves showed number of peaks. Each peak indicates the precipitation of a phase. All the phases those precipitates during solidification of Al-Si are tabulated in Figure 4.4.

Table 4.4 Phases that Precipitate During Solidification of Al-Si Alloys.[17,44,45,46]

Element	**Effect on Mechanical properties**	**Primary phases**	**Secondary phases**
Al	Increases castablility, decreases density.	Al dendrites	
Si	Increases castablility, corrosion resistance and welding/machining properties	Eutectic Si, Primary Si crystals.	
Fe	Decreases ductility and tensile strength		Less common: δ- Al_4FeSi_2 ρ- $Al_8MgFeSi_6$ More common: α - $Al_{15}Fe_3Si_2$ – Looks like a Chinese script β - Al_5FeSi – Looks like needles.
Mg	Increases tensile strength and hardness. Decreases ductility		Mg_2Si
Cu	Increases strength and fatigue properties.	$CuAl_2$	$Al_5Cu_2Mg_8Si_6$

4.2.4 Comparison of First Derivative Curves for the alloys with 12,18 and 25% Si Content

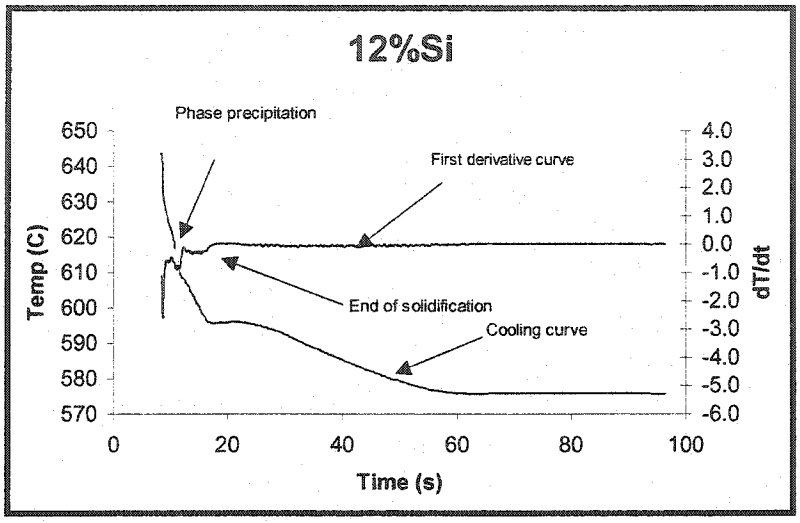

Figure 4.29 First Derivative Curve for 12% Si at 150°C Superheat.

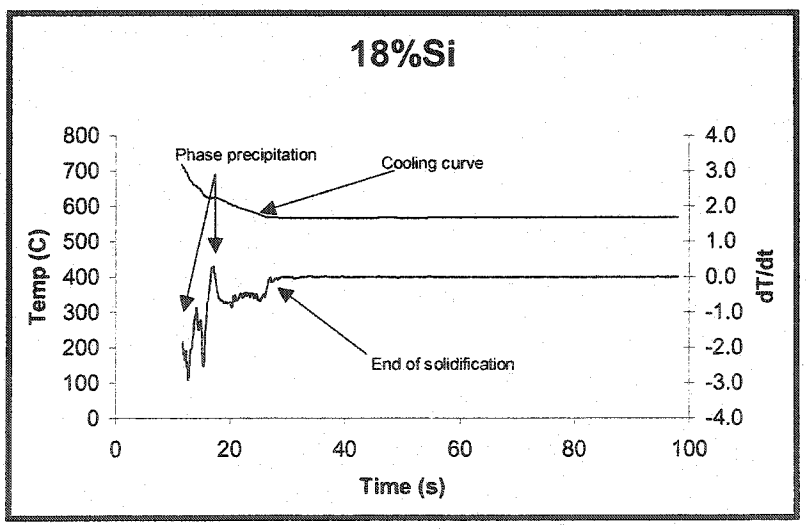

Figure 4.30 First Derivative Curve for 18% Si at 150°C Superheat.

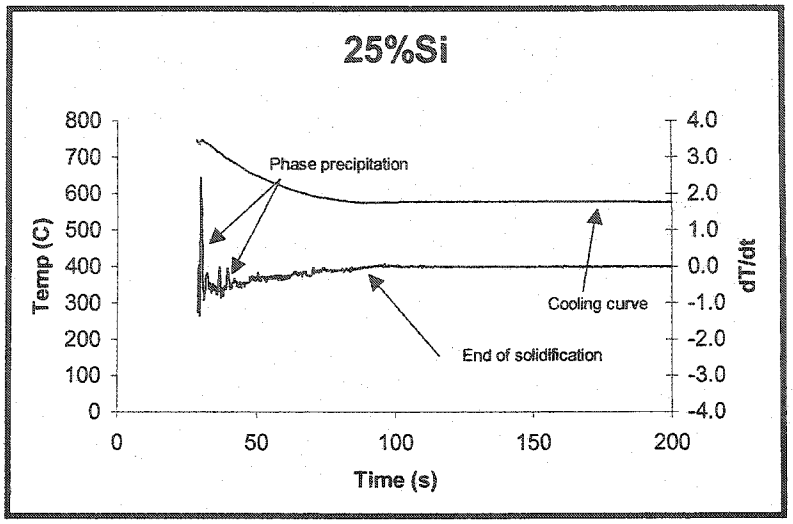

Figure 4.31 First Derivative Curve for 25% Si at 150°C Superheat.

4.2.5 Comparison of First Derivative Curves for the Alloys with 12, 18 , 25% Si and 2.5% Cu Addition

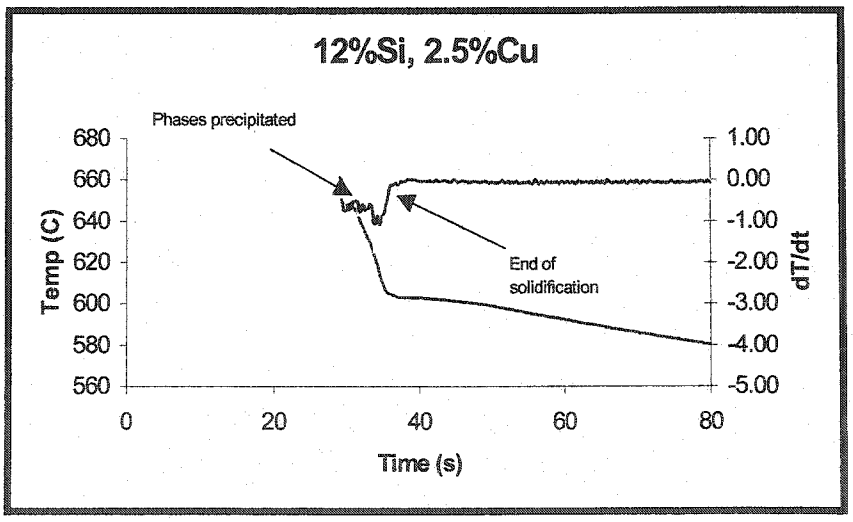

Figure 4.32 First Derivative Curve for 12% Si ,2.5% Cu at 150°C superheat.

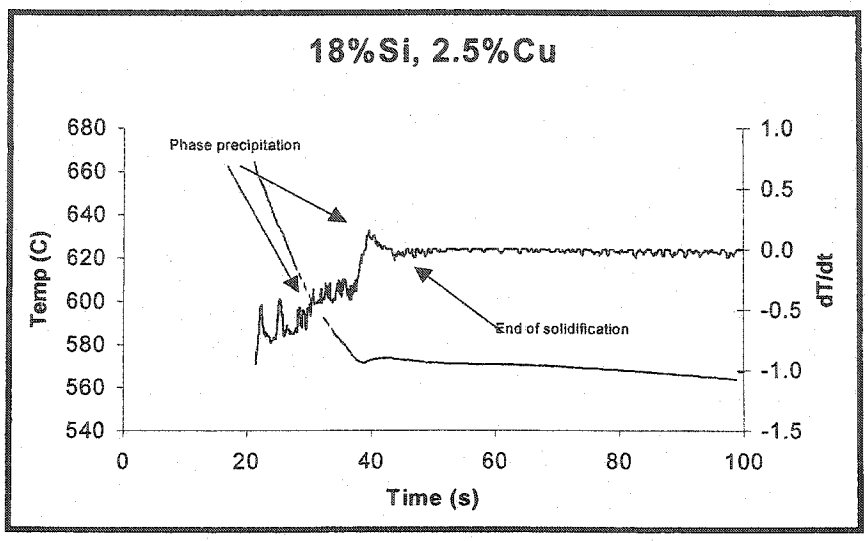

Figure 4.33 First Derivative Curve for 18% Si, 2.5%Cu at 150°C Superheat.

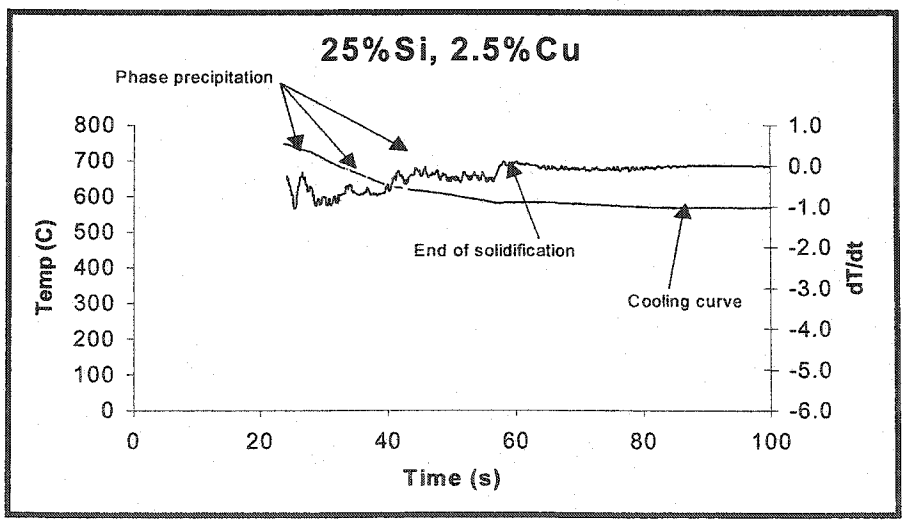

Figure 4.34 First Derivative Curve for 25% Si, 2.5%Cu at 150°C Superheat.

CHAPTER 5

CONCLUSIONS

1) Maximum velocity (fluidity) was observed for the alloys with 18% Si content in all the pouring sets. The high heat of fusion of Si should increase the velocity of an alloy with an increase in Si content and this did not happen. Velocity decreased for the alloys with Si content more than 18% Si content at higher section thickness (>18mm). It was suggested in the present study that the precipitation of PSC played a major role in controlling the fluidity of hypereutectic Al-Si alloys whereas process parameters (superheat, composition and gating design) played a minor role.

2) Cooling rate analysis revealed that the PSC has a tendency to flow with the molten metal to the end of the casting, and this decreases the cooling rate due to the high heat of fusion of the PSC. This behavior was prominently observed for higher section thickness bar (>18mm). It was also observed that the change in process parameters (superheat, gating design and composition) does not reduce the higher concentration of PSC at the end of the casting.

3) Strong correlation was observed between the cooling rate, pouring temperature and the size of PSC. This was explained through the principles of nucleation and growth of precipitated particles (PSC) during solidification.

4) Addition of Cu caused nonlinearity in the velocity curves for all the three alloy compositions (12,18 and 25% Si contents) unlike the pourings without Cu addition (nonlinearity was observed mainly for the alloy with 25% Si content). This curve behavior was related to melt sluggishness caused by precipitation of

the $CuAl_2$ phase. SEM work showed that the $CuAl_2$ phase forms in different odd shapes thus increasing the possibility of interlocking with each other.

5) Micrographs showed PSC interlocking and melt sluggishness (with contribution from $CuAl_2$ phases.) This was observed prominently for the alloys with Si content higher than 18% and with the addition of Cu.

6) The lamellar flow mechanism of LFC resulted in the smooth distribution of PSC in microstructure as well as in controlling the size of PSC in an acceptable range (<100 μm). This was achieved without phosphorous grain refinement and eutectic Si modification. The size control was due to endothermic nature of LFC.

7) The fraction of solid at the instant of flow stoppage decreased with an increase in Si content. This was correlated to an increase in the heat content of the melt at higher Si content. Decrease in fraction of solid with an increase in Si content should increase the velocity of the melt, but this was not observed. First derivative curves revealed that the number of phase precipitation increased with an increase in Si content. This resulted in melt sluggishness, thus decreasing the fluidity of an alloy.

8) The first derivative curves also revealed that the number of phases precipitated increased with the addition of Cu, thus retarding the metal flow. Cu increased the cooling rate by decreasing the latent heat release. This can also be observed in the first derivative curves.

9) Size and distribution of PSC was correlated with cooling rate, fluidity and fraction of solid at the instant of flow stoppage for different pouring conditions (changing superheat, composition and gating system). Maximum velocity was observed in the case of the top gating system for the alloy with 18% Si content at 150°C superheat without Cu addition. A minimum velocity was observed in the bottom gating system for the alloy with 12% Si and 5% Cu content at 150°C superheat.

CHAPTER 6

SUGGESTIONS FOR FUTURE WORK

1) To determine the dendritic coherency in hypoeutectic Al-Si alloys by using fraction of solid calculation. Dendritic coherency plays a major role in the flow stoppage of an alloy. A Change in process parameters could increase the dendritic coherency point and ultimately the fluidity of an alloy.

2) To improve the fluidity of hypereutectic Al-Si alloy above 18% Si content. This can be achieved by studying methods to avoid interlocking and melt sluggishness through phosphorous grain refinement and eutectic Si modification.

3) To calculate the fraction of solid at any instant of time in the mushy zone by using other models of fraction of solid (for e.g. the heat balance model). It will reveal the details of phase precipitation at any time instant and its role in the flow stoppage mechanism. This model can also calculate latent heat release by each phase.

4) To study the effect of addition of other elements like Fe, Mg, Zn, P and Sr on the flow stoppage mechanism of hypereutectic Al-Si alloys.

5) To compare the flow stoppage mechanism and fraction of solid of LFC with other conventional casting processes (e.g., Sand Casting and Die Casting processes) and to develop the fluidity model for each casting process.

CHAPTER 7

REFERENCES

1. J. Jorstad, "The Hypereutectic Al-Si Alloy Used to Cast the Vega Engine Block," AFS Transactions, 1971, Vol. 16, pp. 85-91.
2. C. Loper, Jr., "Fluidity of Aluminum Silicon Casting Alloys," AFS Transactions, 1992, Vol. 100, pp. 533-537.
3. J. Kim and C. Loper, Jr., "Effect of Solidification Mechanism on Fluidity of Al-Si Casting Alloys," AFS Transactions, 1995, Vol. 103, pp. 521-530.
4. E. Pan and J. Hu , "Study on Fluidity of Al-Si Alloys," AFS Transactions, 1997, Vol. 105, pp. 413-417.
5. E. Pan and J. Hu, "Fluidity of Al-Si (Cu) Alloys as Affected by Alloy Solidification Modes," AFS Transactions, 1998, Vol. 106, pp. 609-616.
6. E. Pan and K. Liao, "Study on flowability of EPC A356 Al Alloy," AFS Transactions, 1998, Vol. 106, pp. 233-237.
7. M. Flemings, E. Niyama and H. Taylor, "Fluidity of Aluminum Alloys," AFS Transactions, 1961, Vol. 69, pp. 625-635.
8. R. Monroe, "Expandable Pattern Casting," AFS, Des Plaines, Illinois, U.S.A., 1992, pp. 13-15.
9. R. Walling and J. Dantzig, "Mechanisms of Mold Filling in the EPC Process," AFS Transactions, 1994,Vol. 102, pp. 851-852.
10. S. Shivkumar, L. Wang and D. Apelian, "The Lost Foam Casting of Aluminum Alloy Components" JOM, 1990, Vol. 42, pp. 38-40.
11. S. Mehta and S. Shivkumar, "Fluidity of Al Alloys and Composites in the Lost Foam Process," AFS Transactions, 1998, Vol.106, pp. 663-668.
12. W. Hesterberg, R. Donahue and T. Cleary, " Evaporable Foam Casting System Utilizing a Hypereutectic Aluminum-Silicon Alloy," United states Patent, No. 340555, 14 April 1989.

13. J. Jorstad, "Hypereutectic Al-Si Casting Alloys: 25 Years, What's Next?" AFS Transactions, 1996, Vol. 104, pp. 665-669.
14. J. Davis, "ASM Specialty Handbook: Aluminum and Aluminum Alloys," ASM International, Ohio, 1994, pp. 706.
15. T. Lyman, " Metallography, Structures and Phase Diagrams," American Society for Metals, Ohio, Vol.8, Edition 8, pp. 263.
16. J. Gruzleski and B. Closset, "The Treatment of Liquid Aluminum-Silicon Alloys," Des Plaines III, AFS, 1990, pp. 107-113.
17. S. Gowri and F. Samuel, "Effect of Mg on the Solidification Behavior of Two Al-Si-Cu-Fe-Mg (380) Die Casting Alloys," AFS Transactions, 1993, Vol. 101, pp. 611-617.
18. L. Wang and D. Apelian, "Solidification of Eutectic in Hypoeutectic Al-Si Alloys," AFS Transactions, 1999, Vol. 107, pp. 249-256.
19. T. Layman, "Metallography, Structures and Phase diagrams: Metals Handbook," American Society for Metals, Ohio,1972, Vol.8, Edition 8, pp.389.
20. M. Flemings, "Solidification Processing," McGraw-Hill, New York, (1974).
21. L. Backerud, G. Chai and J. Tamminen, "Solidification Characteristics of Aluminum Alloys," Vol. 2, Foundry alloys , pp. 71-72.
22. L. Arnberg and L. Backerud, "Solidification Characteristics of Aluminum Alloys," Volume 3: Dendritic Coherency, AFS, 1996, pp. 210.
23. http://www.beckracing.com/page02.htm, Beck Racing, Al Alloys for Pistons, Sept 2002.
24. http://www.dynacast.com/die-casting/benefits-myths.html, Dynacast, Die Casting, June 2003
25. http://strategic.ic.gc.ca/SSG/mm01267e.html#control, American Foundrymen's Society 101st Casting Conference, June 2003.
26. L. Arnberg and L. Backerud, "Solidification Characteristics of Aluminum Alloys," Volume 3: Dendritic Coherency, AFS, 1996, pp. 211-212.
27. http://www.moderndiecasting.com/faq_dcd.html, Modern die Casting, June 2003.
28. http://www.portalenergy.com/casddet/ee/R379.pdf, CADDET, Lost Foam Casting Improves Production and Uses Less Energy, June 2003.

29. L. Backerud, G. Chai and J. Tamminen, "Solidification Characteristics of Aluminum Alloys", Vol. 2, Foundry Alloys, pp 4-5.
30. K. Upadhya, D. Stefanescu, K. Lieu and D. Yeager, "Computer-Aided Cooling Curve Analysis: Principles and Applications in Metal Casting", AFS Transactions, 1989, Vol. 97, pp. 61-66.
31. Dwyer, "Gaters and Risers for Castings," Third edition, The Penton Publishing Co. Clevland13, Ohio, 1952.
32. C. Ravindran, B. Jue and J. Karpynczyk, "A Study of the Effect of Vibration on the Permeability of Unbonded Sand in Expendable Foam Casting," AFS Transactions, Vol.102, 1994, pp. 915-920.
33. J. Davis, "ASM Specialty Handbook: Aluminum and Aluminum Alloys," ASM International, Ohio, 1994, pp. 223.
34. J. Davis, "ASM Specialty Handbook: Aluminum and Aluminum Alloys," ASM International, Ohio, 1994, pp. 207.
35. J. Davis, "ASM Specialty Handbook: Aluminum and Aluminum Alloys," ASM International, Ohio, 1994, pp. 200.
36. Gas-Tech Instruction manual, Kingsville, Missouri 64061.
37. E. Pan and K. Liao, "Filling Behavior of EPC A356 Alloy Casting," AFS Transactions, 2000, Vol.108, pp. 751-760.
38. X. Liu, C. Ramsay and D. Askeland, "Study on Mold Filling Control Mechanisms in the EPC Process," AFS Transactions, 1994, Vol.102, pp. 900-905.
39. S. Bennett, M. Tschopp, A. Vrieze , E. Zelkovich, C. Ramsay and D. Askeland, "Observation on the Effect of Gating Design on Metal Flow and Defect Formation in Aluminum Lost Foam Casting: Part 1," AFS Transactions, 2001, Vol. 109, pp. 1473-1487.
40. C. Tseng and D. Askeland, "A Study of Selected Process Parameters for the Evaporative Pattern Casting Process," AFS Transactions, 1992, Vol.100, pp. 519-527.
41. Y. Sun, H. Tsai and D. Askeland, "Effects of Silicon Content, Coating Material and Gating Design on Casting Defects in the Aluminum Lost Foam Process," AFS Transactions, 1996,Vol.104, pp. 271-279.

42. T. Kobayashi and Y. Kasuya, "Behavior of Produced Gas and Thermal Decomposition in the Evaporative Pattern," IMONO, 1992, Vol.6, pp. 318-324.
43. X. Yao and S. Shivkumar, " Mold filling and Solidification in the Lost Foam Process," AFS Transactions, 1995, Vol.95, pp. 761-764.
44. L. Ananthanarayanan, F. Samueland and J. Gruzleski, "Crystallization Behavior of Iron Containing Intermetallic Compounds in 319 Aluminum Alloy," Metall. Trans. A, 1994, Vol. 25A, pp. 1761-1773.
45. S. Murali, K. Raman and K.S.S Murthy, "Effect of Magnesium, Iron (impurity) and Cooling Rates on the Fracture Toughness of Al-7 Si-0.3 Mg Casting Alloy," Material Science and Engineering, A151, 1992, pp. 1-10.
46. G. Gustafsson, T. Thorvaldsson and G. Dunlop, "The Influence of Fe and Cr on the Microstructure of Cast Al-Si-Mg alloys," Metallurgical Transactions A, 1986, Vol. 17A, pp. 45-52.
47. M. Djurdjevic, W. Kierkus, G. Byczynski , T. Stockwell and J. Sokolowski, "Modeling of Fraction of Solid for 319 Aluminum Alloy," AFS Transactions, 1999, Vol.107, pp. 173-179.
48. A. Savitzky and M. Golay, "Smoothening and Differntiation of Data by Simplified Least Squares Procedure," Analytical Chemistry, 1964, Vol.36, pp. 1627-1639.
49. W. Back, " Solidification of Metals," AFS Transactions, 1960, Vol.68, pp. 693-698.
50. J. Kim, H. Kwon and C. Loper, " Feeding Behavior of Modified and Unmodified Al-Si Alloys," AFS Transactions, 1996, Vol.104, pp.743-749.

APPENDIX A

CHEMICAL ANALYSIS

Chemical Analyses of Experimental Alloys:

Table A.1 Average Chemical Analyses of 3 pourings (pourings with 30°C superheat, pourings with 150°C superheat and pourings with top gating system) for the alloy with 12% Si content

E.	%	E.	%	E.	%	E.	%	E.	%
Al	86.552	Fe	0.3192	Mg	0.325	Zn	0.136	**Si**	**12.276**
Cu	**0.0397**	Li	0.0001	Mn	0.0301	Sn	0.009	Cr	0.0064
Sr	0.0002	Pb	0.0073	Ni	0.0083	P	0.0005	Ti	0.0299
Be	0.0001								

Table A.2 Chemical Analysis for the Alloy with 12% Si, 2.5% Cu

E.	%	E.	%	E.	%	E.	%	E.	%
Al	85.05	Fe	0.2292	Mg	0.124	Zn	0.0164	**Si**	**11.789**
Cu	**2.71**	Li	0.0001	Mn	0.0215	Sn	0.001	Cr	0.0049
Sr	0.0002	Pb	0.0077	Ni	0.0092	P	0.0005	Ti	0.0280
Be	0.0001								

Table A.3 Average Chemical Analyses of 3 pourings (pourings with 30°C superheat, pourings with 150°C superheat and pourings with top gating system) for the alloy with 18% Si content

E.	%	E.	%	E.	%	E.	%	E.	%
Al	81.477	Fe	0.2502	Mg	0.160	Zn	0.0075	**Si**	**18.009**
Cu	**0.0200**	Li	0.0001	Mn	0.0168	Sn	0.013	Cr	0.0033
Sr	0.0004	Pb	0.0056	Ni	0.0053	P	0.0008	Ti	0.0312
Be	0.0001								

Table A.4 Chemical Analysis for the Alloy with 18% Si and 2.5% Cu

Element	%	E.	%	E.	%	E.	%	E.	%
Al	79.983	Fe	0.1992	Mg	0.000	Zn	0.0126	**Si**	**17.08**
Cu	**2.64**	Li	0.0001	Mn	0.0233	Sn	0.008	Cr	0.0048
Sr	0.0002	Pb	0.0076	Ni	0.0073	P	0.0004	Ti	0.0292
Be	0.0001								

Table A.5 Average Chemical Analyses of 3 pourings (pourings with 30°C superheat, pourings with 150°C superheat and pourings with top gating system) for the alloy with 18% Si content

Element	%	E.	%	E.	%	E.	%	E.	%
Al	74.644	Fe	0.2652	Mg	0.081	Zn	0.0385	**Si**	**24.812**
Cu	**0.0201**	Li	0.0001	Mn	0.0193	Sn	0.013	Cr	0.0050
Sr	0.0030	Pb	0.0451	Ni	0.0183	P	0.0026	Ti	0.0332
Be	0.0001								

Table A.6 Chemical Analysis for the Alloy with 25% Si, 2.5% Cu

Element	%	E.	%	E.	%	E.	%	E.	%
Al	71.735	Fe	0.2232	Mg	0.104	Zn	0.0211	**Si**	**24.936**
Cu	**2.8976**	Li	0.0001	Mn	0.0245	Sn	0.001	Cr	0.0057
Sr	0.0002	Pb	0.0087	Ni	0.0120	P	0.0002	Ti	0.0287
Be	0.0001								

Note: Chemical analyses for the alloy with 5% Cu additions were not carried out because the Gamma foundry has Cu limit of 3%.

E : Element

APPENDIX B

COOLING RATE AND VELOCITY CURVES FOR 30^{0}C SUPERHEAT POURINGS

A.1 Cooling Rate Curves:

Cooling rate and velocity curves for the alloys with 12, 15, 18, 21 and 25% Si content at 30°C are shown in figure B.1, B.2, B.3, B.4, and B.5.

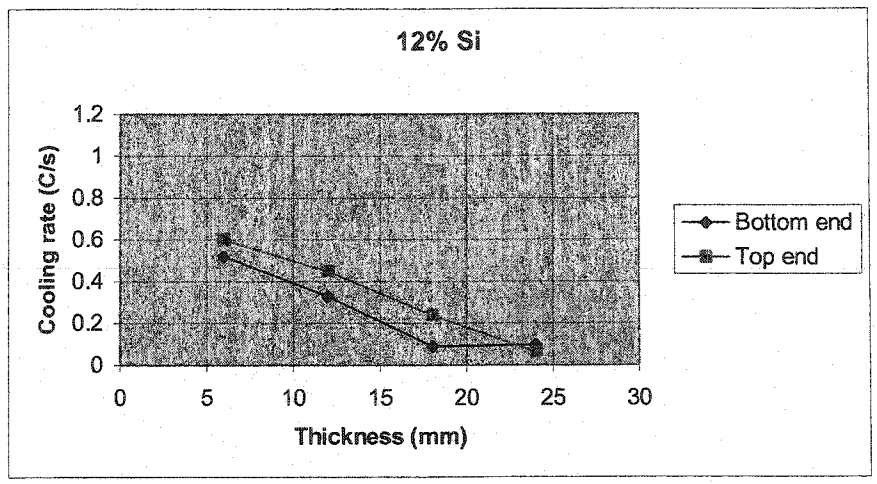

Figure B.1 Cooling Rate Curve for the Alloy with 12% Si Content.

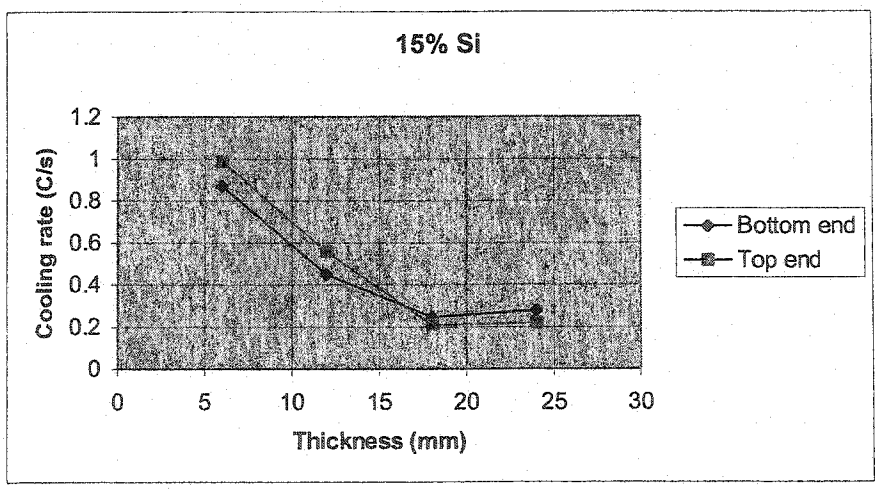

Figure B.2 Cooling Rate Curve for the Alloy with 15% Si Content

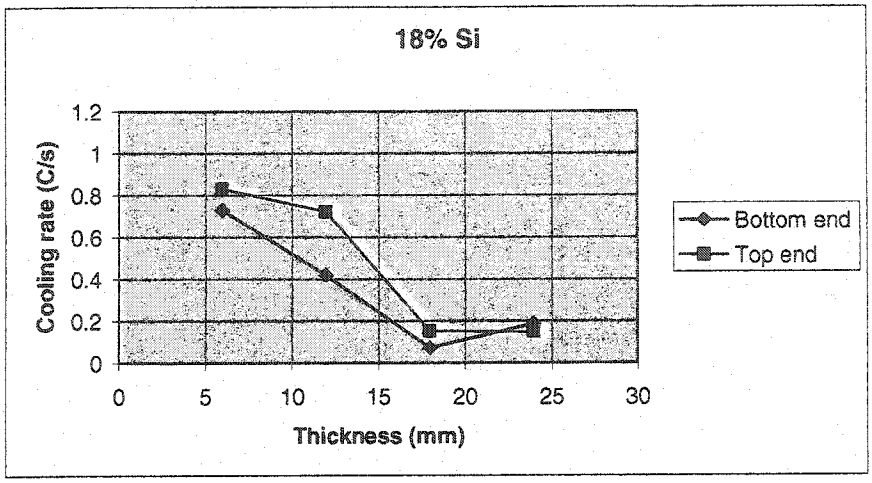

Figure B.3 Cooling rate Curve for the Alloy with 18% Si Content.

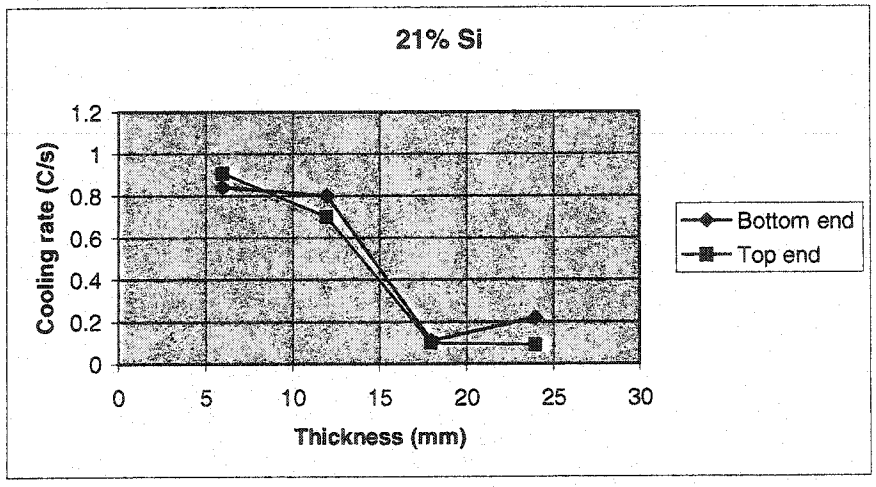

Figure B.4 Cooling Rate Curve for the Alloy with 21% Si Content.

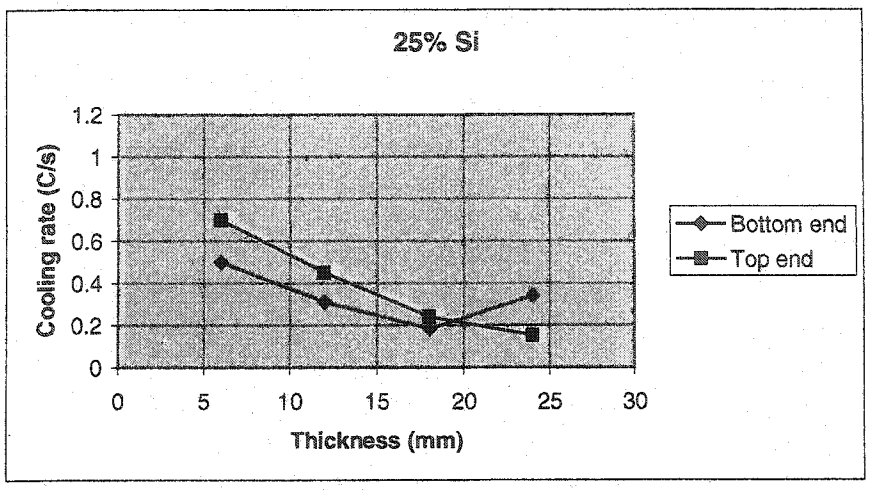

Figure B.5 Cooling Rate Curve for the Alloy with 25% Si Content.

B.2 Velocity curves:

Velocity Curves for the alloy with 12, 15, 18, 21 and 25% Si content at 30°C is shown in figure B.6.

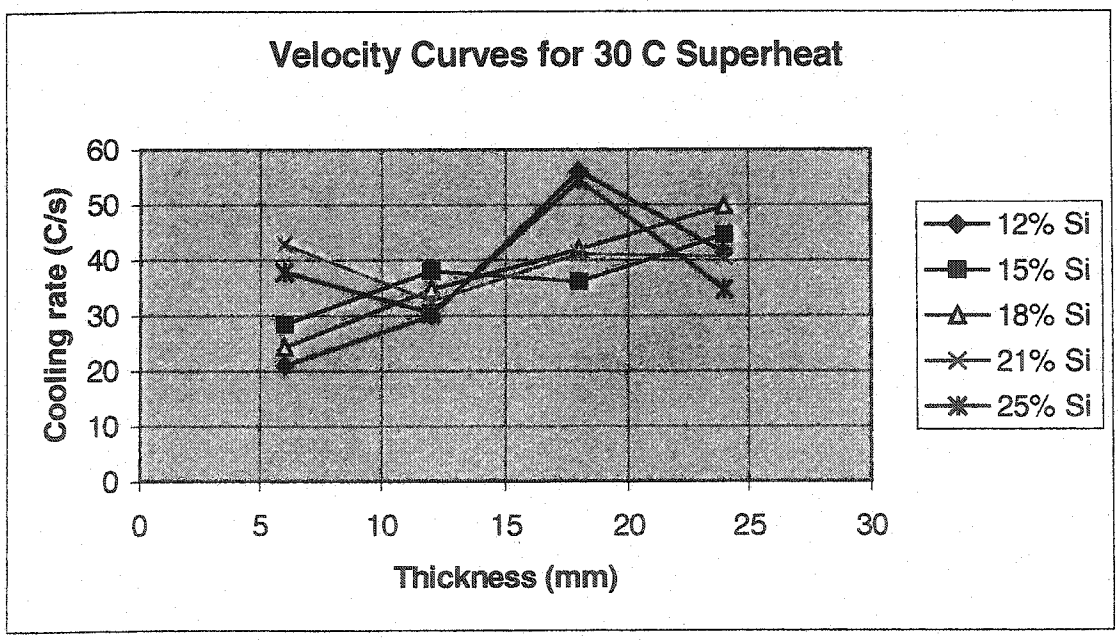

Figure B.6 Velocity curves for the Alloy with 12, 15, 18, 21, 25% Si content.

APPENDIX C

COOLING RATE AND VELCITY CURVES FOR THE POURINGS WITH 5% Cu ADDITION

C.1 Cooling rate:

Cooling rate curves for the alloy with 12,18 and 25% Si content by addition of 5% Cu at 150°C superheat.

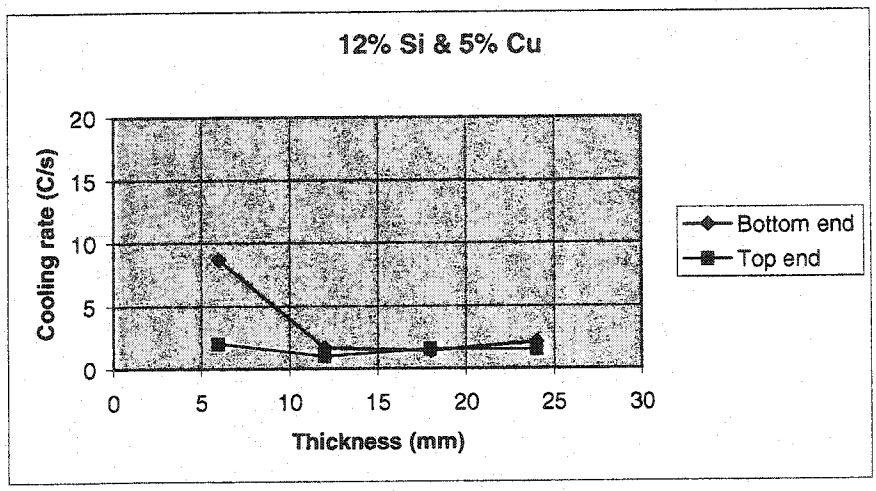

Figure C.1 Cooling Rate Curve for the Alloy with 12% Si and 5% Cu Content.

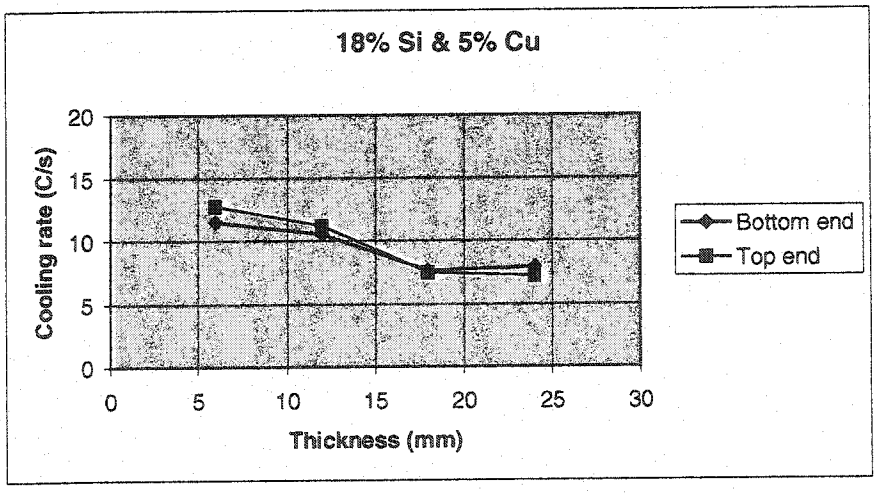

Figure C.2 Cooling Rate Curves for the Alloy with 18% Si and 5% Cu Content

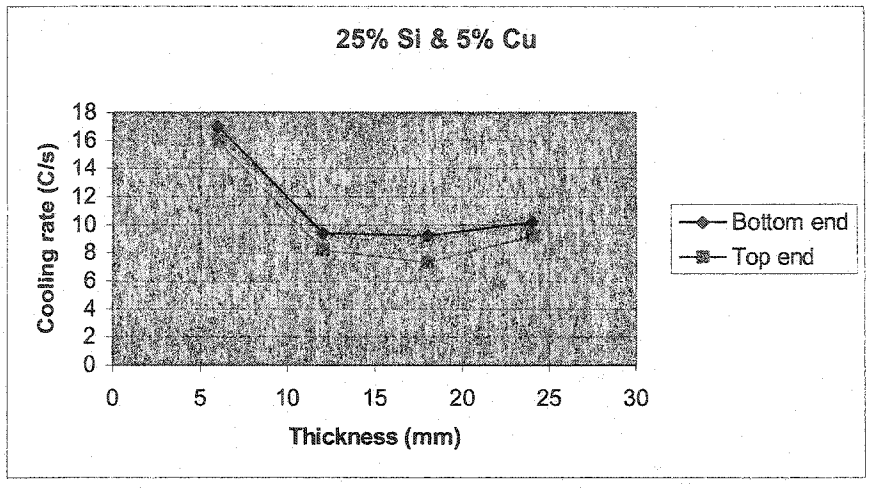

Figure C.3 Cooling Rate Curves for the Alloy with 25% Si and 5% Cu Content

C.2 Velocity Curves:

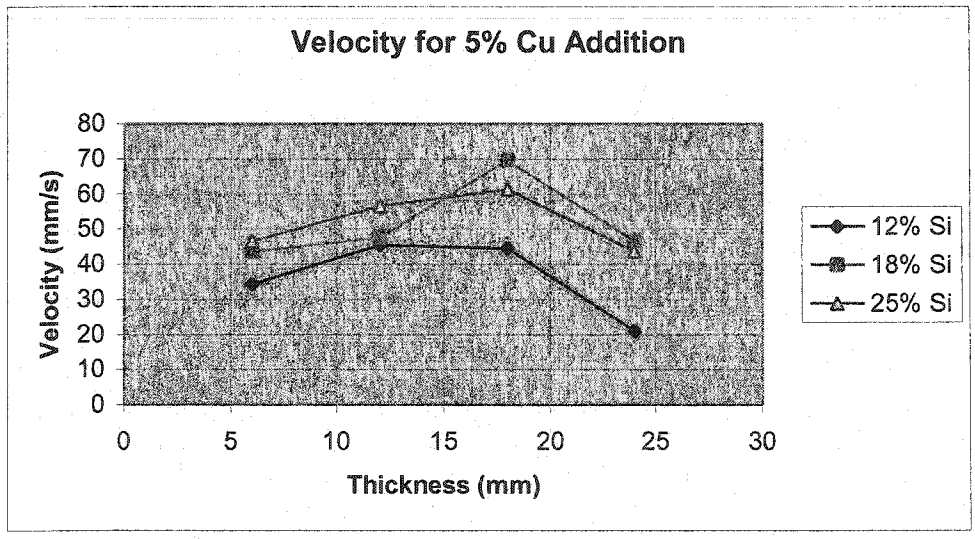

Figure C.4 Velocity Curves for 12,18 and 25% Si Content by Addition of 5% Cu.